UNIVERSITY OF CALIFORNIA

Los Angeles

Mechanisms of Parasympathetic Dysfunction Following Myocardial Infarction

A dissertation submitted in partial satisfaction of the

requirement for the degree of Doctor of Philosophy

in Molecular, Cellular, and Integrative Physiology

by

Jonathan Duy-Thach Hoang

2022

ABSTRACT OF THE DISSERTATION

Mechanisms of Parasympathetic Dysfunction Following Myocardial Infarction

by

Jonathan Duy-Thach Hoang

Doctor of Philosophy in Molecular, Cellular, and Integrative Physiology

University of California, Los Angeles, 2022

Professor Marmar Vaseghi, Chair

The sympathetic and the parasympathetic nervous systems (PNS), exert opposing control over beat-to-beat cardiac function but following myocardial infarction (MI), their balance is disrupted. Sustained sympathetic hyperactivity coupled with PNS withdrawal promotes cardiac electrical heterogeneity and predisposes to ventricular tachycardia (VT). PNS blockade is pro-arrhythmic and the restoration of PNS function is anti-arrhythmic, in part through prolonging ventricular action potential duration (APD) and reducing electrical heterogeneity. Thus, expanding our understanding on PNS dysfunction is paramount to designing better therapies. This dissertation aims to dissect the neural circuitry underlying PNS withdrawal post-MI.

Chapters 1 and 2 expand the therapeutic potential and applicability of augmenting PNS activity. Chapter 2 demonstrated that vagal nerve stimulation (VNS) remains anti-arrhythmic despite sympathoexcitation post-MI. These cardioprotective effects were mediated by prolongation of ventricular APD and reductions in electrical heterogeneity in the scar and border zone, known regions of arrhythmogenesis. Chapter 3 extends these potential anti-arrhythmic effects to patients with chronic MI.

Chapter 3 assesses the role of vagal afferents in mediating vagal efferent dysfunction. In health, nociceptive afferent activation increase vagal efferent outflow. However, *in vivo* neural recording and detailed histology revealed that post-MI, nociceptive afferents may instead decrease PNS tone through augmented release of GABA, a novel pathway of vagal inhibition.

Chapter 4 examines the role of spinal afferent signaling in suppressing central PNS outflow. Thoracic epidural anesthesia (TEA), a neuromodulatory approach under investigation for its anti-arrhythmic effects, is generally regarded as a sympatho-inhibitory technique. However, we show herein that the anti-arrhythmic effects of TEA may in part be mediated by PNS augmentation. Moreover, these studies implicate an important role for spinal afferents in post-MI PNS inhibition.

Lastly, Chapter 5 explores the role of the sympathetic co-transmitter, neuropeptide Y (NPY), in cardiac control. We established the frequency dependent release of NPY in healthy pigs, *in vivo*. We observed that high frequency sympathetic stimulation circumvents traditional therapy with beta-blockers, even at supramaximal doses. However, the NPY Y_1 receptor-selective antagonist, BIBO 3304, mitigated the residual electrophysiological effects of sympathetic stimulation. These studies set the stage for further investigations into other NPY receptor subtypes, such as the Y_2 receptor, which is expressed on PNS neurons. Agonism of the Y_2 receptor reduces neuronal calcium influx and the release of acetylcholine, a potential mechanism for reductions in cardiac PNS tone.

In conclusion, PNS augmentation is anti-arrhythmic despite sympathoexcitation, suggesting that relief of central PNS suppression may also be independently anti-arrhythmic. However, post-MI PNS withdrawal may be mediated at several levels of the cardiac neuraxis by nociceptive afferent inhibition (vagal reflexes), spinal sympathetic afferent signaling (spinal reflexes), and/or excessive sympathetic efferent tone causing release of NPY (sympathetic – parasympathetic crosstalk). Therapies targeting these novel pathways may restore central parasympathetic tone and suppress arrhythmogenesis, especially in patients who are refractory to traditional therapy.

The dissertation of Jonathan Duy-Thach Hoang is approved.

Jeffrey Laurence Ardell

Thomas J. O'Dell

Tamer I. Sallam

Thomas M. Vondriska

Marmar Vaseghi, Committee Chair

University of California, Los Angeles

2022

Dedicated to

My friends, family, and mentors who this work possible.

TABLE OF CONTENTS

LIST OF FIGURES

CHAPTER 1

CHAPTER 2

CHAPTER 3

CHAPTER 4

CHAPTER 5

LIST OF TABLES

CHAPTER 1

CHAPTER 5

LIST OF ACRONYMS

AH = atrio-His conduction

AT = activation time

ARI = activation recovery interval

BRS = baroreflex sensitivity

BSS = bilateral stellate ganglia stimulation

CM = cardiomyopathy

ECG = electrocardiogram

HR = heart rate

HV = His-ventricle conduction

LV = left ventricle

PE = phenylephrine

RV = right ventricle

MI = myocardial infarction

RT = recovery time

SBP = systolic blood pressure

SNH = structurally normal hearts

TEA = thoracic epidural anesthesia

VNS = vagal nerve stimulation

VT = ventricular tachyarrhythmias

VF = ventricular fibrillation

SUPPLEMENTARY TABLES AND FIGURES

CHAPTER 3

CHAPTER 5

PREFACE

Chapter I is a version of a published manuscript. Hoang JD, Yamakawa K, Rajendran PS, Chan CA, Yagishita D, Nakamura K, Lux RL, Vaseghi M. Proarrhythmic Effects of Sympathetic Activation Are Mitigated by Vagal Nerve Stimulation in Infarcted Hearts. JACC: Clinical Electrophysiology. 2022; 8(4):513-525. doi: 10.1016/j.jacep.2022.01.018. Author contributions are as follows. JDH, KY, RLL, and MV conceived and designed research; JDH, KY, PSR, CAC, DY, KN, RLL, and MV performed experiments; JDH, KY, and MV analyzed data; JDH and MV interpreted results of experiments; JDH and MV prepared figures; JDH and MV drafted the manuscript; JDH, KY, PSR, CAC, DY, KN, RLL, and MV edited, revised, and approved the final version of the manuscript.

Chapter II is in preparation for publication. Hoang JD, Lokhandwala ZA, Buckley U, Jani NR, Bradfield JS, Krokhaleva Y, Khakpour H, Ajijola OA, Boyle NG, Shivkumar K, Vaseghi M. Ventricular Electrophysiological Effects of Vagal Nerve Stimulation in Humans With and Without Structural Heart Disease. Author contributions are as follows. JDH, ZAL, UB, NRJ, JSB, YK, HK, OAA, NGB, KS, and MV performed experiments; JDH, ZAL, UB and MV analyzed data; JDH and MV interpreted results of experiments; JDH and MV prepared figures; JDH and MV drafted the manuscript.

Chapter III is a version of a published manuscript. Salavatian S,* Hoang JD,* Yamaguchi N,* Lokhandwala ZA, Swid MA, Armour JA, Ardell JL, Vaseghi M. Myocardial infarction reduces cardiac nociceptive neurotransmission through the vagal ganglia. JCI Insight. 2022;7(4). Epub 2022/01/12. doi: 10.1172/jci.insight.155747. PubMed PMID: 35015733; PMCID: PMC8876456. Author contributions are as follows. SS, JAA, and MV conceived and designed research; SS, JDH, NY, MAS, and MV performed experiments; SS, JDH, NY, ZAL, and MV analyzed data; SS, JDH, JAA, and JLA, ZAL and MV interpreted results of experiments; SS, JDH, NY, and MV prepared figures; SS, JDH, and MV drafted the manuscript; SS, NY, JDH, ZAL, MAS, JAA, JLA, and MV

edited, revised, and approved the final version of the manuscript. First authorship order position was noted based on intellectual contribution to design of the study and interpretation of data.

Chapter IV is in preparation for publication. Hoang JD, Swid MA, Kang KW, Chan CA, Jani NR, Vaseghi M. Autonomic and Electrophysiological Effects of Thoracic Epidural Anesthesia on Infarcted Porcine Hearts. Author contributions are as follows. JDH, MAS, KWK, CAC, NRJ and MV performed experiments; JDH, KWK, and MV analyzed data; JDH and MV interpreted results of experiments; JDH and MV prepared figures; JDH and MV drafted the manuscript.

Chapter V is a version of a published manuscript. Hoang JD,* Salavatian S,* Yamaguchi N,* Swid MA, Hamon D, Vaseghi M. Cardiac sympathetic activation circumvents high-dose beta blocker therapy in part through release of neuropeptide Y. JCI Insight. 2020;5(11). Epub 2020/06/05. doi: 10.1172/jci.insight.135519. PubMed PMID: 32493842; PMCID: PMC7308065. Author contributions are as follows. JDH, SS, and MV contributed to the conception and design of the experiments. JDH, SS, NY, and MAS performed experiments, and JDH, SS, NY, and MV analyzed the data. DH contributed to the initial design of the study and helped perform preliminary experiments. JDH and MV drafted the manuscript, and all authors revised and approved the final version of the manuscript.

This work was supported by NIH DP2HL132356, NIH R01HL148190, and SPARC OT2OD023848 to Marmar Vaseghi and NIH T32GM065823 to Jonathan D Hoang.

ACKNOWLEDGMENTS

Thanks to you, the reader, for finding your way to my dissertation. I hope you find that the enclosed work is informative and interesting but also appreciate that none of this would be possible without the endless support of my loving friends & family and guidance from my many mentors & advisors throughout the years.

Thank you to my mentor and doctoral advisor, Dr. **Marmar Vaseghi**. I will always be grateful that you took a chance on me, both as an undergraduate student and again as a doctoral student. You are the only person capable of taking me to where I needed to go and making me into the scientist I am now; you pushed me when I needed to be pushed, let me find my way when I needed to explore, and directed me whenever I started to wander.

Thank you to my excellent committee members: Drs. **Jeffrey Ardell**, **Thomas Vondriska**, **Tamer Sallam**, and **Thomas O'Dell**. Throughout my graduate career you have all been valued mentors and advisors. All of this work was only truly capable by following the example of scientific curiosity and passion you have all set for me.

Thank you to Dr. **Viviana Gradinaru** for accepting me as a post-doctoral fellow. I am incredibly excited for the opportunity to learn from you and your team. I cannot wait to contribute to your work and see where the research will take me. Thank you for seeing the potential in me.

A heartfelt thank you to our collaborators, not only for their guidance in our experiments, but also for their advice to me over the years. Dr. **John Andrew Armour**, I deeply appreciate the time you always took to talk to me. I will always remember your humility and how you not only accepted, but actually welcomed, that there was still so much we did not know. Even though I was a nobody, you always pulled me in to introduce me to all the important people you were talking with at the time. Dr. **John Tompkins**, thank you for your scientific and professional advice over the years. I have truly enjoyed working alongside you and learned so much from you over the years through your talks and our random late night conversations in the lab. Dr. **Corey Smith**,

thank you for your constant encouragement throughout the years. I remember meeting you at the beginning of my career and very shyly approaching you after your talk. Thank you for showing me around Cleveland and especially being a mentor over these many years.

My deep appreciation to all the post-doctoral fellows I have had the pleasure to train under and alongside, especially when I was just an undergraduate student. Thank you to Dr. **Kentaro Yamakawa** for sharing with me the elegance of the heart from my first day in the lab and instilling me with a fascination for science and research. Working closely with you set me down a path of success that I will always be grateful for. Thank you to Dr. **Pradeep Rajendran** for his endless patience in taking the time to teach a bunch of undergraduate students like myself how to be scientists. More than that, I am grateful for your mentorship and advice throughout my graduate career and beyond.

Throughout my PhD I had the fortune of working with so many talented and patient post-doctoral fellows as well. I am grateful for all of your patience and for sharing a wealth of knowledge with me along this journey. Thank you to Dr. **Una Buckley**, working with you closely at the beginning of my graduate career really instilled me with the confidence I needed to survive graduate school. I am thankful for all of your support and patience with me as I was starting off. Thank you Dr. **Siamak Salavatian** for not only being a life-long mentor, but also a dear friend. I wish for everyone in their training to have a friend and colleague like you with whom they feel comfortable to ask stupid questions, but also have esoteric scientific discussions with. I learned so much trying to keep up with you while you were here and trying to fill your shoes after you left. Thank you to Dr. **Naoko Yamaguchi** for always humbling me and showing me how simple and common sense cardiology could be. I still use the Naoko method to show everyone how to place a coronary sinus catheter. Most of all though, I will never forget that the only time I ever amazed you was when I turned a high five into a turkey. Thank you to Dr. **Veronica Dusi**, you were always so incredibly patient with me. I am especially grateful for all that I learned through our late nights

working in the office and deep conversations about cardiology. I will always remember how you loved Brugada syndrome as an example of basic electrophysiology principles, but I must admit that I still do not understand it! Thank you to Dr. **Ki-Woon Kang** for all your lessons. I was incredibly lucky to have the opportunity to work alongside you and ask you questions about cardiac electrophysiology and intervention. It is only with your guidance that I was able to master the infarct model and I share the lessons I learned from you with everyone I work with. Thank you to Dr. **Valerie van Weperen** for being a dear friend. Somehow you have always arrived just when I needed you most. From the first time I was submitting a paper to when I was preparing for my defense, you always knew just what I needed to hear and when I needed to hear it.

I am appreciative to have the opportunity to work with so many talented project scientists and technicians who have become so much more than just that. Thank you to Dr. **Asokan Devarajan**, your greeting cards and notes always make me smile. Thank you to Dr. **Ke Wang**, I really enjoyed our small chats on the bus and learning from your dissections; I hope I can be as good as you one day. Thank you to Dr. **Mohammed Amer Swid**, I know we did not get along at first but that makes it all the more surprising how close of a friend and even a brother you have become to me. Thank you to **Amit Tsanhani**, **Jaime Contreras**, **Christopher Chan**, and **Zulfiqar Ali Lokhandwala**. You were more than just colleagues; you were lifelong friends who made the lab bearable. Thank you for tolerating my obsessive personality and helping me survive graduate school. Amit, I am glad we could share Taylor Swift memes instead of actual conversation. Jaime, I am happy we could nerd out over Jurassic Park and thank you for helping me through some hard times throughout COVID. Chris, thank you so much for being such a loyal friend and for always doing what you thought was right above all else. Ali, all your nonsense always lightened the atmosphere. Thank you to Dr. **Neil Jani**, I have never heard someone use so much Latin and medical jargon before working with you. Thank you to Dr. **Maryam Emamimeybodi**, I have never had this many pictures of myself before you joined.

To all the fellows in the lab, it was my pleasure to work with you over the years throughout our PhDs. Congratulations to us all for surviving! Thank you to Dr. **Peter Hanna**, I enjoyed all our little conversations about Orange County while you were here. You were an endless wealth of knowledge and glad I could grow and learn in the lab alongside you. I am always glad to see you when I get to visit the catheterization lab! Thank you to Dr. **Joseph Hadaya**, I am happy to have had someone in the lab to celebrate the wins and share in the losses together; glad we could catch up in Philadelphia. Thank you to Dr. **Ching Zhu**, I am glad someone else in the lab understood my obsessiveness and shared my passion for organization and labeling.

Thank you to all of the students I have been able to work with over the years. Thank you especially to Dr. **Janki Mistry**, **Raeann Salonga**, **Sahar Nadafian**, and **Sartaj Bal**. Having the opportunity to work with and teach such amazing students was really my pleasure. I learned just as much from you as I hope you learned from me. Thank you to **Al-Hassan Dajani**, I am so incredibly impressed to see the bright-eyed kid who used to share the desk next to me now leaving for medical school. I really enjoyed working with you and I can hardly believe I have known you for so many years. Go crush it, boss. Thank you to **Cameron Carlson** for always being a pleasure to work with. Your genuine attitude, excitement to learn, and humility will take you far.

Thank you to Dr. **Koji Yoshie**, Dr. **Yuichi Hori**, Dr. **Taro Temma**, and Dr. **Sachin Sharma** Simply sharing the same office and lab as all of you was inspiring. I am truly thankful to have been able to learn so much just through this simple diffusion of knowledge.

Thank you to Dr. **Douglas Chapski**, I almost cringe now thinking about all the stupid questions I asked you about biology and about R. You were incredibly patient and kind to me and the lessons I learned while working with you are invaluable. I owe you a Diet Coke! Thank you to Dr. **Jiayi Yao**, you were one of my first mentors in graduate school and I will never forget you. Not only did you teach me in class and deeply questioned when I said I would do co-culture, but you were my post-doc while I was a rotation student. I will always remember the way you would

squint your eyes really hard when you thought you saw me across the hall, the way you would gasp nervously when watching me do cell culture, and how you would yell at me to go faster when I was helping you with FACS. Most of all though, I will never forget your patience. Thank you for your mentorship and for your friendship, you are incredibly missed.

I am deeply grateful for the opportunity to have worked at the Larry Hillblom Islet Research Center, for all that I learned while I was there, and all the friends I made. A special thank you to Dr. **Aleksey Matveyenko** and Dr. **Anthony Thomas** for taking a chance on me and taking me in after I had graduated. I will never forget how humbling it was to work with you, thank you for all your patience and everything you taught me. Thank you to my first ever students, Dr. **Kenny Vongbunyong** and **Andrew Nguyen** for not only being the best undergraduates I could ask for, but also for being great friends. Hopefully we will never have to do another 2 AM oral glucose tolerance test in red light!

Thank you to Dr. **Peter Butler**, Dr. **Tatyana Gurlo**, and Dr. **Sangeeta Dhawan** for their guidance when I felt lost and did not know what to do with my life. It was in large part due to your kindness and mentorship that I decided to pursue graduate school. Thank you to Dr. Butler for telling me that you thought I would excel in graduate school, you really gave me the confidence to make it. Thank you to Tatyana for working with me so closely and teaching me everything I know. I use the lessons I learned while working with you every single day, we will always be a team. Thank you to Sangeeta for your friendship throughout my time in the lab and even now. I always take lessons from my time here and bring them with me wherever I go; whether it is scientific protocols or birthday celebrations, your passion and cheer is always with me.

Thank you to my life-long friends **Paul Sung**, **Nick Kim**, and **Kydric Luyen**. You always cheered for me in whatever I pursued. No matter what was going on or how long it had been since we caught up, you were always right there for me whenever I needed you. You never held it

against me for being busy and not responding for weeks at a time and we always picked up right where we left off. Thank you for always staying by my side.

Thank you to my entire PhD cohort for their support and friendship. Special thank you to Dr. **Nathaniel Elia** & Dr. **Artin Soroosh** for keeping me fed and sane throughout graduate school with our Saturday morning coffee clubs, Korean barbeque nights, and hot pot dinners. We need to start up SMCC again.

Lastly, thank you to my loving and supportive family. A special thank you to my **Grandparents**, I wish you could have been here with me to celebrate. You have been cheering for me my whole life to become Dr. Hoang. I hope I have made you proud.

To my sisters, **Jessica Hoang** and **Justina Hoang**, thank you for always carrying me and keeping me standing. I would not be here if not for the countless trips between Los Angeles and Orange, the free meals and fast-food breaks, and all the times you took care of me when I was sick. When I felt like I was losing my way, you helped me to find my path. I am so incredibly lucky to have two big sisters who did everything for me so I would never have to worry. Your baby brother finally did it!

Thank you for everything **Bố Mẹ** (mom and dad). I cannot begin to express my appreciation of your life-long support. I am truly a product of your love, your generosity, your kindness, and your curiosity. You have always put us first no matter the circumstances and it is only by standing on your shoulders that I have been capable of anything. You have supported me throughout my entire career and showed me the unconditional love that gave me the strength and courage to do something that had at many points did not feel possible. My success is your success. Everything I do is in service to how wonderful and loving my parents are. Thank you for all that you do every day.

VITA

EDUCATION

UNIVERSITY OF CALIFORNIA, LOS ANGELES — Los Angeles, CA

PhD Candidate - Molecular, Cellular, & Integrative Physiology — *2016 - Present*

Thesis: Mechanisms of Parasympathetic Dysfunction Following Myocardial Infarction

UNIVERSITY OF CALIFORNIA, LOS ANGELES — Los Angeles, CA

Bachelor of Science, Biology *(Minor: Evolutionary Medicine)* — *2010 - 2014*

PUBLICATIONS

1. **Pro-arrhythmic Effects of Sympathetic Activation Are Mitigated by Vagal Nerve Stimulation in Infarcted Hearts by Electrical Stabilization of Infarct Border Zone and Scar Regions** (*Accepted to JACC: Clinical Electrophysiology. Preprint. doi:* 10.2139/ssrn.3950133.)
   HOANG JD, Yamakawa K, Rajendran PS, Chan CA, Yagishita D, Nakamura K, Lux RL, Shivkumar K, Vaseghi M
2. **Myocardial infarction reduces cardiac nociceptive neurotransmission through the vagal ganglia** (*JCI Insight. 2022 Jan 11;e155747. doi:* 10.1172/jci.insight.155747.)
   HOANG JD, Salavatian S, Yamaguchi N, Lokhandwala ZA, Swid MA, Armour JA, Ardell JL, Vaseghi M
3. **Scalable and reversible axonal modulation of the sympathetic chain for cardiovascular control** (*Am J Physiol Heart Circ Physiol. 2022 Jan 1;322(1):H105-H115. doi:* 10.1152/ajpheart.00568.2021. *Epub 2021 Dec 3.*)
   Hadaya J, Buckley U, Gurel NZ, Chan CA, Swid MA, Bhadra N, Vrabec TL, **HOANG JD**, Ardell JL
4. **Cardiac Sympathetic Activation Circumvents High Dose Beta-blocker Therapy in Part Through Neuropeptide-Y** (*JCI Insight. 2020 Jun 4;5(11):e135519. doi:* 10.1172/jci.insight.135519.)
   HOANG JD, Salavatian S, Yamaguchi N, Swid MA, Vaseghi M
5. **Stellate ganglion stimulation causes spatiotemporal changes of ventricular repolarization in pig** (*Heart Rhythm. 2020 May;17(5 Pt A):795-803. doi:* 10.1016/j.hrthm.2019.12.022. *Epub 2020 Jan 7.*)
   Meijborg VMF, Boukens BJD, Janse MJ, Salavatian S, Dacey M, Yoshie K, Opthof T, Swid MA, **HOANG JD**, Hanna P, Ardell J, Shivkumar K, Coronel R
6. **Premature ventricular contractions activate vagal afferents and alter autonomic tone: implications for premature ventricular contraction-induced cardiomyopathy** (*Am J Physiol Heart Circ Physiol. 2022 Jan 1;322(1):H105-H115. doi:* 10.1152/ajpheart.00568.2021. *Epub 2021 Dec 3.*)
   Salavatian S, Yamaguchi N, **HOANG JD**, Lin N, Patel S, Ardell JL, Armour JA, Vaseghi M
7. **Beta-cell specific increased expression of calpastatin prevents diabetes induced by Islet Amyloid Polypeptide toxicity** (*JCI Insight. 2016 Nov 3;1(18):e89590. doi:* 10.1172/jci.insight.89590.)
   Gurlo T, Costes S, **HOANG JD**, Rivera J, Butler AE, Butler PC
8. **Administration of melatonin and metformin prevents deleterious effects of circadian**

disruption and obesity in male rats *(Endocrinology. 2016 Dec;157(12):4720-4731. doi: 10.1210/en.2016-1309. Epub 2016 Sep 21.)*
Thomas AP, **HOANG JD**, Vongbunyong K, Nguyen A, Rakshit K, Matveyenko AV

9. **CHOP contributes to, but is not the only mediator of, IAPP induced beta-cell apoptosis** (*Mol Endocrinol. 2016 Apr;30(4):446-54. doi: 10.1210/me.2015-1255. Epub 2016 Feb 22.)*
Gurlo T, Rivera JF, Butler AE, Cory M, **HOANG JD**, Costes S, Butler PC

10. **Beta-cell deficit in Obese Type 2 Diabetes, the Role of Beta-cell Dedifferentiation and Degranulation** (*J Clin Endocrinol Metab. 2016 Feb;101(2):523-32. doi: 10.1210/jc.2015-3566. Epub 2015 Dec 23.*)
Butler AE, Dhawan S, **HOANG JD**, Cory M, Zeng K, Fritsch H, Meier JJ, Rizza RA, Butler PC

11. **Electrophysiological Effects of Left and Right Vagal Nerve Stimulation on Ventricular Myocardium** (*Am J Physiol Heart Circ Physiol. 2014 Sep 1;307(5):H722-31. doi: 10.1152/ajpheart.00279.2014. Epub 2014 Jul 11.*)
Yamakawa K, So EL, Rajendran P, **HOANG JD**, Makkar N, Mahajan A, Shivkumar K, Vaseghi M

BOOK CHAPTERS, REVIEWS & EDITORIALS

1. **Neurocardiología: Aspectos fisiopatológicos e implicaciones clínicas** (*June 2018)*
Capítulo 20: Invervación autonómica cardíaca y rol de los tratamientos neuromoduladores
HOANG JD, Vaseghi M

2. **No Sympathy for the Hypoxic – The Role of Fetal Oxygenation in Autonomic Dysfunction** (*Am J Physiol Heart Circ Physiol. 2022 Jan 1;322(1):H105-H115. doi: 10.1152/ajpheart.00568.2021. Epub 2021 Dec 3.)*
HOANG JD, Vaseghi M

3. **A Novel Mechanism for Regulation of Cardiac Ca^{2+} Current by Estradiol: cAMP-ing Out at the Basal Epicardium** (*Heart Rhythm. 2018 May;15(5):750-751. doi: 10.1016/j.hrthm.2018.01.025. Epub 2018 Jan 31.*)
HOANG JD, Vaseghi M

SELECTED ABSTRACTS

1. **Ventricular Electrophysiological Effects of Vagal Nerve Stimulation in Humans With and Without Structural Heart Disease** (*Accepted to Experimental Biology, April 2022*)
HOANG JD, Lokhandwala ZA, Buckley U, Bradfield JS, Krokhaleva Y, Khakpour H, Ajijola OA, Boyle NG, Shivkumar K, Vaseghi M

2. **Epidural Sympathetic Afferent Blockade by Resiniferatoxin Reverses Vagal Dysfunction Following Myocardial Infarction** (*AHA Scientific Sessions, Nov 2021. Circulation. 2021 Nov 16;144(Suppl_1):A10597;* abstract)
HOANG JD, Swid MA, Kang K, Lokhandwala ZA, Chan CA, Jani NR, Vaseghi M

3. **Autonomic and Electrophysiological Effects of Thoracic Epidural Anesthesia on Infarcted Porcine Hearts** (*Heart Rhythm Scientific Sessions, 2020;* abstract)
HOANG JD, Swid MA, Kang K, Chan CA, Vaseghi M

Chapter 1

Pro-arrhythmic Effects of Sympathetic Activation Are Mitigated by Vagal Nerve Stimulation in Infarcted Hearts

Jonathan D Hoang, Kentaro Yamakawa, Pradeep S Rajendran, Christopher A Chan, Daigo Yagishita, Keijiro Nakamura, Robert L Lux, Marmar Vaseghi

Hoang JD, Yamakawa K, Rajendran PS, Chan CA, Yagishita D, Nakamura K, Lux RL, Vaseghi M. Proarrhythmic Effects of Sympathetic Activation Are Mitigated by Vagal Nerve Stimulation in Infarcted Hearts. JACC Clin Electrophysiol. 2022;8(4):513-25. Epub 2022/04/23. doi: 10.1016/j.jacep.2022.01.018.

ABSTRACT

Background: Sympathoexcitation increases risk of ventricular tachyarrhythmias (VT). Vagal nerve stimulation (VNS) has been anti-arrhythmic in the setting of ischemia-driven arrhythmias, but it is unclear if it can overcome the electrophysiological effects of sympathoexcitation in the setting of chronic myocardial infarction (MI). The goal of this study was to evaluate whether intermittent VNS reduces electrical heterogeneities and arrhythmia inducibility during sympathoexcitation.

Methods: In Yorkshire pigs after chronic MI, a sternotomy was performed, a 56-electrode sock was placed over the ventricles (*n*=17), and a basket catheter was positioned in the left ventricle (*n*=6). Continuous unipolar electrograms from sock and basket arrays were obtained to analyze activation recovery interval (ARI), a surrogate of action potential duration. Bipolar voltage mapping was performed to define scar, border zone, or viable myocardium. Hemodynamic and electrical parameters, and VT inducibility were evaluated during sympathoexcitation with bilateral stellate ganglia stimulation (BSS) and during combined BSS with intermittent VNS.

Results: During BSS, global epicardial ARIs shortened from 384±59 to 297±63 ms and endocardial ARIs from 359±36 to 318±40 ms. Dispersion in ARIs increased in all regions, with the greatest increase observed in scar and border zone regions. VNS mitigated the effects of BSS on border zone ARIs (from -18.3±6.3% to -2.1±14.7%) and ARI dispersion (from 104 ms^2 [1, 1108] to -108 ms^2 [-588, 30]). VNS reduced VT inducibility during sympathoexcitation (from 75% to 40%, $p<0.05$).

Conclusions: After chronic myocardial infarction, VNS overcomes the detrimental effects of sympathoexcitation by reducing electrophysiological heterogeneities exacerbated by sympathetic stimulation, decreasing VT inducibility.

INTRODUCTION

Sympathetic activation due to pathological neural remodeling resulting from heart disease is known to contribute to ventricular arrhythmias.[1,2] Sympathoexcitation exacerbates existing electrophysiological heterogeneities in the myocardium and increases the occurrence of early and delayed after depolarizations.[3-5] *In-vivo* in healthy hearts, vagal nerve stimulation (VNS) has been shown to increase ventricular action potential duration and ventricular fibrillation (VF) threshold, as well as reduce the burden of ventricular arrhythmias if initiated prior to or at the time of ischemia.[6-9] However, in chronically infarcted animals, ventricular tachyarrhythmias (VT) often occur in the setting of stress and sympathoexcitation without ischemia. It is unclear if in chronically remodeled and diseased hearts, VNS can overcome the detrimental electrophysiological effects of sympathoexcitation by reducing electrophysiological heterogeneities exacerbated by sympathetic stimulation and decrease VT inducibility.

Early *in-vivo* studies by Levy *et al*. suggested that in healthy canine hearts, vagal nerve stimulation may blunt myocardial norepinephrine levels. In addition, the parasympathetic nervous system is also regulated by the sympathetic nervous system. Cardiac sympathetic activation causes release of norepinephrine, which can bind to parasympathetic neurons and inhibit release of acetylcholine.[10] Thus, while acetylcholine levels may be preserved throughout the heart following infarction, they may be functionally suppressed.[11] The ventricular electrophysiological effects of vagal nerve stimulation during sympathoexcitation in structurally diseased hearts is thereby unclear. It is possible, that even during states of elevated sympathetic tone, such as electrical storm, implementation of vagal nerve stimulation in diseased hearts may reduce arrhythmias. In this study, we hypothesized that vagal nerve stimulation can be anti-arrhythmic even during sympathetic activation and reduce inducibility of VT that occurs with sympathetic stimulation. We tested this hypothesis in a chronic large animal porcine infarct model using detailed electrophysiological mapping.

METHODS

Ethical approval

Seventeen Yorkshire pigs (*Sus scrofa*; S&S Farms) weighing 48–56 kg were used for this study. Care of animals conformed to the National Institutes of Health Guide for the Care and Use of Laboratory Animals. The study protocol was approved by the University of California, Los Angeles Institutional Animal Care and Use Committee.

Creation of myocardial infarcts

Percutaneous MI in the region of left anterior descending (LAD) coronary artery was created in 17 pigs (30–35 kg) as previously described under general anesthesia (isoflurane, 1-2%).[11,12] Briefly, an AL2 guide catheter (Boston Scientific, Marlborough, MA) was advanced from the femoral artery to the left main coronary artery. A percutaneous transluminal angioplasty (PTA) balloon catheter (Abbott, Chicago, IL) was advanced over a coronary guidewire into the LAD and positioned after the take-off of the first diagonal branch (Figure 1b). The balloon was inflated, and 3–5 mL of polystyrene microspheres (Polybead® 90.0µm, Polysciences, PA) followed by 5 mL normal saline were injected through the lumen of the catheter. The balloon was then deflated and removed. MI was confirmed by the presence of ST-elevation or T-wave inversion on ECG and coronary angiography showing a lack of flow in the artery (Figure 1c-d). After the procedure, ECG and blood pressure were monitored for 20 min prior to extubation. Immediate external defibrillation was performed if the animal developed VT or VF. After extubation, animals were monitored until they could ambulate.

Surgical preparation

Six to eight weeks post-MI, animals were sedated, intubated, and placed under anesthesia with isoflurane (1–2% INH). After completion of the surgical procedures, including sternotomy, anesthesia was transitioned to α-chloralose (Sigma-Aldrich; 50 mg/kg initial bolus, then 20–35 mg/kg/hr IV). Depth of anesthesia was adjusted based on hemodynamic indices, corneal reflex, and jaw tone. Arterial blood gases were monitored throughout the experiments; ventilation was

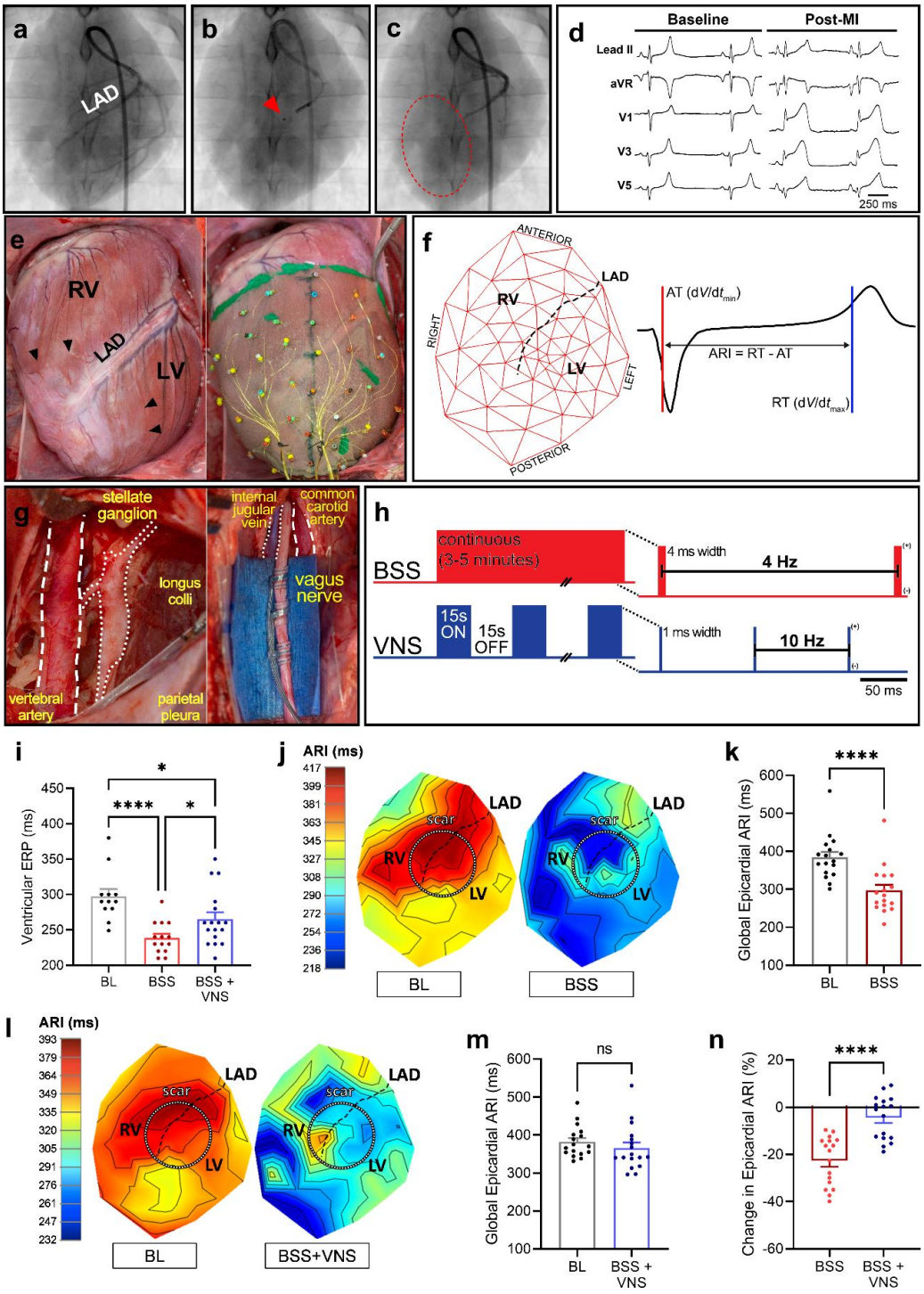

Figure 1-1. ***Ventricular epicardial effects of sympathetic stimulation and its attenuation by VNS following MI.*** (**a-b**) Percutaneous creation of MI in region of the LAD coronary artery via injection of microspheres through a transluminal angioplasty catheter (red arrowhead indicates tip of catheter). (**c-d**) Following injection of microspheres, lack of flow is observed in the distal portion of the LAD (red circle), accompanied by ST-segment elevation. (**e**) Six to eight weeks after MI, prominent scarring of the anterior RV and LV is observed along with regions of patchy sc6ar (black arrowheads) and a 56-electrode sock is

placed around the ventricles to record unipolar electrograms. (**f**) Electrograms are then mapped onto a 2-D polar map for the assessment of regional electrophysiological differences. The difference in time between activation and recovery time (AT and RT, respectively) is defined as ARI and used a surrogate of local action potential duration at each electrode/site. (**g-h**) The stellate ganglia and cervical vagus nerves are isolated for bipolar stimulation. Stimulation of the bilateral stellate ganglia are performed at 4 Hz for 3-5 minutes with and without concomitant 10 Hz VNS (50% duty cycle). (**i**) ERP from the RV endocardium was significantly shortened by BSS. Concomitant bilateral VNS reduced effects on ERP. (**j-k**) Representative polar maps at baseline (BL) and during BSS indicates a shortening of ARIs in infarct and remote regions of the RV and LV. Accordingly, a significant shortening of global epicardial ARIs across animals is observed. **(l-m)** Representative polar map at BL and during BSS+VNS suggests attenuation of BSS-induced ARI shortening. **(n)** Changes in epicardial ARIs from baseline (pre-stimulation) with BSS were significantly attenuated by concomitant VNS. BSS=bilateral stellate stimulation, VNS=bilateral vagus nerve stimulation, ERP=effective refractory period. Data are shown as mean ± SEM (n = 17). *p<0.05, ****p<0.0001, ns=not significant.

adjusted, or sodium bicarbonate was administered to maintain normal pH. The CardioLab System (GE Healthcare) was used to record continuous 12-lead electrocardiograms. Ventral precordial leads were placed posteriorly given sternotomy. The femoral and carotid arteries were cannulated to measure blood pressure continuously and obtain access to the left ventricle (LV) for basket catheter placement, respectively. Sheaths were placed in the femoral veins for delivery of medications and saline. Fentanyl boluses (20–30 mcg/kg) were used during sternotomy to reduce discomfort. Sodium pentobarbital (Med-Pharmex Inc.; 100 mg/kg IV) followed by saturated KCl (Sigma-Aldrich; 1–2 mg/kg IV) was used for euthanasia.

Stellate ganglia and vagal nerve stimulations

For bilateral stellate ganglia stimulation (BSS), the stellate ganglia were isolated behind the parietal pleura (Figure 1g), as previously described and stimulated by bipolar needle electrodes using a Grass stimulator (Grass Technologies Model S88).[3,12] Stimulation current was set at an amplitude that led to a greater than 10% increase in heart rate (HR) and/or systolic blood pressure (SBP) for each ganglion.[3]

For bilateral VNS, after neck cutdown, the vagi were isolated in the carotid sheaths. The vagus was carefully dissected away from the sympathetic chain and insulated from the

surrounding tissue. Bipolar cuff electrodes were placed around each vagi (Figure 1g). Threshold current for each vagus was defined as the amplitude that led to a 10% decrease in heart rate (10 Hz, 1 ms pulse-width).[7] Intermittent bilateral VNS (15 sec ON, 15 sec OFF) was performed at 1.2 times this current during BSS.

BSS was performed continuously at threshold current (4 Hz and 4 ms pulse-width) for both electrophysiological/hemodynamic recordings and during VT inducibility testing (described below). Similarly, BSS was performed continuously with concomitant intermittent VNS to determine the effects of VNS on mitigating the electrophysiological effects of BSS.

Electrophysiological study and mapping

Epicardial unipolar electrograms were continuously recorded using a 56-electrode sock placed over the ventricles (n = 17, Figure 1), *in-vivo* (Cardio Lab, GE Healthcare). In 6 animals, the 56-electrode sock was attached to customized multielectrode recording system (University of Utah, Salt Lake City, Utah) and a Constellation basket catheter (Boston Scientific, Marlborough, MA) was placed via a retrograde aortic approach from the left carotid artery into the LV, under fluoroscopic and ultrasound guidance (Figure 2) to record endocardial unipolar electrograms. Bipolar voltage electroanatomic mapping was performed, and location of each sock electrode overlying scar (defined as bipolar voltage < 0.5 mV), border zone (defined as bipolar voltage between 0.5 and 1.5 mV), or viable myocardium (defined as bipolar voltage > 1.5 mV) was meticulously measured using a duodecapolar catheter (2-2-2 interelectrode spacing, Abbott Medical, IL) and regional epicardial ARIs (scar, viable, border zone) quantified in 12 of 17 hearts. Very dense scar regions (voltage < 0.05 mV) with little to no definable bipolar recordings were excluded from analysis. Electroanatomic mapping of the heart was performed using the Ensite system (Abbott).

Activation recovery intervals (ARI) were analyzed from unipolar electrograms of each electrode using iScaldyn software (University of Utah, Salt Lake City, UT).[13,14] Activation time was defined from the origin to the minimum dV/dt of the activation wavefront of the unipolar

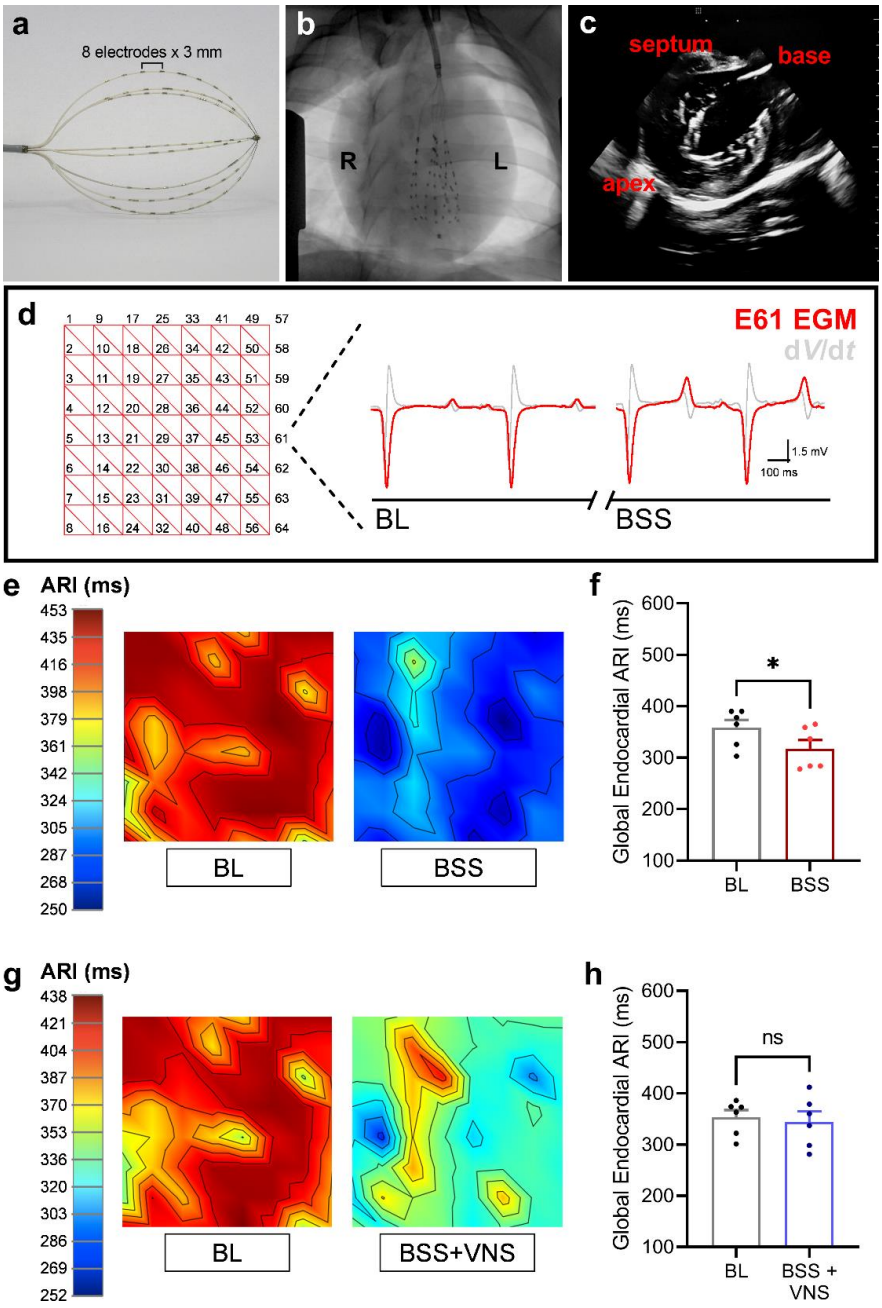

Figure 1-2. ***Ventricular endocardial effects of sympathetic stimulation and attenuation by VNS.*** (**a-c**) A 64-electrode Constellation catheter was advanced into the LV for assessment of local endocardial unipolar electrograms. Sufficient contact of the basket catheter with the endocardium was confirmed by echocardiography. (**d**) Local unipolar electrograms from the endocardium were mapped onto a 2-D polar map. (**e**) A representative polar map of ARIs at baseline and during BSS indicates significant shortening of endocardial ARIs. (**f**) There was no significant ARI change during BSS+VNS relative to baseline. (**g-h**) BSS-induced shortening in endocardial ARI was significantly blunted by concomitant bilateral VNS. BSS=bilateral stellate stimulation, VNS=bilateral vagus nerve stimulation. Data are shown as mean ± SEM (n = 6). *p<0.05.

electrogram and recovery time was defined as the start of activation to the maximum d*V*/d*t* of repolarization wavefront. ARI was calculated by subtracting activation time from repolarization time (Figure 1). ARI has been previously validated as a faithful correlate of local action potential duration.[13-16]

ARIs and hemodynamic variables including heart rate and blood pressure were analyzed before and during nerve stimulations (before and during BSS and before and during BSS+VNS). A minimum of 30 minutes was allowed between stimulations and the order of stimulations was randomized. After 45 seconds of BSS or BSS+VNS, during which electrical and hemodynamic data were obtained, effective refractory period was evaluated and VT inducibility testing performed as described below. The duration of nerve stimulations ranged between 3 to 5 minutes depending on the number extra-stimuli required to induce VT.

Effective refractory period measurement and VT inducibility testing

Effective refractory period (ERP) was measured by placement of a quadripolar catheter in the right ventricular (RV) apex. Pacing was performed at 3-5 mA and 2 ms pulse width, and capture confirmed by ventricular morphology on the surface ECG. A drive cycle length 10-20% faster than the baseline heart rate was used and a single extra-stimulus placed and decremented by 10 ms interval to measure ERP at baseline (prior to any nerve stimulation), during BSS, and during concomitant BSS and VNS from the same RV apical position.

VT inducibility was also assessed during BSS alone and during concomitant BSS and VNS by programmed ventricular stimulation (Micropace, New South Wales, Australia) with the same pacing parameters. Inducibility was determined at two different drive cycle lengths with up to three extra-stimuli (10 ms decrement, down to 200 ms or ERP), from two different sites (RV endocardium and LV anterior epicardium). If VT was induced from one specific site, this same site was used to induce VT during subsequent stimulations. If sustained VT or VF was inducible at baseline, a minimum wait period of 30 minutes was allowed after cardioversion before repeat stimulation/inducibility testing. Both VT inducibility (defined as occurrence of sustained VT or VF

requiring anti-tachycardia pacing or defibrillation) or non-sustained VT (defined as occurrence of greater than 3 premature ventricular contractions) was quantified during each nerve stimulation.

Statistical analysis

Data are reported as means ± standard deviation (SD) for normally-distributed data, unless stated otherwise. Non-normal data are reported and shown as median [1st quartile, 3rd quartile]. Normality of data distributions was assessed using the Shapiro-Wilk test. Global ventricular ARIs were calculated as the mean ARI across all electrodes. Regional dispersion in ARI was defined as variance across electrodes from a specific region (i.e., scar, border zone, or viable regions). Paired Student's *t*-test was performed to compare responses between BSS and BSS+VNS in each animal. Paired Wilcoxon signed-rank test was performed to compare changes in regional dispersion between BSS and BSS+VNS. Changes in regional ARIs and dispersion in ARI from baseline were compared using one-way repeated measure analysis of variance and the Friedman test, respectively, with the false discovery rate corrected by the Benjamini-Hochberg procedure. Percentage change in ARI or change in dispersion in ARI in each region with nerve stimulation were compared by paired Student's *t*-test and the Friedman test, respectively. Inducibility for VT during each stimulation were compared by the exact binomial test. A p value ≤ 0.05 was considered statistically significant. All statistical analyses were performed with GraphPad Prism software v8.

RESULTS

Hemodynamic effects of BSS and BSS combined with VNS

In chronically infarcted pigs ($n = 17$), BSS significantly increased all hemodynamic indices, including heart rate, systolic blood pressure, diastolic blood pressure and mean arterial pressure (Table 1). On the other hand, concomitant VNS with BSS mitigated the increases in all hemodynamic parameters.

	BL	BSS	%	BL	BSS + VNS	%
Heart Rate (bpm)	79.6 ± 13.1	104.7 ± 21.2***	32.0 ± 20.1	80.3 ± 9.0	77.4 ± 14.5	-3.2 ± 17.2ǂ
Systolic Pressure (mmHg)	113.0 ± 18.0	154.6 ± 39.0***	36.1 ± 31.8	110.7 ± 18.7	131.1 ± 34.5***	17.1 ± 17.9ł
Diastolic Pressure (mmHg)	73.5 ± 18.8	106.1 ± 27.4***	54.8 ± 73.3	74.4 ± 18.3	84.5 ± 28.9	11.4 ± 27.7ł
Mean Arterial Pressure (mmHg)	87.1 ± 18.0	122.6 ± 20.3***	44.1 ± 24.2	86.5 ± 17.5	100.3 ± 29.9*	13.0 ± 20.9ǂ

Table 1-1. ***Hemodynamic responses to sympathetic stimulation alone and concurrent vagal nerve stimulation with sympathetic stimulation.*** Values are shown as mean±SD. BL=baseline, BSS=bilateral stellate ganglia stimulation, VNS=bilateral vagus nerve stimulation. *p<0.05, ** p<0.01, ***p<0.001 *vs* BL. ł p<0.05, ǂ p<0.001 *vs* BSS alone. Red values denote a significant increase and blue values denote a significant decrease.

Global ventricular electrophysiological effects

BSS shortened ventricular ERP from 297±36 ms at baseline to 239±22 ms (p < 0.001). During combined stimulation, ventricular ERP only decreased to 265±39 ms (p < 0.05), Figure 1. However, ERP was still shortened as compared to baseline (p < 0.05).

In a similar fashion as ERP, BSS shortened ventricular epicardial global ARIs (defined as the mean ARI across all 56 electrodes) from 384±59 ms at baseline to 297±63 ms (n = 17, p < 0.001, Figure 1). ARI did not significantly change compared to pre-stimulation during BSS+VNS (382±41 ms at baseline to 366±60 ms during BSS+VNS, p = 0.1, Figure 1). Therefore, VNS during BSS markedly blunted sympathetically-induced ARI shortening (-22.7±10.4% during BSS *vs* -4.5±9.2% during BSS+VNS, p < 0.001, Figure 1). Global epicardial dispersion in ventricular ARIs (variance across all electrodes) significantly increased during BSS from 648 ms^2 [509, 826 ms^2] at baseline to 992 ms^2 [594, 1400 ms^2] (p < 0.01). VNS added to BSS significantly mitigated these effects of sympathoexcitation on dispersion (baseline pre-stimulation global dispersion in ARI: 609 ms^2 [493, 747 ms^2], BSS+VNS: 743 ms^2 [592, 1000 ms^2], p = 0.1).

The endocardium followed the same trend as the epicardium, and during BSS, ventricular endocardial ARIs decreased from 359±36 ms at baseline to 318±40 ms during stimulation (n = 6,

$p < 0.05$, Figure 2). Conversely, BSS+VNS did not elicit any significant shortening of global ARIs, (Figure 2).

Regional differences in ventricular electrophysiological effects

The genesis of ventricular arrhythmias in ischemic cardiomyopathies is known to be initiated and propagated within the scar and border zone regions.[1] While this is in part due to altered excitability of the border zone combined with the anatomic substrate of these regions allowing for reentrant circuits, the distinct pattern of sympathetic denervation and hyperinnervation in these regions augments these heterogeneities,[17,18] and the complex interaction of the sympathetic and parasympathetic nervous systems in these discrete functional domains is yet to be identified. To this end, the scar, border zone, and viable regions of the myocardium underlying the epicardial sock arrays were identified by epicardial voltage mapping and validated by electroanatomic mapping (Figure 3).

Detailed analysis of regional changes ($n = 12$) revealed that the effects of BSS on global epicardial ARI were paralleled by significant shortening in scar, border zone, and viable regions of the epicardium (Figure 3). Notably, benefits of VNS in blunting the effects of BSS were not restricted to any particular region; scar, border zone and viable regions alike showed a blunting of sympathetic effects during VNS (Figure 3). Despite a sustained background of BSS, ARI shortening was significantly less during BSS+VNS than BSS alone in the scar (-13.6±5.3% with BSS *vs* -4.9±12.4% with BSS+VNS; $p < 0.05$), border zone (-18.3±6.3% with BSS *vs* -2.1±14.7% with BSS+VNS; $p < 0.01$), and viable regions (-14.3±6.2% with BSS *vs* -1.0±10.2% with BSS+VNS; $p < 0.01$, Figure 3).

BSS also increased local electrophysiological heterogeneities as reflected by variances in regional ARIs; these changes in dispersion were also stabilized by VNS. The regional dispersion of scar was significantly increased from 72 ms^2 [12, 177 ms^2] at baseline to 232 ms^2 [23, 1276 ms^2] during BSS ($p < 0.01$, Figure 3) as was dispersion in border zone (194 ms^2 [66, 399 ms^2] at baseline *vs* 355 ms^2 [100, 1457 ms^2] during BSS; $p < 0.05$) and viable regions (124

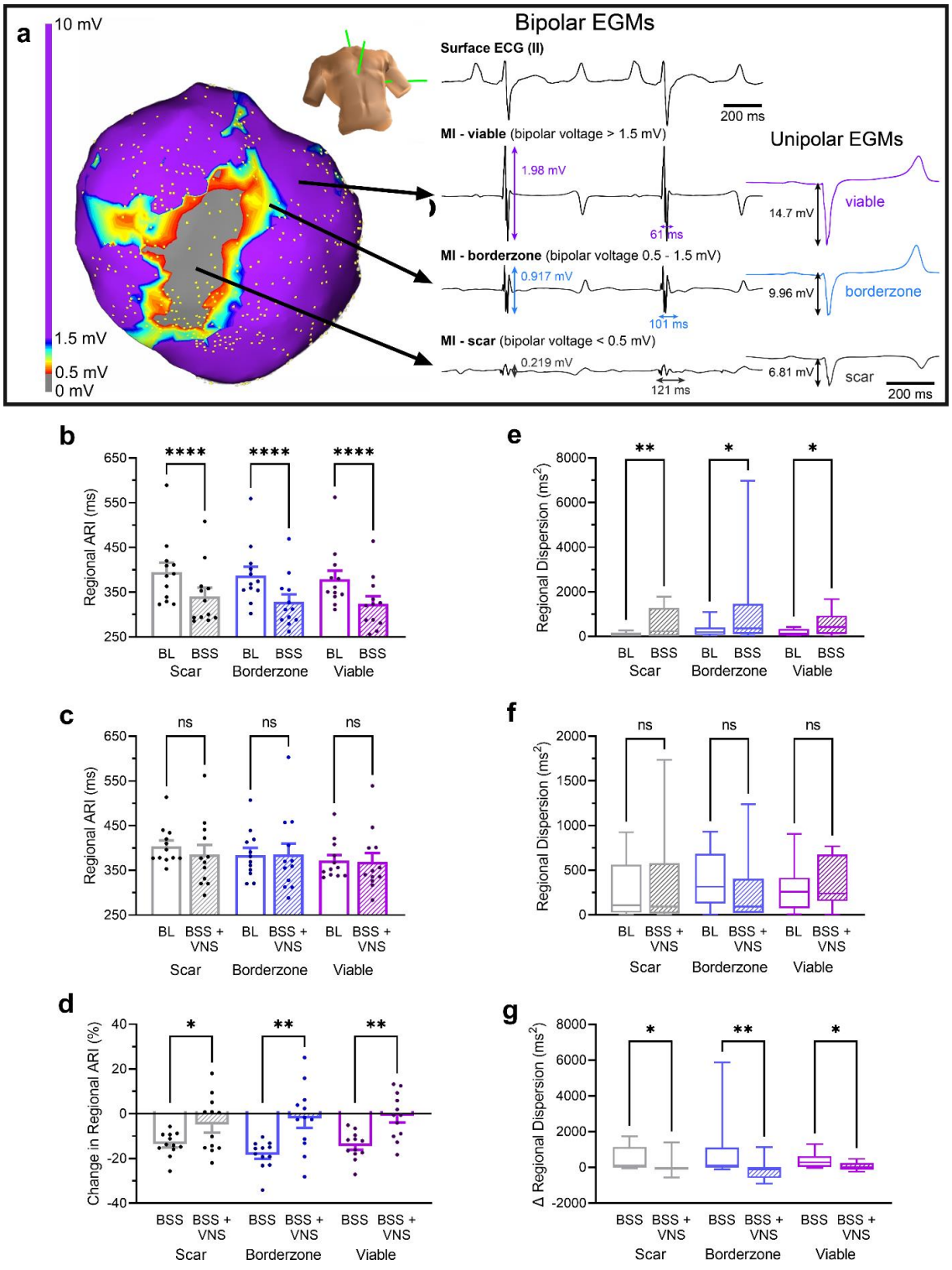

Figure 1-3. ***VNS mitigates ventricular ARI shortening and heterogeneities induced by sympathetic activation.*** (**a**) Representative electroanatomic map confirms the presence of a dense antero-apical scar encircled by broad regions of heterogenous electrical border zone and remote, healthy myocardium. Based on the bipolar voltage at each site, electrodes were designated as viable (> 1.5 mV), border zone (0.5 – 1.5 mV) or scar (< 0.5 mV) with sample electrograms shown. (**b**) BSS induced significant shortening of ARIs in

all regions (**c-d**) and these effects were significantly attenuated by concomitant VNS. (**e**) Importantly, BSS led to significant increases in regional dispersion, a measure of local heterogeneity in ARIs. (**f-g**) Increases in regional dispersion with BSS were attenuated by concomitant bilateral VNS. BSS=bilateral stellate stimulation, VNS=bilateral vagus nerve stimulation. Regional ARI data are shown as mean ± SEM and regional dispersion as median and interquartile range (n = 12). *p<0.05, **p<0.01, ****p<0.0001, ns=not significant.

ms^2 [30, 337 ms^2] at baseline *vs* 432 ms^2 [107, 927 ms^2] during BSS; $p < 0.05$). On the other hand, VNS during BSS significantly reduced dispersion in all regions, Figure 3, and mitigated BSS-induced increases in local dispersion of viable (Δ regional dispersion: 297 ms^2 [22, 639 ms^2] with BSS *vs* 2 ms^2 [-111, 248 ms^2] with BSS+VNS; $p < 0.05$) and scar regions (Δ regional dispersion: 110 ms^2 [5, 1146 ms^2] with BSS *vs* -18 ms^2 [-111, 6 ms^2] with BSS+VNS; $p < 0.05$). Notably, in the border zone regions, effects of VNS during BSS reduced dispersion to levels even below baseline (pre-stimulation) values (Δ regional dispersion: 104 ms^2 [1, 1108 ms^2] with BSS *vs* -108 ms^2 [-588, 30 ms^2] with BSS+VNS; $p < 0.01$, Figure 3).

Effects of concomitant stimulation on susceptibility for ventricular arrhythmias

During BSS alone, 13 of 17 animals (>75%; Figure 4d) were inducible for any sustained or non-sustained VT with up to triple extra-stimuli (Figure 4). NSVT only was observed in 3 of these 13 animals. Animals with sustained VT exhibited repeated bouts of NSVT at less aggressive programmed stimulation before being inducible for sustained VT, which required cardioversion, with one animal experiencing spontaneous degeneration of sinus rhythm to VT/VF during BSS alone (i.e., without any ventricular pacing having been performed), Figure 4b.

However, VT inducibility was significantly reduced in the setting of BSS+VNS, with only 7 of 17 animals (~40%) still inducible for VT/VF. In addition, a decrease in episodes of NSVT observed during BSS were observed during combined BSS+VNS (Figure 4).

DISCUSSION

Major findings

The major findings of this study are as follows:

1) Despite a high background of sympathetic activation, vagus nerve stimulation is capable of mitigating the effects of bilateral stellate ganglia stimulation on global and regional ventricular ARI shortening.
2) Vagal nerve stimulation can reduce electrophysiological heterogeneities in regional ARIs across viable, border zone, and scar regions, as reflected by dispersion in ARI.
3) Vagal nerve stimulation reduces VT inducibility during sympathoexcitation.

Neuromodulatory approaches aimed at augmenting the parasympathetic nervous system (e.g., vagal nerve stimulation) are currently under intense investigation for the treatment of cardiovascular disease.[19] Previous studies have suggested that vagal nerve stimulation may reduce the burden of ventricular arrhythmias through the stabilization of existing heterogeneities in peri-infarct border zone action potential duration.[11] However, it is yet unknown if and how these interventions may act in the context of elevated sympathetic tone, a known trigger for ventricular arrhythmias where elevated norepinephrine levels, for example, may reduce acetylcholine release.[1]

This is the first study to evaluate detailed electrophysiological effects of concomitant stimulation of the stellate ganglia (sympathetic nervous system) and vagal nerves (parasympathetic nervous system). In this study, a porcine model of chronic myocardial infarction was used as it closely recapitulates both electrophysiological and autonomic changes seen in humans with structural heart disease.[20] While previous studies have suggested that vagal nerve stimulation may be antiarrhythmic in the setting of structural heart disease,[11] it remained unclear whether these effects may persist and be sufficient to combat the effects of sympathoexcitation.

Pro-arrhythmic mechanisms of sympathoexcitation

Stimulation of the bilateral stellate ganglia evoked significant increases in ventricular excitability, causing shortening of ERP as well as epicardial and endocardial action potential duration as reflected by ARIs. Importantly, electrophysiological heterogeneity of scar and border zone regions of the myocardium were markedly increased by sympathetic stimulation. Notably, sympathetic

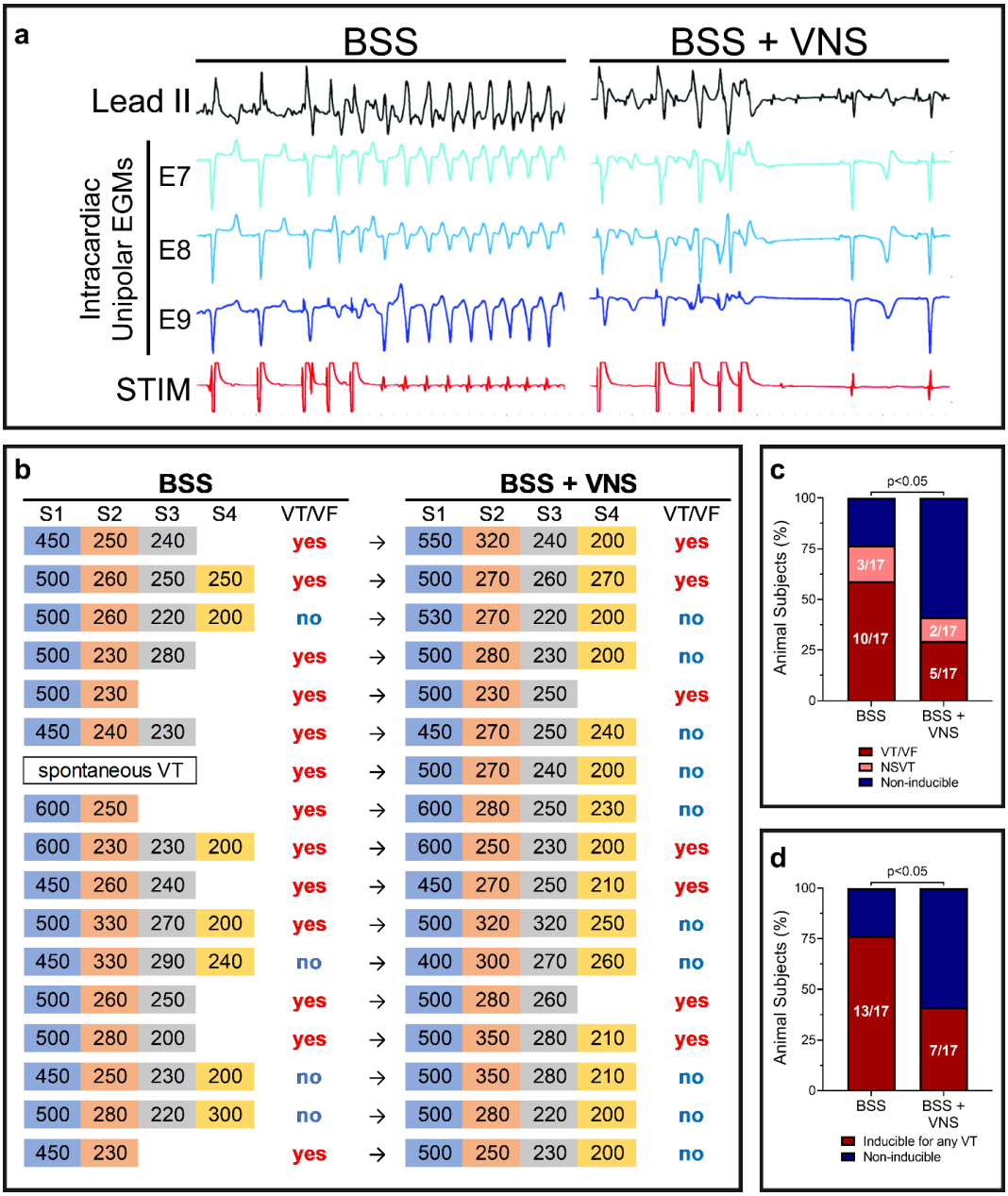

Figure 1-4. ***VNS reduces ventricular arrhythmias despite sympathoexcitation.*** (**a**) Representative examples of programmed electrical stimulation during BSS alone or with concomitant VNS. (**b**) Pacing protocols used to induce VT/VF in each animal are shown. (**c-d**) During BSS alone, 13 of 17 animals were inducible. Concomitant VNS caused a significant reduction in VT inducibility with only 7 animals remaining inducible for VT. One animal had spontaneous VT during BSS without any extra-stimulus pacing. BSS = bilateral stellate stimulation, VNS = bilateral vagus nerve stimulation, NSVT = non-sustained VT.

stimulation alone was sufficient to induce premature ventricular contractions, non-sustained ventricular tachycardia (NSVT) and ventricular tachyarrhythmias (VT/VF) in some animals.

Cardioprotective effects of vagal nerve stimulation

VNS has been shown to decrease the incidence of sudden cardiac death.[19] In addition in normal and infarcted porcine hearts, intermittent moderate levels of vagal nerve stimulation was shown to increase action potential duration.[7,11] The mechanism by which VNS increases action potential duration is an ongoing area of investigation and may occur through direct release and action of acetylcholine on muscarinic receptors, via inhibition of norepinephrine and neuropeptide Y release at the nerve-myocyte interface, or via interactions at the stellate ganglia.[21-23] In addition, chronic myocardial infarction and heart failure have been shown to be associated with significant neural remodeling in the intrinsic cardiac, vagal (nodose), and stellate ganglia.[24-26] Interestingly, while chronic VNS has been shown to decrease stellate ganglion nerve activity,[23,27] other studies have suggested that acute VNS may paradoxically increase stellate ganglion nerve activity, potentially through anastomosing sympathetic fibers and/or afferent fiber activation, responses that may be frequency dependent.[28-30] In this study, the frequency of stimulation was similar to where cardiomotor vagal efferent fibers were shown to be engaged, close to the neural fulcrum, in a canine model.[29] The same frequency of stimulation was used in the ANTHEM-HF study, which showed improvement in echocardiographic and New York Heart Association class parameters in patients with heart failure,[31,32] and was also previously demonstrated to increase action potential duration in normal porcine hearts.[7] However, whether the beneficial electrophysiological effects of VNS would persist during states of sympathoexcitation in diseased hearts, in whom pre-existing baseline electrophysiological heterogeneities are exacerbated by sympathetic activation, remained unknown. The present study shows that VNS caused nearly a 70 ms prolongation of global ARIs (80% reduction in effects of BSS) during sympathoexcitation, with even more prominent effects observed in border zone regions (90% reduction in effects of BSS), areas that are specifically implicated in ventricular arrhythmogenesis. Moreover, VNS stabilized the cardiac electrophysiological heterogeneity within the border zone regions despite concomitant sympathetic stimulation. Border zone regions are known to serve as pro-arrhythmic

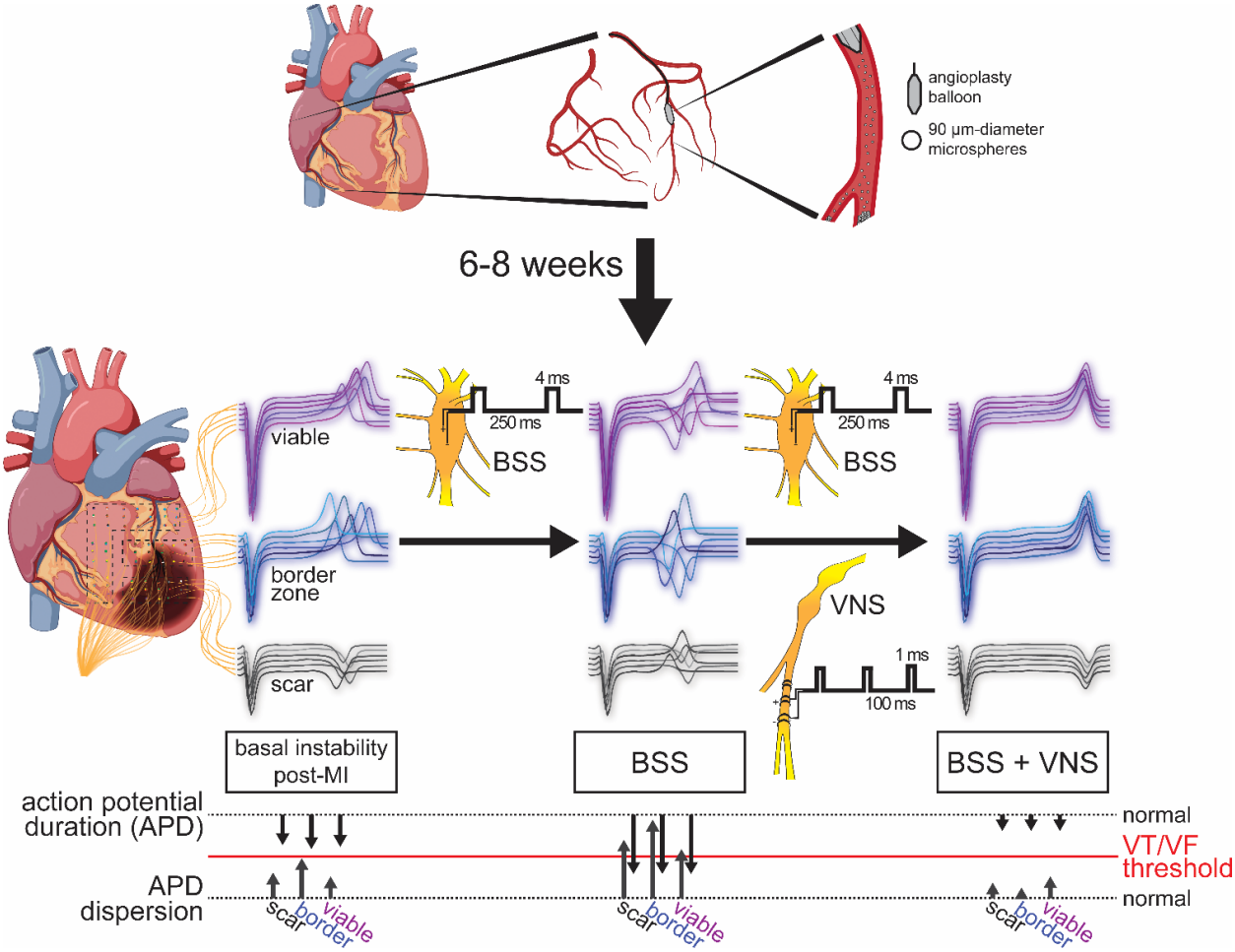

Figure 1-5. ***Summary.*** Sympathoexcitation exacerbates baseline electrophysiological heterogeneities in chronically infarcted hearts, predisposing to VT/VF. These heterogeneities are reduced back to baseline, and even further mitigated below baseline in border zone regions, by intermittent vagal nerve stimulation. Vagal nerves stimulation reduces VT inducibility during states of elevated sympathetic tone.

regions responsible for both triggers and maintenance of ventricular arrhythmias. This is potentially related to both their structural heterogeneity consisting of areas of fibrosis intermixed with viable myocardium,[33-35] but also due to neural remodeling which leads to sympathetic nerve-sprouting after MI in this region.[17,36,37] This underlying structural and neural heterogeneity can further contribute to occurrence of arrhythmias, particularly in the setting of sympathoexcitation. Therefore, the potential beneficial effects of VNS in stabilizing these particular regions have significant electrophysiological implications.

Clinical significance

In this study, inducibility of ventricular arrhythmias was reduced by nearly 50% despite sustained sympathetic activation. These results, taken together with the global and regional electrical data suggest that vagal nerve stimulation can increase electrical stability, even during states of high sympathetic tone (Figure 5, Central Illustration), and may present a promising therapeutic option for treatment of ventricular tachyarrhythmias, even if acutely.

Limitations

General anesthesia with isoflurane is known to blunt autonomic responses. To limit this effect, anesthesia was switched to α-chloralose to reduce anesthetic effects on autonomic responses.[29] In addition, our results reflect the effects of acute sympathetic and vagal nerve stimulation. Chronic effects of intermittent vagal nerve stimulation during states of sympathoexcitation require further study.

Moreover, while scar and border zones are known to play important roles in harboring circuits that cause VT in ischemic heart disease, transmural gradients between these sites may compound myocardial heterogeneities.[38] In this study, however, accurate pairing of electrodes was not possible. Therefore, the role of transmural gradients in exacerbating arrhythmias could not be assessed.

PERSPECTIVES

Competency in medical knowledge

While beta-blockers remain a part of standard anti-arrhythmic therapy for patients with ventricular arrhythmias, sympathoexcitation may amplify arrhythmogenicity through non-adrenergic pathways, leaving patients refractory to traditional therapies. Detailed electrophysiological mapping in a chronically infarcted porcine model in this study demonstrated that modest levels of vagal nerve stimulation mitigated sympathetically-driven shortening of action

potential duration and exacerbation of electrical heterogeneity, particularly in border zone and scar regions, significantly reducing VT during sympathoexcitation.

Translational outlook

This study demonstrates the acute beneficial effects of vagal nerve stimulation in mitigating the pro-arrhythmic effects of sympathoexcitation in a large animal model of chronic myocardial infarction. These findings add to the growing body of literature on the safety and efficacy of vagal nerve stimulation for treating heart failure. Further studies are needed to determine whether these effects are also observed in patients with ventricular arrhythmias, and whether vagal nerve stimulation can reduce burden of ventricular arrhythmias in the setting of ischemic cardiomyopathy.

ACKNOWLEDGEMENTS

We would like to thank Dr. Jeffrey Ardell and Dr. Kalyanam Shivkumar for their guidance. We would like to thank Drs. Tadanobu Irie and David Hamon with their assistance for some of the experiments.

FUNDING SUPPORT AND AUTHOR DISCLOSURES

This study was funded by National Institutes of Health R01 HL148190 (to Dr Vaseghi). Dr Vaseghi has shares in NeuCures Inc; and has patents on neuromodulation at University of California, Los Angeles. All other authors have reported that they have no relationships relevant to the contents of this paper to disclose.

REFERENCES

1 Vaseghi, M. & Shivkumar, K. The role of the autonomic nervous system in sudden cardiac death. Prog Cardiovasc Dis 50, 404-419, doi:10.1016/j.pcad.2008.01.003 (2008).

2 Zipes, D. P. & Rubart, M. Neural modulation of cardiac arrhythmias and sudden cardiac death. Heart Rhythm 3, 108-113 (2006).

3 Yagishita, D. et al. Sympathetic nerve stimulation, not circulating norepinephrine, modulates T-peak to T-end interval by increasing global dispersion of repolarization. Circulation. Arrhythmia and electrophysiology 8, 174-185, doi:10.1161/CIRCEP.114.002195 (2015).

4 Priori, S. G., Mantica, M. & Schwartz, P. J. Delayed afterdepolarizations elicited in vivo by left stellate ganglion stimulation. Circulation 78, 178-185 (1988).

5 Ben-David, J. & Zipes, D. P. Differential response to right and left ansae subclaviae stimulation of early afterdepolarizations and ventricular tachycardia induced by cesium in dogs. Circulation 78, 1241-1250 (1988).

6 Yamakawa, K. et al. Vagal nerve stimulation activates vagal afferent fibers that reduce cardiac efferent parasympathetic effects. American journal of physiology. Heart and circulatory physiology 309, H1579-1590, doi:10.1152/ajpheart.00558.2015 (2015).

7 Yamakawa, K. et al. Electrophysiological effects of right and left vagal nerve stimulation on the ventricular myocardium. American journal of physiology. Heart and circulatory physiology 307, H722-731, doi:10.1152/ajpheart.00279.2014 (2014).

8 Brack, K. E., Coote, J. H. & Ng, G. A. Vagus nerve stimulation protects against ventricular fibrillation independent of muscarinic receptor activation. Cardiovascular research 91, 437-446, doi:10.1093/cvr/cvr105 (2011).

9 Myers, R. W. et al. Beneficial Effects of Vagal Stimulation and Bradycardia During Experimental Acute Myocardial Ischemia. Circulation 49, 943-947, doi:10.1161/01.cir.49.5.943 (1974).

10 Xu, Z. J. & Adams, D. J. Alpha-adrenergic modulation of ionic currents in cultured parasympathetic neurons from rat intracardiac ganglia. J Neurophysiol 69, 1060-1070, doi:10.1152/jn.1993.69.4.1060 (1993).

11 Vaseghi, M. et al. Parasympathetic dysfunction and antiarrhythmic effect of vagal nerve stimulation following myocardial infarction. JCI Insight 2, doi:10.1172/jci.insight.86715 (2017).

12 Irie, T. et al. Cardiac sympathetic innervation via middle cervical and stellate ganglia and antiarrhythmic mechanism of bilateral stellectomy. American journal of physiology. Heart and circulatory physiology 312, H392-H405, doi:10.1152/ajpheart.00644.2016 (2017).

13 Haws, C. W. & Lux, R. L. Correlation between in vivo transmembrane action potential durations and activation-recovery intervals from electrograms. Effects of interventions that alter repolarization time. Circulation 81, 281-288 (1990).

14 Millar, C. K., Kralios, F. A. & Lux, R. L. Correlation between refractory periods and activation-recovery intervals from electrograms: effects of rate and adrenergic interventions. Circulation 72, 1372-1379 (1985).

15 Chinushi, M. et al. Correlation between the effective refractory period and activation-recovery interval calculated from the intracardiac unipolar electrogram of humans with and without dl-sotalol treatment. Jpn Circ J 65, 702-706 (2001).

16 Yue, A. M. et al. Determination of human ventricular repolarization by noncontact mapping: validation with monophasic action potential recordings. Circulation 110, 1343-1350, doi:10.1161/01.CIR.0000141734.43393.BE

1) 01.CIR.0000141734.43393.BE [pii] (2004).

17 Cao, J. M. et al. Relationship between regional cardiac hyperinnervation and ventricular arrhythmia. Circulation 101, 1960-1969, doi:10.1161/01.cir.101.16.1960 (2000).

18 Habecker, B. A. et al. Molecular and cellular neurocardiology: development, and cellular and molecular adaptations to heart disease. J Physiol 594, 3853-3875, doi:10.1113/JP271840 (2016).

19 Brack, K. E., Winter, J. & Ng, G. A. Mechanisms underlying the autonomic modulation of ventricular fibrillation initiation--tentative prophylactic properties of vagus nerve stimulation on malignant arrhythmias in heart failure. Heart Fail Rev 18, 389-408, doi:10.1007/s10741-012-9314-2 (2013).

20 Nakahara, S. et al. Characterization of myocardial scars: electrophysiological imaging correlates in a porcine infarct model. Heart Rhythm 8, 1060-1067, doi:10.1016/j.hrthm.2011.02.029 (2011).

21 Herring, N. et al. The cardiac sympathetic co-transmitter galanin reduces acetylcholine release and vagal bradycardia: implications for neural control of cardiac excitability. J Mol Cell Cardiol 52, 667-676, doi:10.1016/j.yjmcc.2011.11.016 (2012).

22 Hoang, J. D. et al. Cardiac sympathetic activation circumvents high-dose beta blocker therapy in part through release of neuropeptide Y. JCI Insight 5, doi:10.1172/jci.insight.135519 (2020).

23 Shen, M. J. et al. Continuous low-level vagus nerve stimulation reduces stellate ganglion nerve activity and paroxysmal atrial tachyarrhythmias in ambulatory canines. Circulation 123, 2204-2212, doi:10.1161/CIRCULATIONAHA.111.018028 (2011).

24 Li, W., Knowlton, D., Van Winkle, D. M. & Habecker, B. A. Infarction alters both the distribution and noradrenergic properties of cardiac sympathetic neurons. American journal of physiology. Heart and circulatory physiology 286, H2229-2236, doi:10.1152/ajpheart.00768.2003 (2004).

25 Rajendran, P. S. et al. Myocardial infarction induces structural and functional remodelling of the intrinsic cardiac nervous system. J Physiol 594, 321-341, doi:10.1113/JP271165 (2016).

26 Salavatian, S. et al. Myocardial Infarction Alters Cardiac Nociception in the Vagal Ganglia: Implications for Parasympathetic Dysfunction in Heart Disease. JCI Insight (2022).

27 Shen, M. J. et al. Low-level vagus nerve stimulation upregulates small conductance calcium-activated potassium channels in the stellate ganglion. Heart Rhythm 10, 910-915, doi:10.1016/j.hrthm.2013.01.029 (2013).

28 Seki, A. et al. Sympathetic nerve fibers in human cervical and thoracic vagus nerves. Heart Rhythm 11, 1411-1417, doi:10.1016/j.hrthm.2014.04.032 (2014).

29 Ardell, J. L. et al. Defining the neural fulcrum for chronic vagus nerve stimulation: implications for integrated cardiac control. J Physiol 595, 6887-6903, doi:10.1113/JP274678 (2017).

30 Rhee, K. S. et al. Cervical vagal nerve stimulation activates the stellate ganglion in ambulatory dogs. Korean Circ J 45, 149-157, doi:10.4070/kcj.2015.45.2.149 (2015).

31 Anand, I. S. et al. Comparison of symptomatic and functional responses to vagus nerve stimulation in ANTHEM-HF, INOVATE-HF, and NECTAR-HF. ESC Heart Fail 7, 75-83, doi:10.1002/ehf2.12592 (2020).

32 Premchand, R. K. et al. Autonomic regulation therapy via left or right cervical vagus nerve stimulation in patients with chronic heart failure: results of the ANTHEM-HF trial. J Card Fail 20, 808-816, doi:10.1016/j.cardfail.2014.08.009 (2014).

33 Schmidt, A. et al. Infarct tissue heterogeneity by magnetic resonance imaging identifies enhanced cardiac arrhythmia susceptibility in patients with left ventricular dysfunction. Circulation 115, 2006-2014, doi:10.1161/CIRCULATIONAHA.106.653568 (2007).

34 Yan, A. T. et al. Characterization of the peri-infarct zone by contrast-enhanced cardiac magnetic resonance imaging is a powerful predictor of post-myocardial infarction mortality. Circulation 114, 32-39, doi:10.1161/CIRCULATIONAHA.106.613414 (2006).

35 Rutherford, S. L., Trew, M. L., Sands, G. B., LeGrice, I. J. & Smaill, B. H. High-resolution 3-dimensional reconstruction of the infarct border zone: impact of structural remodeling on electrical activation. Circ Res 111, 301-311, doi:10.1161/CIRCRESAHA.111.260943 (2012).

36 Chen, P. S. et al. Sympathetic nerve sprouting, electrical remodeling and the mechanisms of sudden cardiac death. Cardiovascular research 50, 409-416, doi:10.1016/s0008-6363(00)00308-4 (2001).

37 Cao, J. M. et al. Nerve sprouting and sudden cardiac death. Circ Res 86, 816-821, doi:10.1161/01.res.86.7.816 (2000).

38 Srinivasan, N. T. et al. Prolonged action potential duration and dynamic transmural action potential duration heterogeneity underlie vulnerability to ventricular tachycardia in patients undergoing ventricular tachycardia ablation. Europace 21, 616-625, doi:10.1093/europace/euy260 (2019).

Chapter 2

Ventricular Electrophysiological Effects of Vagal Nerve Stimulation in Humans With and Without Structural Heart Disease

Jonathan D Hoang, Zulfiqar A Lokhandwala, Una Buckley, Neil R Jani, Jason S Bradfield, Yuliya Krokhaleva, Houman Khakpour, Olujimi A Ajijola, Noel G Boyle, Kalyanam Shivkumar, Marmar Vaseghi

In preparation.

ABSTRACT

Background: Clinical trials of vagus nerve stimulation (VNS) in heart failure show mixed results, in part due to varied stimulation parameters, which may fail to stimulate cardiomotor fibers required for cardio-protection. However, overstimulation of the vagus nerve may cause adverse effects. Thus, the aim of this study was to assess the beneficial effects of moderate frequency VNS in patients with structurally normal hearts (SNH) and those with cardiomyopathy (CM). Thus, we hypothesized that moderate frequency VNS (10 Hz) confers sufficient ventricular electrophysiological effects.

Methods: Patients with SNH and supraventricular tachycardia (*n* = 5) and cardiomyopathy patients with ventricular tachycardia (CM, *n* = 6) undergoing electrophysiology procedures were recruited. A multi-electrode circular electrophysiology catheter was advanced from the femoral to the right internal jugular vein via a long sheath. Bipolar electrode pairs were serially stimulated and capture/stimulation of the vagus nerve identified by a negative chronotropic response. Threshold current was defined as a 10-15% decrease in heart rate (HR) at 20 Hz and 1 ms pulse-width. Stimulation was then performed at threshold current for 10 seconds at 10 and 20 Hz. Endocardial unipolar electrograms were continuously recorded using ventricular multielectrode mapping catheters and used to calculate activation recovery intervals (ARI), a validated surrogate of local action potential duration (APD). Electrodes were designated as overlying scar, border zone, or viable myocardium based on standard bipolar voltage mapping criteria in CM patients. ARIs were corrected for HR by the Framingham method.

Results: The current of stimulation was 13.2 ± 1.7 mA in SNH and 14.4 ± 3.1 mA in CM (*p* = ns). VNS at 20 Hz significantly decreased HR ($p \leq 0.01$) in both SNH and CM patients (12.6 ± 1.4% in SNH *vs* 12.9 ± 1.7% in CM, *p* = ns) while significantly prolonging global ventricular ARIs (2.2 ± 0.4% in SNH *vs* 4.6 ± 1.0% in CM, *p* = ns). The chronotropic effects of 10 Hz VNS were similar to 20 Hz in SNH (12.0 ± 1.4% at 10 Hz *vs* 12.6 ± 1.4% at 20 Hz, *p* = ns) but blunted in CM patients (12.0 ± 1.4% in SNH *vs* 4.9 ± 2.4% in CM, $p \leq 0.05$). Surprisingly, despite reduced chronotropic

responses, global ARI prolongation persisted (4.0 ± 0.7% at 10 Hz *vs* 4.6 ± 1.0% at 20 Hz, p = ns) in CM patients. Importantly, ARI prolongation was observed in scar (326 ± 23 to 340 ± 22 ms, $p \leq 0.05$) and border zone regions (312 ± 18 ms to 323 ± 17 ms, $p \leq 0.05$). Moreover, after correcting ARI for heart rate (ARIc), 10 Hz VNS in CM patients caused significantly greater prolongation in ARIc than 20 Hz (1.8 ± 0.6% at 10 Hz *vs* -1.0 ± 0.6% at 20 Hz, $p \leq 0.05$), suggesting that higher frequency VNS may potentially cause a net shortening of ventricular APD.

Conclusions: Acute application of moderate frequency VNS (10 Hz) demonstrated ventricular electrophysiological effects, with ARI prolongation observed in scar and border zone regions in diseased hearts. This human data validates previously reported effects of moderate frequency VNS in large animal infarct models. Stimulation at 20 Hz is unnecessary and may have negative ventricular electrophysiological effects. Further clinical trials assessing electrophysiological effects of chronic VNS in humans are required.

INTRODUCTION

Clinical trials investigating the benefits of vagal nerve stimulation (VNS) in heart failure (HF) have shown mixed results. This variation is perhaps due to inconsistent stimulation parameters,[1-3] which may fail to adequately stimulate cardiomotor fibers required for cardio-protection.[4] However, overstimulation of the vagus nerve may cause adverse off-target effects, such as cough and dyspnea due to unintended activation of the recurrent and superior laryngeal nerves.[5] Additionally, vagal nerve stimulation may have undesirable effects system-wide, such as gut discomfort, via its afferent and efferent innervation of numerous organ systems.[6,7]

The INcrease Of VAgal TonE in CHF (INOVATE-HF) trial starting in 2011 performed VNS at 1-2 Hz via a closed-loop delivery system,[2] mimicking parameters that were previously successful in the CardioFit Pilot study by De Ferrari et al.[8,9] However, it was determined that they failed to reach their primary end points of reductions in death and HF events.[10] Later that same year, the Neural Cardiac Therapy for Heart Failure Study (NECTAR-HF) trial began, instead employing VNS at 20 Hz in an open-loop implementation.[3] However, while NECTAR-HF seemed to show some improvement of quality of life parameters (Minnesota Living with Heart Failure Questionnaire, New York Heart Association class, and SF-36 Physical Component), it failed to show improvements in cardiac remodeling and functional capacity at either 6 or 12 months.[11,12] Lastly, the Autonomic Neural Regulation Therapy to Enhance Myocardial Function in Heart Failure (ANTHEM-HF) trial looked for benefit of VNS at 10 Hz of stimulation.[1] Despite the apparent failure of the prior two trials, ANTHEM-HF has shown benefit as early as 6 months lasting throughout the current observation period of 4 to 5 years.[13] The improvements seen in the ANTHEM-HF trial are reflected by improvements in cardiac mechanical, electrical, and autonomic function.[14-20] Moreover, studies further suggest that that VNS may be a favorable adjunct treatment to guideline directed medical therapy,[21] and notably beta-blockade.[22]

However, experimental evidence suggests large frequency dependent differences and benefits,[4,23,24] perhaps underlying the differential results stemming from these clinical trials.

NECTAR-HF, which employed a relatively high frequency stimulation of 20 Hz, was limited by off-target effects during up-titration. ANTHEM-HF on the other hand which employed a moderate frequency of stimulation at 10 Hz allowed up-titration until a negative chronotropic response was seen.

Clinical trials for vagus nerve stimulation thus far have relied on changes in heart rate dynamics to guide VNS titration,[1-3] also causing dysphonia in some patients at amplitudes required to cause heart rate changes.[16] However, while current guidelines suggest that bradycardia is the accepted biomarker for efficacy of VNS,[25] experimental data suggests that heart rate effects may not be necessary to achieve the ventricular benefit that is of interest in this patient population.[29,30] Thus, the optimal parameters for focused ventricular cardioprotection remain unclear.

To date, no study has directly examined the ventricular electrophysiological effects of vagal nerve stimulation in humans. Prior studies assessing data from clinical trials are limited by their episodic assessment of functional, but non-invasive parameters which lack mechanistic power. While moderate frequency VNS (10 Hz) shows support for treating heart failure and cardiovascular dysfunction, it remains unclear 1) what the ventricular electrophysiological benefits of VNS are and 2) if it has any potential as an acute anti-arrhythmic intervention. Moreover, evidence for relatively limited parasympathetic innervation of the ventricles[26] coupled with studies indicating a functional parasympathetic denervation in infarcted and ischemic regions[27] suggests that direct ventricular effects in the setting of chronic structural heart disease may be limited. It is thus possible that many of the benefits of chronic VNS may be driven primarily via control of sinus rate or even general inflammation.[28] Lastly, it remains to be seen whether high frequency VNS (20 Hz) may confer additional benefits over moderate frequencies of stimulation (10 Hz), especially in patients with structural heart disease. Thus, the aim of this study was to assess the beneficial ventricular effects of moderate frequency VNS in patients with structurally normal hearts (SNH) and those with cardiomyopathy (CM).

METHODS

This study was approved by the University of California, Los Angeles, Human Institutional Review Board. Patients with ischemic cardiomyopathy (CM, n = 6) and recurrent ventricular arrhythmias referred for catheter ablation were recruited. Patients with structurally normal hearts (n = 5) referred for electrophysiological study for possible supraventricular tachycardia also underwent the same experimental protocol as patients with CM, Figure 1. Detailed written informed consent for the study was obtained from all patients. Patients with hemodynamic instability were excluded from the protocol at the discretion of the investigator.

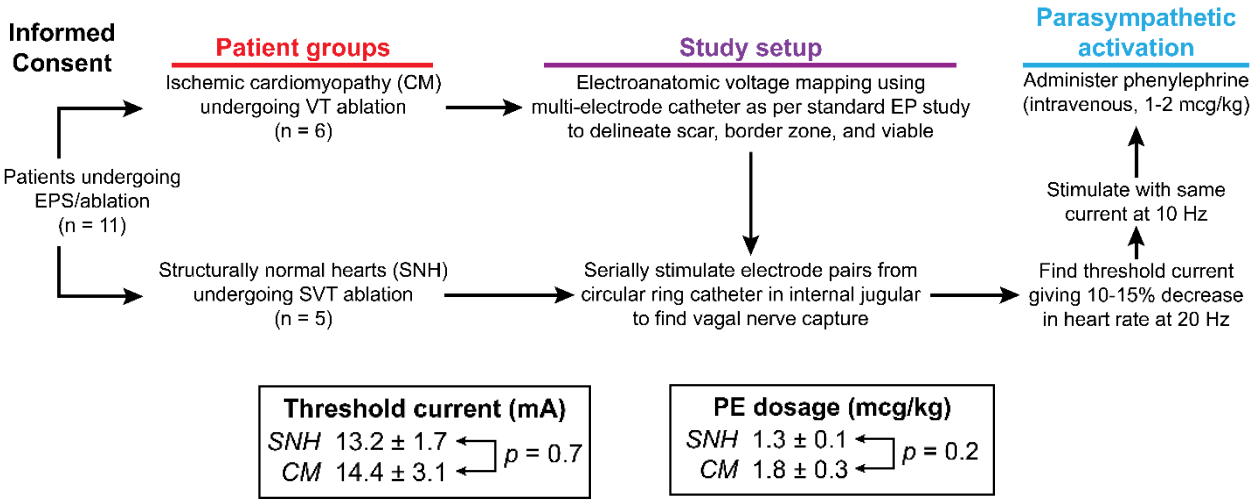

Figure 2-1. ***Study protocol and procedure.***

Electrophysiology study and electroanatomic mapping

All antiarrhythmic medications were discontinued a minimum of 12 hours before electrophysiology study. Single or double transseptal catheterization was performed in all patients with ICM but only in those normal patients whose electrophysiology study dictated the necessity for left atrial or LV access. When necessary, epicardial access was obtained in patients with ICM using the method described by Sosa et al. An endocardial, and when necessary, an epicardial voltage map was created to assess for the presence of normal, scar, and border zone regions in all patients with ICM using either the CARTO (CARTO XP; Biosense-Webster, Diamond Bar, CA) or Nav-X (St.

Jude Medical, St. Paul, MN) electroanatomic mapping systems. Scar was defined as areas with electrogram (EGM) amplitude <0.5 mV. Border zone regions were defined by areas with EGM amplitude between 0.5 and 1.5 mV. Viable myocardium was defined as areas with EGM amplitude >1.5 mV.

Ventricular electrophysiological recording and analysis

Duodecapolar (20-electrode) or HD GRID (16-electrode) electrophysiology catheters were placed in the left ventricle to continuously record local unipolar electrograms via a GE CardioLab System (Boston, MA). Unipolar electrograms were bandpass filtered 0.05 Hz to 500 Hz. Electrodes in the distal inferior vena cava were used as the unipolar references for this catheter. Catheters were carefully positioned to obtain a minimum of 4-5 electrodes per electrical region and the location of each electrode with respect to the electroanatomic map was noted.

Activation recovery intervals (ARIs) were analyzed to estimate regional action potential durations, using customized software, iScaldyn (University of Utah, Salt Lake City, UT).[29,30] ARI is a reliable surrogate for action potential duration and has been validated in both animal models and humans.[29,31] Activation time was measured as the time of dV/dt_{min} of depolarization from the initial deflection, and repolarization time was measured as the time of dV/dt_{max} of repolarization; the difference, ARI, reflects action potential duration at the electrode site and correlates well with APD during different interventions.[32]

Electrograms with unclear or biphasic repolarization waves were excluded after visual confirmation. Electrodes overlying very dense scar (voltage < 0.05 mV) that did not give rise to a discernable electrogram were also excluded. Based on its electrode location on the electroanatomic map, and as confirmed by fluoroscopy, the local changes in ARI were categorized as reflecting changes in the normal, border zone, or scar regions of the myocardium. In the case of structurally normal hearts, the average change in ARI of all electrodes reflected healthy myocardium.

Parasympathetic activation via vagal nerve stimulation and baroreflex activation

A circular electrophysiology catheter (7-Fr Inquiry Optima, 2-2-2 electrode spacing, 20 electrodes; St. Jude Medical) was introduced via the femoral vein to the right internal jugular vein via a long sheath (Figure 2A). Bipolar electrode pairs were serially stimulated using a Micropace EPS320, and capture/stimulation of the vagus nerve was identified by a negative chronotropic response. The right vagal nerve was chosen to better compare results of clinical trails which generally looked at right-sided stimulation.[1,2,3] The vagal nerve was stimulated at a frequency of 20 Hz and pulse-width of 1 ms. The current of stimulation was gradually titrated to a response yielding a 10-15% decrease in heart rate (HR) which was defined as the threshold current. The threshold current was not significantly different between SNH and CM patients (13.2 ± 1.7 mA in SNH *vs* 14.4 ± 3.1 mA; $p = 0.7$), Figure 1. Stimulation was then performed at threshold current for 10 seconds at 10 Hz and 20 Hz.

The parasympathetic arm of the baroreflex response was engaged by bolus administration of the alpha-1 selective agonist, phenylephrine (PE). PE (intravenous, 1-2 mcg/kg) was administered to increase systolic blood pressure by 20-30 mmHg. The dosage of PE was similar between SNH and CM patients (1.3 ± 0.1 mcg/kg *vs* 1.8 ± 0.3 mcg/kg; $p = 0.2$), Figure 1.

Statistical analysis

Data are reported as mean ± SEM. Global ARIs were calculated as the mean ARI across all electrodes and regional ARIs as the mean ARI of the electrodes classified by electroanatomic mapping. Paired two-tailed Student's *t*-test was used to compare parameters before and during parasympathetic activation. For responses to VNS and PE, percent changes in parameters from baseline were calculated first; then paired two-tailed Student's *t*-test was used to compare efficacy of different frequencies of VNS and unpaired two-tailed Student's *t*-test was used to make comparisons between SNH and CM patients. Repeated measures mixed effects analysis was used to assess differences between VNS and PE and corrected for the false discovery rate by the Benjamini Hochberg method. All statistical analyses were performed with GraphPad Prism software v9. $P < 0.05$ was considered statistically significant.

RESULTS

Chronotropic effects of moderate frequency vagal nerve stimulation in patients with structurally normal hearts and cardiomyopathy

Given that the accepted biomarker for VNS efficacy is changes in heart rate dynamics, we first sought to determine the differential chronotropic effects of 10 Hz and 20 Hz VNS in health and disease. High frequency VNS (20 Hz) significantly decreased heart rate in SNH (84.8 ± 5.3 bpm to 74.0 ± 4.3 bpm, $p \leq 0.05$) and CM (74.2 ± 6.4 bpm to 65.4 ± 5.5 bpm, $p \leq 0.05$), Figure 2B. However, while moderate frequency VNS (10 Hz) significantly lowered heart rate in SNH (84.4 ± 5.5 bpm to 73.5 ± 4.4 bpm, $p \leq 0.05$), it did not have an effect in CM patients (74.8 ± 6.3 bpm to 70.5 ± 5.7 bpm, non-significant), Figure 2B.

Both 10 and 20 Hz VNS exhibited similar bradycardic effects in SNH patients (-12.7 ± 1.1% with 10 Hz *vs* -12.6 ± 1.6% with 20 Hz, non-significant), Figure 2C. Interestingly, while 20 Hz VNS was in SNH was comparable to 20 Hz VNS in CM (-12.6 ± 1.6% in SNH patients *vs* -12.3 ± 1.7% in CM patients, non-significant), effects of 10 Hz VNS were significantly blunted (-5.3 ± 2.3%, $p \leq 0.05$ *vs* 10 Hz in SNH patients, $p \leq 0.01$ *vs* 20 Hz in CM patients).

Ventricular electrophysiological effects of vagal nerve stimulation

Although in CM patients, 10 Hz VNS lacked significant chronotropic effects and seemed less effective in patients with CM compared to 20 Hz of the same amplitude, we next sought to determine if these effects were consistent with changes at the ventricular level. Ventricular multipolar catheters allowed us to record unipolar electrograms directly from the ventricular myocardium and assess local changes in action potential duration (Figure 2D, example of duodecapolar catheter in SNH patient).

In concordance with the chronotropic effects of VNS, 20 Hz VNS prolonged global ventricular ARIs by an average of 7 ms in SNH (298 ± 16 ms to 304 ± 16 ms, $p \leq 0.05$) and 14 ms in CM (318 ± 17 ms to 332 ± 18 ms, $p \leq 0.05$), Figure 2E. Similarly, 10 Hz VNS prolonged global ventricular ARI by 9 ms in SNH (297 ± 15 ms to 306 ± 17 ms, $p \leq 0.05$), Figure 2E.

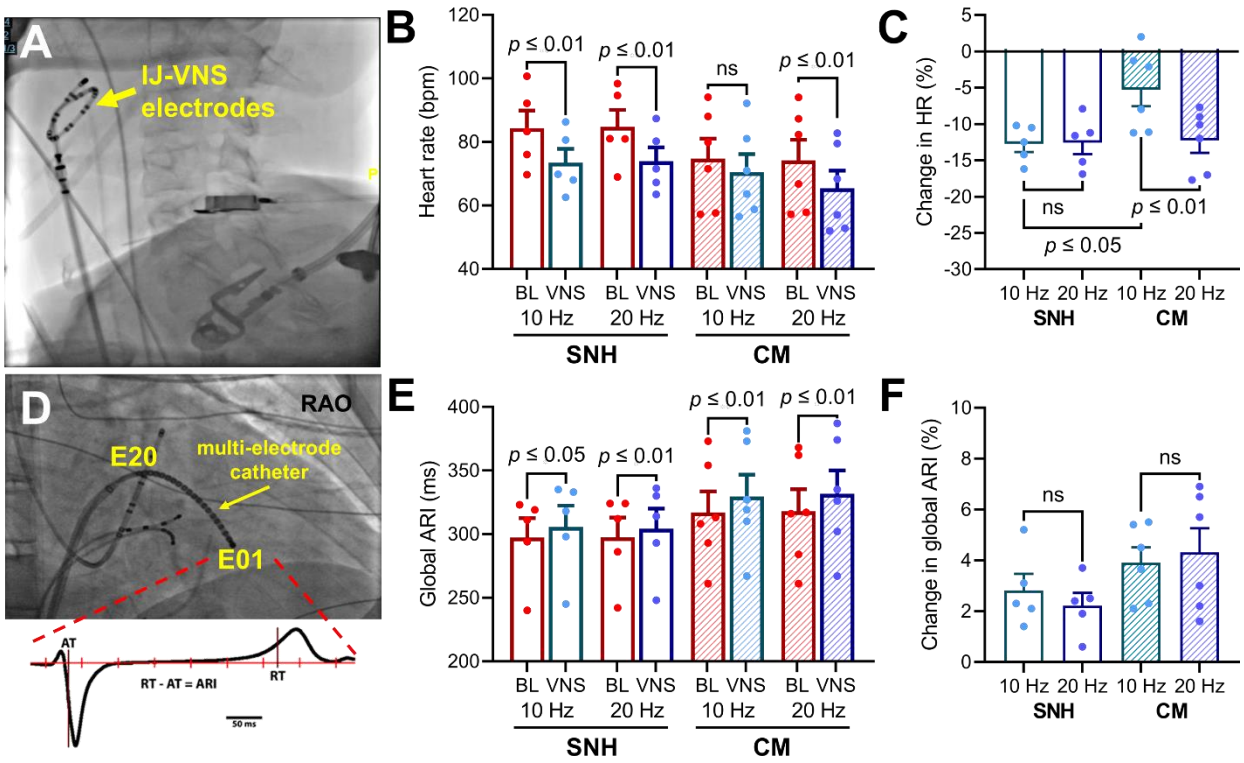

Figure 2-2. ***Effects of frequency on vagal nerve stimulation effects in structurally normal hearts and cardiomyopathy.*** (**A**) A circular electrophysiology catheter was positioned in the internal jugular vein (IJ) for trans-jugular vagal nerve stimulation (VNS). (**B, C**) VNS lowered heart rate (HR) at both 10 Hz and 20 Hz in structurally normal hearts (SNH), but HR effects of 10 Hz VNS were blunted in cardiomyopathy (CM) patients. (**D**) Unipolar electrograms were acquired via endocardial multi-electrode electrophysiology catheters for ARI measurement (example from SNH). (**E, F**) Global ARIs were prolonged by VNS in both SNH and CM patients, but not significantly different between 10 Hz and 20 Hz. RAO = right anterior oblique; ARI = activation recovery intervals.

However, while 10 Hz VNS in CM patients failed to elicit a significant chronotropic response, it significantly prolonged ventricular ARI (317 ± 17 ms to 330 ± 17 ms, p ≤ 0.05), Figure 2E.

While high frequency (20 Hz) VNS was necessary to achieve significant bradycardic effect in CM patients, moderate frequency (10 Hz) VNS was sufficient to achieve ventricular effect. The ventricular benefit yielded by 10 Hz VNS in CM patients was thus not dissimilar from 20 Hz in CM or 10 Hz in SNH (3.9 ± 0.6% with CM-10 Hz, non-significant *vs* CM-20 Hz and SNH-10 Hz), Figure 2F.

Regional differences of different frequency vagal nerve stimulation in patients with structural heart disease

To determine whether these effects may be potentially anti-arrhythmic, we specifically evaluated distinct electrical regions in CM patients by positioning the electrodes of the multipolar catheter across regions of scar, border zone, and viable myocardium as identified by electroanatomic mapping (Figure 3A, example of 16-electrode HD-GRID catheter in CM patient). Electrograms from each of these electrodes w spatially mapped onto a 2D-schematic (Figure 3B) to assess functional differences in the effects of VNS.

As 10 Hz and 20 Hz VNS differed in their chronotropic effects while bearing similar ventricular effects, we first controlled for the effects of sinus rate on ventricular action potential duration to better distinguish between direct and indirect ventricular benefits of VNS. Interestingly, while 10 Hz VNS prolonged HR-corrected ARIs (ARIc) by 5 ms (343 ± 11 ms to 348 ± 11 ms, $p \leq 0.05$), 20 Hz VNS tended to shorten ARIc by 5 ms (343 ± 11 ms to 338 ± 10 ms, non-significant), Figure 3C. Effects of 10 Hz VNS on ARIc were significantly greater than 20 Hz VNS (1.6 ± 0.6% with 10 Hz *vs* -1.3 ± 0.6% with 20 Hz, $p \leq 0.05$), suggesting that 10 Hz VNS may have greater direct ventricular effects, Figure 3C.

Given that 10 Hz VNS appeared to have greater direct effects on the ventricles than 20 Hz VNS, we assessed the specific localization of the effects of 10 Hz VNS within the ventricles. As ventricular infarct (scar) and peri-infarct (border zone) sites are known to play roles in the initiation and propagation of ventricular tachyarrhythmias,[33] we specifically aimed to map these effects to these electrical subregions. Although 10 Hz VNS exhibited global effects, viable regions of the myocardium specifically did not significantly prolong (318 ± 14 ms to 325 ± 14 ms, non-significant), Figure 3E. However, regional ARIs of both scar (323 ± 21 ms to 336 ± 20 ms, $p \leq 0.05$) and border zone (311 ± 16 ms to 323 ± 16 ms, $p \leq 0.05$) regions significantly prolonged, Figure 3E. However, these differences were not significantly different between regions.

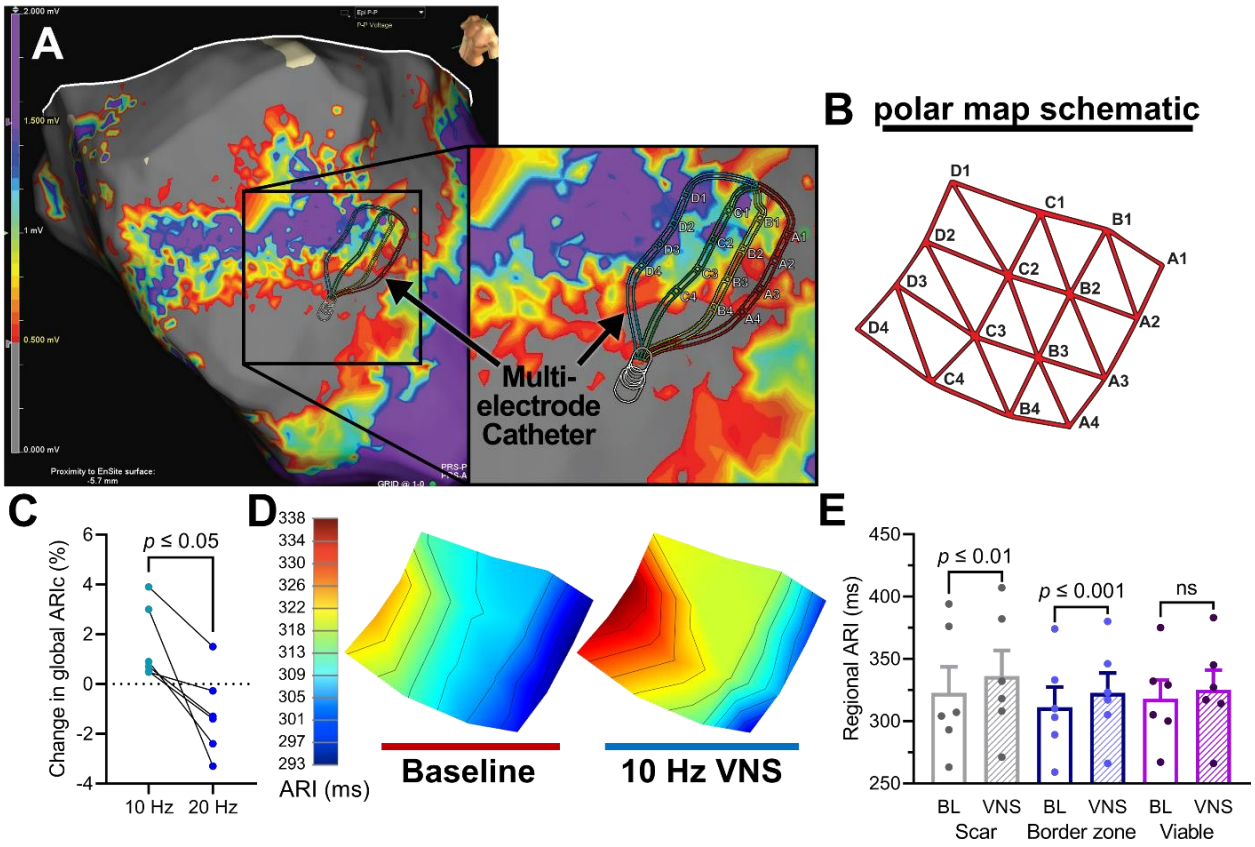

Figure 2-3. ***Regional effects of vagal nerve stimulation in cardiomyopathy patients.*** (**A**) Representative bipolar voltage map of a cardiomyopathy (CM) patient with a 16-electrode HD GRID mapping catheter. Electrodes are overlying viable (purple, voltage >1.5 mV), border zone (multicolor, between 0.5-1.5 mV) and scar (grey, <0.5 mV) regions. (**B**) Schematic of electrode positions used to assess regional changes in activation recovery interval (ARI). (**C**) Correcting ARI for HR (ARIc) revealed that 10 Hz VNS may have greater ventricular electrophysiologic effects than 20 Hz VNS. (**D**) Example of polar map before and during 10 Hz VNS showing global prolongation of ARI. (**E**) ARIs prolonged in scar and border zone areas, regions known to play a key role in arrhythmogenesis.

Effects of baroreflex engagement on ventricular electrical parameters

Lastly, we sought to test endogenous vagal function in SNH and CM patients by pressor test. Given our findings of moderate frequency of VNS on ventricular APD but not heart rate, we questioned whether these findings would extend into the baroreflex response. Importantly, the cardiovascular reflex to a pressor challenge is thought to be reflective of native parasympathetic function and is known to be depressed in the setting of chronic disease.

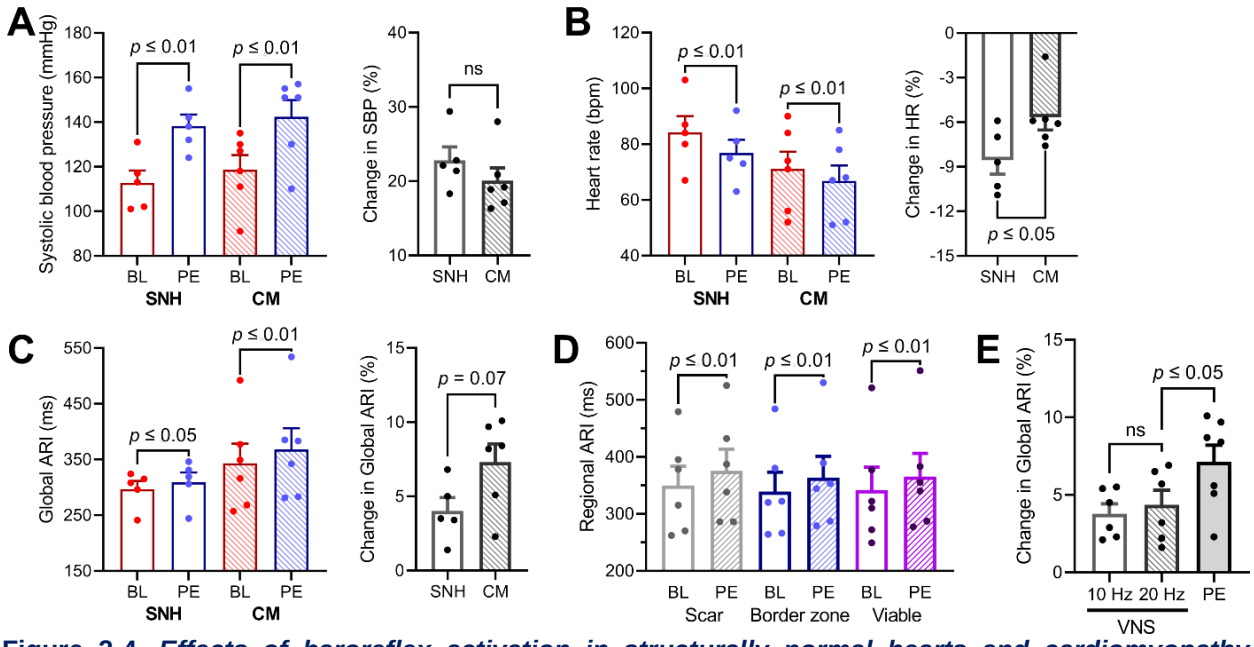

Figure 2-4. ***Effects of baroreflex activation in structurally normal hearts and cardiomyopathy patients.*** (**A**) Phenylephrine (PE) significantly increased systolic blood pressure in both structurally normal hearts (SNH) and cardiomyopathy (CM) patients without significant differences between groups. (**B**) Baroreflex activation significantly decreased heart rate (HR) in both groups but this response was blunted in CM patients. (**C**) Ventricular activation recovery intervals (ARIs) significantly prolonged in both SNH and CM patients with a trend for greater effects in CM patients. (**D**) Effects on ventricular ARI were not limited to any electrical region in CM patients. (**E**) High frequency VNS caused similar prolongation to moderate frequency VNS but was significantly less than PE administration.

Administration of phenylephrine significantly increased blood pressure in SNH (113 ± 5 mmHg to 138 ± 5 mmHg, p ≤ 0.01) and CM (119 ± 7 mmHg to 142 ± 8 mmHg, p ≤ 0.01). Phenylephrine caused a reflex-driven bradycardic response in SNH (84 ± 6 bpm to 77 ± 5 bpm, p ≤ 0.01) and CM (71 ± 6 bpm to 67 ± 6 bpm, p ≤ 0.01). However, while there was no significant difference in the direct response to alpha-adrenergic agonism (22.8 ± 1.8% in SNH *vs* 20.1 ± 1.7% in CM, non-significant), the indirect response of a decrease in heart rate was significantly blunted (-8.6 ± 0.9% in SNH *vs* -5.7 ± 0.9% in CM, p ≤ 0.05).

Phenylephrine administration significantly prolonged global ventricular ARI in both SNH (297 ± 15 ms to 309 ± 18 ms, p ≤ 0.05) and CM (343 ± 35 ms to 368 ± 38 ms, p ≤ 0.01). Similar to vagal nerve stimulation, the chronotropic effects of baroreflex activation were not reflective of the

ventricular benefit. Despite its diminished effects on heart rate in CM patients, phenylephrine administration prolonged ventricular ARI significantly more in CM patients than SNH patients (4.0 ± 0.9% in SNH *vs* 7.3 ± 1.2% in CM, p = 0.07).

In CM patients the ventricular effects of baroreflex activation by phenylephrine administration were significantly greater than either 10 Hz or 20 Hz VNS (3.8 ± 0.6% in CM, p ≤ 0.05 *vs* 10 Hz and *vs* 20 Hz VNS), suggesting an important role for afferent activation in addition to vagal efferent activation, in translating the beneficial effects of parasympathetic nervous system activation.

DISCUSSION

This is the first study in humans to assess in detail the direct ventricular effects of vagus nerve stimulation. The present investigation combined myocardial unipolar electrical recordings from the ventricles with detailed electrophysiological mapping to assess functional changes in the acute efficacy of moderate frequency VNS (10 Hz), high frequency VNS (20 Hz), and baroreflex activation (phenylephrine bolus). The major findings of this study in CM patients are:

1) Chronotropic effects of 10 Hz VNS are limited in comparison to 20 Hz VNS, but ventricular effects are present at both frequencies.
2) Electrophysiological effects of 10 Hz VNS are focused to ventricular scar and border zone regions as compared to 20 Hz VNS.
3) Baroreflex activation by phenylephrine showed a similar reduction in HR as 20 Hz VNS but had significantly greater ventricular effects.

Effects of moderate versus high frequency vagal nerve stimulation in the setting of chronic structural heart disease

Higher frequency nerve stimulation not only increases the frequency of neuronal depolarization and proportionally the amount of neurotransmitter release, but may also alter the identity of neurotransmitters and neuropeptides released.[23] Thus, it is not unexpected that high frequency VNS (20 Hz) as employed in NECTAR-HF, is expected to behave differently with perhaps

greater benefit than the moderate frequency VNS (10 Hz) employed in ANTHEM-HF. However, with the failure of NECTAR-HF to titrate 20 Hz VNS to the cardiac threshold due to incidence of off-target effects, these additional cardiac benefits remain to be seen. Studies by Ardell *et al.* (2017)[4] which investigated the "neural fulcrum" in healthy dogs corroborate these findings and additionally show that, on the basis of chronotropic effects, high frequency VNS (20 Hz) may have greater efficacy than lower frequency VNS at the same current.

Based on current heart rate criteria for defining amplitude of VNS, the absence of clear chronotropic effects of 10 Hz VNS in CM patients may suggest that there was minimal cardiac benefit in the present study. In these patients with structural heart disease, an established setting of altered cardiac autonomic control,[34] vagal nerve stimulation may thus be less effective. However, experimental evidence from large animals suggests that 1) vagal nerve stimulation may be anti-arrhythmic independent of its effects on heart rate,[35,36] and 2) vagal nerve stimulation may have more potent ventricular effects, especially within scar and border zone regions,[37] known regions of arrhythmogenesis in ischemic cardiomyopathies.[33] These results may owe in part to a preservation, or even increase of acetylcholine levels in these regions,[37] and to the increased cardiac expression of muscarinic receptors in heart failure.[38]

The present study recapitulated these findings for the first time in humans, suggesting that ventricular effects of vagal nerve stimulation may actually be enhanced in patients with cardiomyopathy. Moreover, these data may be in line with findings that, although the synaptic efficacy (coupling of stimulation frequency to depolarization frequency) of intrinsic cardiac neurons to higher frequencies (≥ 20 Hz) was augmented shortly following myocardial infarction, these results tend to normalize by 14 days after infarction.[24] Thus, in the setting of chronic structural heart disease, the ventricular benefits of vagal nerve stimulation may saturate at 10 Hz of stimulation.[24] In the present study, high frequency VNS (20 Hz) caused significant slowing of sinoatrial rate but without further prolongation of ventricular action potential duration.

While the neural fulcrum has provided invaluable experimental evidence for guiding clinical trials of vagal nerve stimulation for heart failure, it may poorly reflect ventricular anti-arrhythmic strategy. Taken together, these data reinforce the successes of the ANTHEM-HF trial, but further suggest that optimal and focused ventricular benefit may be obtained with lower amplitude of stimulation. Titration to the point of altered heart rate dynamics followed by a reduction in amplitude may be ideal to balance ventricular benefit with avoidance of off-target effects and assuage concerns of eventual tachyphylaxis.

Vagal nerve stimulation as an acute anti-arrhythmic strategy

Experimental evidence from animal models of chronic myocardial infarction suggest that vagus nerve stimulation may be acutely anti-arrhythmic.[37] The present study showed for the first time in humans with structural heart disease that vagus nerve stimulation may, similar to what has been shown in animal models, prolong ventricular action potential duration across scar and border zone regions by almost 15 ms. This extent of prolongation mimics what has been seen in animal models to be of a therapeutic threshold of VNS,[37] and greater prolongation than other highly anti-arrhythmic neuromodulatory approaches such as cardiac sympathetic denervation.[39]

Importantly, these data suggest the potential for closed-loop VNS as a first line of defense against sudden cardiac death, adjuvant to an implantable cardioverter defibrillator, that may increase quality of life.[40-44] Closed-loop VNS is currently under investigation for suppression of refractory epileptic seizures (responding to pre-ictal tachycardia) with patients showing greater freedom from ictal events than open-loop VNS,[45,46] and the translation of this VNS modality for treatment of refractory ventricular arrhythmias warrants further study.

Baroreflex activation in chronic structural heart disease

In accordance with prior reports of autonomic dysfunction in the setting of cardiovascular disease,[47] CM patients exhibited an orthodox diminished baroreflex response, as reflected by a lesser slowing of heart rate upon increases in arterial blood pressure. Interestingly, baroreflex

activation induced a similar change in heart rate as 20 Hz VNS but caused a significantly greater prolongation in ventricular action potential duration.

Baroreflex sensitivity is thought to be reflective of the function of the parasympathetic nervous system,[48] and has been shown to be a negative prognostic marker.[47] Parasympathetic inputs to sinoatrial node, and thus control of atrial and ultimately ventricular rate, may thus be affected but it may be an incomplete reflection of autonomic activity at the level of the ventricles, let alone within the scar and border zone regions. Although reduced baroreflex sensitivity may be a predictor of cardiac mortality in part due to its insights into overall autonomic tone,[47] the results herein suggest that lack of heart rate effects may be a poor indicator of ventricular benefit of neuromodulatory approaches targeting this pathway.

Limitations

The current of stimulation employed in this study was higher than the range typically employed in clinical trials investigating the effects of vagus nerve stimulation.[49] However, these differences are likely attributed to differences in stimulation modality. Helical cuff electrodes, such as those employed in clinical trials, have the large advantage of direct delivery of current to the vagus nerve combined with circumferential spread of current. Thus, transvascular VNS as used in this study may require greater current to achieve sufficient capture of vagal fibers, especially those distal to the internal jugular vein. Furthermore, anesthesia is known to blunt autonomic function and specifically, the response to vagal nerve stimulation,[4] and as such, may have necessitated higher currents.

Lastly, the present study involved a relatively small number of patients and larger, multi-center clinical trials are required to further corroborate these findings.

CONCLUSIONS

The preliminary assessment of efficacy measures of moderate frequency VNS (10 Hz), as used in ANTHEM-HF, is promising and may be more favorable than 20 Hz VNS. Acute application of 10 Hz VNS demonstrated ventricular electrophysiological effects, with APD prolongation observed

in scar and border zone regions in diseased hearts, a major anti-arrhythmic mechanism. Stimulation at 20 Hz is unnecessary and may not only cause off-target effects but have negative ventricular electrophysiological effects.

REFERENCES

1 Dicarlo, L., Libbus, I., Amurthur, B., Kenknight, B. H. & Anand, I. S. Autonomic regulation therapy for the improvement of left ventricular function and heart failure symptoms: the ANTHEM-HF study. J Card Fail 19, 655-660, doi:10.1016/j.cardfail.2013.07.002 (2013).

2 Hauptman, P. J. et al. Rationale and study design of the increase of vagal tone in heart failure study: INOVATE-HF. Am Heart J 163, 954-962 e951, doi:10.1016/j.ahj.2012.03.021 (2012).

3 De Ferrari, G. M. et al. Rationale and study design of the NEuroCardiac TherApy foR Heart Failure Study: NECTAR-HF. Eur J Heart Fail 16, 692-699, doi:10.1002/ejhf.80 (2014).

4 Ardell, J. L. et al. Defining the neural fulcrum for chronic vagus nerve stimulation: implications for integrated cardiac control. J Physiol 595, 6887-6903, doi:10.1113/JP274678 (2017).

5 Nicolai, E. N. et al. Sources of off-target effects of vagus nerve stimulation using the helical clinical lead in domestic pigs. J Neural Eng 17, 046017, doi:10.1088/1741-2552/ab9db8 (2020).

6 Rush, A. J. & Siefert, S. E. Clinical issues in considering vagus nerve stimulation for treatment-resistant depression. Exp Neurol 219, 36-43, doi:10.1016/j.expneurol.2009.04.015 (2009).

7 Breit, S., Kupferberg, A., Rogler, G. & Hasler, G. Vagus Nerve as Modulator of the Brain-Gut Axis in Psychiatric and Inflammatory Disorders. Front Psychiatry 9, 44, doi:10.3389/fpsyt.2018.00044 (2018).

8 Schwartz, P. J. et al. Long term vagal stimulation in patients with advanced heart failure: first experience in man. Eur J Heart Fail 10, 884-891, doi:10.1016/j.ejheart.2008.07.016 (2008).

9 De Ferrari, G. M. et al. Chronic vagus nerve stimulation: a new and promising therapeutic approach for chronic heart failure. Eur Heart J 32, 847-855, doi:10.1093/eurheartj/ehq391 (2011).

10 Gold, M. R. et al. Vagus Nerve Stimulation for the Treatment of Heart Failure: The INOVATE-HF Trial. J Am Coll Cardiol 68, 149-158, doi:10.1016/j.jacc.2016.03.525 (2016).

11 Zannad, F. et al. Chronic vagal stimulation for the treatment of low ejection fraction heart failure: results of the NEural Cardiac TherApy foR Heart Failure (NECTAR-HF) randomized controlled trial. Eur Heart J 36, 425-433, doi:10.1093/eurheartj/ehu345 (2015).

12 De Ferrari, G. M. et al. Long-term vagal stimulation for heart failure: Eighteen month results from the NEural Cardiac TherApy foR Heart Failure (NECTAR-HF) trial. Int J Cardiol 244, 229-234, doi:10.1016/j.ijcard.2017.06.036 (2017).

13 Libbus, I. et al. Persistent Autonomic Engagement and Cardiac Control After Four or More Years of Autonomic Regulation Therapy Using Vagus Nerve Stimulation. Front Physiol 13, 853617, doi:10.3389/fphys.2022.853617 (2022).

14 Premchand, R. K. et al. Autonomic regulation therapy via left or right cervical vagus nerve stimulation in patients with chronic heart failure: results of the ANTHEM-HF trial. J Card Fail 20, 808-816, doi:10.1016/j.cardfail.2014.08.009 (2014).

15 Libbus, I., Nearing, B. D., Amurthur, B., KenKnight, B. H. & Verrier, R. L. Autonomic regulation therapy suppresses quantitative T-wave alternans and improves baroreflex sensitivity in patients with heart failure enrolled in the ANTHEM-HF study. Heart Rhythm 13, 721-728, doi:10.1016/j.hrthm.2015.11.030 (2016).

16 Premchand, R. K. et al. Extended Follow-Up of Patients With Heart Failure Receiving Autonomic Regulation Therapy in the ANTHEM-HF Study. J Card Fail 22, 639-642, doi:10.1016/j.cardfail.2015.11.002 (2016).

17 Carlson, G. M., Libbus, I., Amurthur, B., KenKnight, B. H. & Verrier, R. L. Novel method to assess intrinsic heart rate recovery in ambulatory ECG recordings tracks cardioprotective effects of chronic autonomic regulation therapy in patients enrolled in the ANTHEM-HF study. Ann Noninvasive Electrocardiol 22, doi:10.1111/anec.12436 (2017).

18 Nearing, B. D. et al. Vagus Nerve Stimulation Provides Multiyear Improvements in Autonomic Function and Cardiac Electrical Stability in the ANTHEM-HF Study. J Card Fail 27, 208-216, doi:10.1016/j.cardfail.2020.10.003 (2021).

19 Nearing, B. D. et al. Chronic vagus nerve stimulation is associated with multi-year improvement in intrinsic heart rate recovery and left ventricular ejection fraction in ANTHEM-HF. Clin Auton Res 31, 453-462, doi:10.1007/s10286-021-00780-y (2021).

20 Sharma, K. et al. Long-term Follow-Up of Patients with Heart Failure and Reduced Ejection Fraction Receiving Autonomic Regulation Therapy in the ANTHEM-HF Pilot Study. Int J Cardiol 323, 175-178, doi:10.1016/j.ijcard.2020.09.072 (2021).

21 Premchand, R. K. et al. Background pharmacological therapy in the ANTHEM-HF: comparison to contemporary trials of novel heart failure therapies. ESC Heart Fail 6, 1052-1056, doi:10.1002/ehf2.12484 (2019).

22 Li, M. et al. Chronic vagal nerve stimulation exerts additional beneficial effects on the beta-blocker-treated failing heart. J Physiol Sci 69, 295-303, doi:10.1007/s12576-018-0646-0 (2019).

23 Feliciano, L. & Henning, R. J. Vagal nerve stimulation releases vasoactive intestinal peptide which significantly increases coronary artery blood flow. Cardiovasc Res 40, 45-55, doi:10.1016/s0008-6363(98)00122-9 (1998).

24 Hardwick, J. C., Southerland, E. M. & Ardell, J. L. Chronic myocardial infarction induces phenotypic and functional remodeling in the guinea pig cardiac plexus. Am J Physiol Regul Integr Comp Physiol 295, R1926-1933, doi:10.1152/ajpregu.90306.2008 (2008).

25 Musselman, E. D., Pelot, N. A. & Grill, W. M. Empirically Based Guidelines for Selecting Vagus Nerve Stimulation Parameters in Epilepsy and Heart Failure. Cold Spring Harb Perspect Med 9, doi:10.1101/cshperspect.a034264 (2019).

26 Wink, J. et al. Human adult cardiac autonomic innervation: Controversies in anatomical knowledge and relevance for cardiac neuromodulation. Auton Neurosci 227, 102674, doi:10.1016/j.autneu.2020.102674 (2020).

27 Zipes, D. P. Influence of myocardial ischemia and infarction on autonomic innervation of heart. Circulation 82, 1095-1105, doi:10.1161/01.cir.82.4.1095 (1990).

28 Verrier, R. L., Libbus, I., Nearing, B. D. & KenKnight, B. H. Multifactorial Benefits of Chronic Vagus Nerve Stimulation on Autonomic Function and Cardiac Electrical Stability in Heart Failure Patients With Reduced Ejection Fraction. Front Physiol 13, 855756, doi:10.3389/fphys.2022.855756 (2022).

29 Millar, C. K., Kralios, F. A. & Lux, R. L. Correlation between refractory periods and activation-recovery intervals from electrograms: effects of rate and adrenergic interventions. Circulation 72, 1372-1379, doi:10.1161/01.cir.72.6.1372 (1985).

30 Coronel, R. et al. Monophasic action potentials and activation recovery intervals as measures of ventricular action potential duration: experimental evidence to resolve some controversies. Heart Rhythm 3, 1043-1050, doi:10.1016/j.hrthm.2006.05.027 (2006).

31 Vaseghi, M., Lux, R. L., Mahajan, A. & Shivkumar, K. Sympathetic stimulation increases dispersion of repolarization in humans with myocardial infarction. Am J Physiol Heart Circ Physiol 302, H1838-1846, doi:10.1152/ajpheart.01106.2011 (2012).

32 Haws, C. W. & Lux, R. L. Correlation between in vivo transmembrane action potential durations and activation-recovery intervals from electrograms. Effects of interventions that alter repolarization time. Circulation 81, 281-288, doi:10.1161/01.cir.81.1.281 (1990).

33 Vaseghi, M. & Shivkumar, K. The role of the autonomic nervous system in sudden cardiac death. Prog Cardiovasc Dis 50, 404-419, doi:10.1016/j.pcad.2008.01.003 (2008).

34 Ardell, J. L. et al. Translational neurocardiology: preclinical models and cardioneural integrative aspects. J Physiol 594, 3877-3909, doi:10.1113/JP271869 (2016).

35 Zhang, Y. et al. Chronic vagus nerve stimulation improves autonomic control and attenuates systemic inflammation and heart failure progression in a canine high-rate pacing model. Circ Heart Fail 2, 692-699, doi:10.1161/CIRCHEARTFAILURE.109.873968 (2009).

36 Vanoli, E. et al. Vagal stimulation and prevention of sudden death in conscious dogs with a healed myocardial infarction. Circ Res 68, 1471-1481, doi:10.1161/01.res.68.5.1471 (1991).

37 Vaseghi, M. et al. Parasympathetic dysfunction and antiarrhythmic effect of vagal nerve stimulation following myocardial infarction. JCI Insight 2, doi:10.1172/jci.insight.86715 (2017).

38 DeMazumder, D., Kass, D. A., O'Rourke, B. & Tomaselli, G. F. Cardiac resynchronization therapy restores sympathovagal balance in the failing heart by differential remodeling of cholinergic signaling. Circ Res 116, 1691-1699, doi:10.1161/CIRCRESAHA.116.305268 (2015).

39 Irie, T. et al. Cardiac sympathetic innervation via middle cervical and stellate ganglia and antiarrhythmic mechanism of bilateral stellectomy. Am J Physiol Heart Circ Physiol 312, H392-H405, doi:10.1152/ajpheart.00644.2016 (2017).

40 Goldenberg, I. et al. Causes and consequences of heart failure after prophylactic implantation of a defibrillator in the multicenter automatic defibrillator implantation trial II. Circulation 113, 2810-2817, doi:10.1161/CIRCULATIONAHA.105.577262 (2006).

41 Hurst, T. M., Hinrichs, M., Breidenbach, C., Katz, N. & Waldecker, B. Detection of myocardial injury during transvenous implantation of automatic cardioverter-defibrillators. J Am Coll Cardiol 34, 402-408, doi:10.1016/s0735-1097(99)00194-1 (1999).

42 Poole, J. E. et al. Prognostic importance of defibrillator shocks in patients with heart failure. N Engl J Med 359, 1009-1017, doi:10.1056/NEJMoa071098 (2008).

43 Runsio, M. et al. Left ventricular function after repeated episodes of ventricular fibrillation and defibrillation assessed by transoesophageal echocardiography. Eur Heart J 18, 124-131, doi:10.1093/oxfordjournals.eurheartj.a015093 (1997).

44 Runsio, M., Kallner, A., Kallner, G., Rosenqvist, M. & Bergfeldt, L. Myocardial injury after electrical therapy for cardiac arrhythmias assessed by troponin-T release. Am J Cardiol 79, 1241-1245, doi:10.1016/s0002-9149(97)00090-8 (1997).

45 Winston, G. M. et al. Closed-loop vagal nerve stimulation for intractable epilepsy: A single-center experience. Seizure 88, 95-101, doi:10.1016/j.seizure.2021.03.030 (2021).

46 Tzadok, M. et al. Clinical outcomes of closed-loop vagal nerve stimulation in patients with refractory epilepsy. Seizure 71, 140-144, doi:10.1016/j.seizure.2019.07.006 (2019).

47 La Rovere, M. T., Bigger, J. T., Jr., Marcus, F. I., Mortara, A. & Schwartz, P. J. Baroreflex sensitivity and heart-rate variability in prediction of total cardiac mortality after myocardial infarction. ATRAMI (Autonomic Tone and Reflexes After Myocardial Infarction) Investigators. Lancet 351, 478-484, doi:10.1016/s0140-6736(97)11144-8 (1998).

48 La Rovere, M. T., Mortara, A. & Schwartz, P. J. Baroreflex sensitivity. J Cardiovasc Electrophysiol 6, 761-774, doi:10.1111/j.1540-8167.1995.tb00452.x (1995).

49 Anand, I. S. et al. Comparison of symptomatic and functional responses to vagus nerve stimulation in ANTHEM-HF, INOVATE-HF, and NECTAR-HF. ESC Heart Fail 7, 75-83, doi:10.1002/ehf2.12592 (2020).

Chapter 3

Myocardial infarction reduces cardiac nociceptive neurotransmission through the vagal ganglia

Siamak Salavatian*, Jonathan D Hoang*, Naoko Yamaguchi*, Zulfiqar Ali Lokhandwala, Mohammed Amer Swid, John Andrew Armour, Jeffrey L. Ardell, Marmar Vaseghi

*These authors share first author position.

Salavatian S, Hoang JD, Yamaguchi N, Lokhandwala ZA, Swid MA, Armour JA, Ardell JL, Vaseghi M. Myocardial infarction reduces cardiac nociceptive neurotransmission through the vagal ganglia. JCI Insight. 2022;7(4). Epub 2022/01/12. doi: 10.1172/jci.insight.155747.

ABSTRACT

Myocardial infarction causes pathological changes in the autonomic nervous system, which exacerbate heart failure and predispose to fatal ventricular arrhythmias and sudden death. These changes are characterized by sympathetic activation and parasympathetic dysfunction (reduced vagal tone). Reasons for the central vagal withdrawal and, specifically, whether myocardial infarction causes changes in cardiac vagal afferent neurotransmission that then affect efferent tone, remain unknown. The objective of this study was to evaluate whether myocardial infarction causes changes in vagal neuronal afferent signaling. Using in vivo neural recordings from the inferior vagal (nodose) ganglia and immunohistochemical analyses, structural and functional alterations in vagal sensory neurons were characterized in a chronic porcine infarct model and compared with normal animals. Myocardial infarction caused an increase in the number of nociceptive neurons but a paradoxical decrease in functional nociceptive signaling. No changes in mechanosensitive neurons were observed. Notably, nociceptive neurons demonstrated an increase in GABAergic expression. Given that nociceptive signaling through the vagal ganglia increases efferent vagal tone, the results of this study suggest that a decrease in functional nociception, possibly due to an increase in expression of inhibitory neurotransmitters, may contribute to vagal withdrawal after myocardial infarction.

GRAPHICAL ABSTRACT

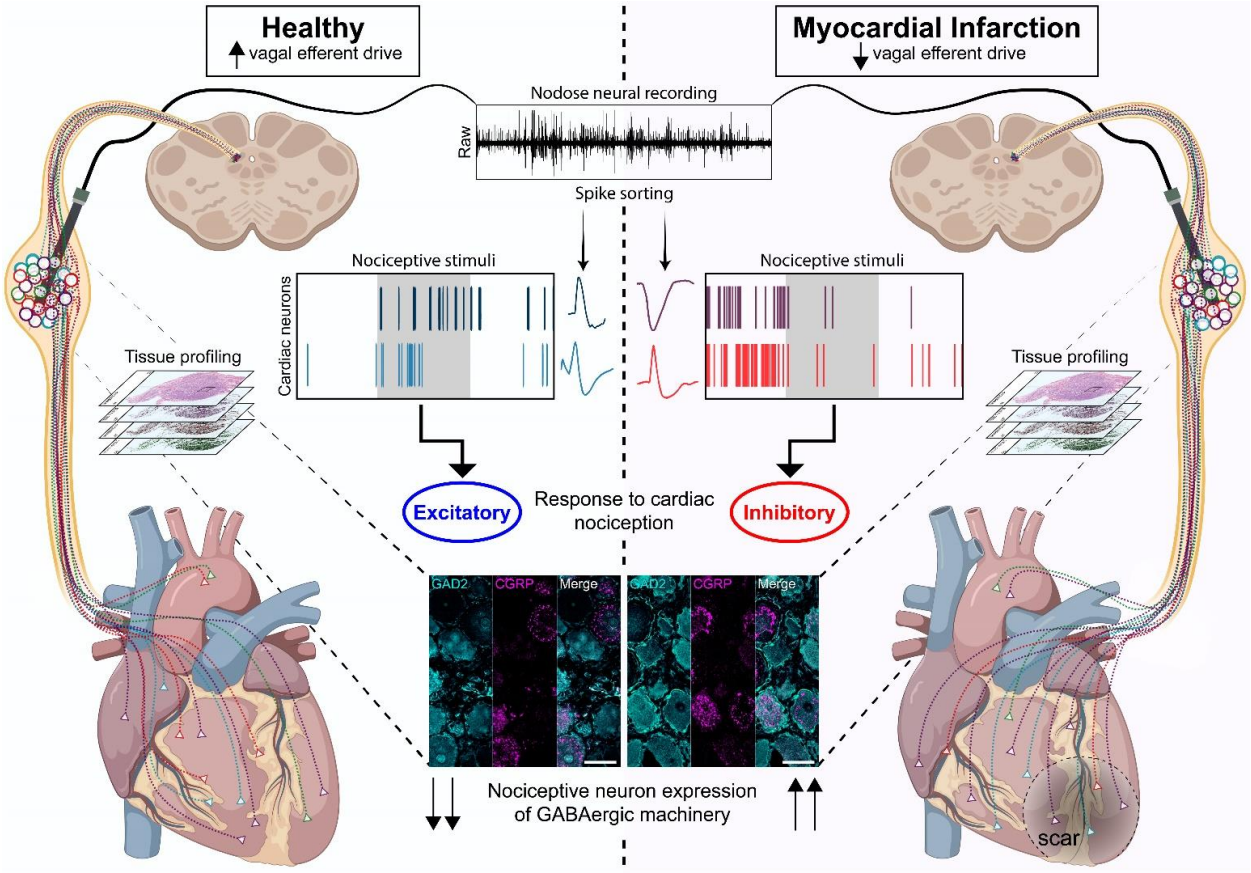

INTRODUCTION

The autonomic nervous system plays an important role in the regulation of cardiac function.[1,2] Cardiac disease causes significant pathological changes in the autonomic nervous system that result in sympathovagal imbalance, as reflected by sympathetic activation and vagal withdrawal.[3,4] Notably, enhanced vagal drive has been shown to be anti-arrhythmic, increasing cardiac action potential duration, slowing heart rate, preventing intracellular calcium overload, and reducing ventricular tachycardia (VT) inducibility.[5,6]

In the setting of myocardial injury, progressive vagal efferent dysfunction occurs, as reflected in noninvasive markers such as decreased heart rate variability. These changes are associated with an increased risk of ventricular arrhythmias in patients with myocardial infarction (MI) and increased mortality in heart failure.[7,8] The mechanisms underlying parasympathetic dysfunction and vagal withdrawal remain unclear.

In normal hearts, activation of cardiac afferent neurons, notably, vagal nociceptive neurons, leads to increased vagal efferent outflow.[9] These pseudo-unipolar cardiac-specific sensory neurons reside in the inferior vagal (nodose) ganglia and transmit signals from the heart to the brainstem,[10] subsequently modulating efferent vagal outflow to the heart.[11] Increased vagal afferent nociceptive neurotransmission is associated with increased efferent vagal drive in normal hearts. However, no studies have evaluated changes in afferent vagal neurotransmission after cardiac disease to delineate abnormalities that may contribute to vagal dysfunction, and it is unknown if myocardial infarction can cause extra-thoracic vagal neuronal remodeling. In this study, we hypothesized that chronic MI causes changes in parasympathetic afferent neurotransmission. To understand these alterations, we probed structural and functional alterations in the nodose ganglia neurons in both normal and chronically infarcted porcine animals.

RESULTS

Effect of myocardial infarction on nodose neurons

It is unknown if MI is associated with phenotypical changes in the neurons of the nodose ganglia. To assess these alterations after MI, ganglia were harvested from chronically infarcted animals as previously described,[5,12] then compared with ganglia from healthy animals. Morphological changes and protein expression profiles were assessed in animals with chronic MI with left anterior descending coronary artery (LAD) occlusion (Figure 1) and in animals with right coronary artery (RCA) infarction, to determine whether the location of the infarct affected the laterality of changes observed (i.e., in right vs. left vagal/nodose ganglia neurons). Overall, there was a modest increase in the size of nodose ganglia neurons after MI. The mean neuronal size in healthy animals was 1204 ± 37 μm^2 (n = 10) versus 1451 ± 61 μm^2 in LAD-infarcted animals (n = 9, P = 0.004 vs. healthy animals) and 1411 ± 56 μm^2 in RCA-infarcted animals (n = 7, P = 0.014 vs. healthy animals, Supplemental Figure 1; supplemental material available online with this article; https://doi.org/10.1172/jci.insight.155747DS1). No change in soma counts was observed between normal and MI animals.

To assess phenotypic changes associated with MI, expression of receptors and peptides involved in purinergic signaling and cardiac nociception, as reflected by expression of adenosine receptor P2RX3 and CGRP, were assessed. Animals with chronic LAD infarcts exhibited significantly higher expression of both P2RX3 (26.2% ± 3.9% in MI vs. 12.2% ± 1.9% in normal animals, P = 0.005) and CGRP (17.3% ± 2.0% in LAD-MI vs. 10.3% ± 0.8% in normal animals, P = 0.005), which are receptors and peptides, respectively, involved in nociceptive neurotransmission. Conversely, the expression of the neuromodulator, neuronal NOS1 (11.6% ± 0.7% in MI vs. 15.5% ± 0.7% in normal animals, P = 0.002), was attenuated after MI (Figure 2). However, there was no change in the expression of PIEZO2, a mechanosensitive ion channel involved in cardiac mechanotransduction (59.8% ± 1.9% in MI vs. 56.0% ± 3.0% in normal animals, P = 0.32, Figure 2).[13] The differences between normal and LAD infarcted animals

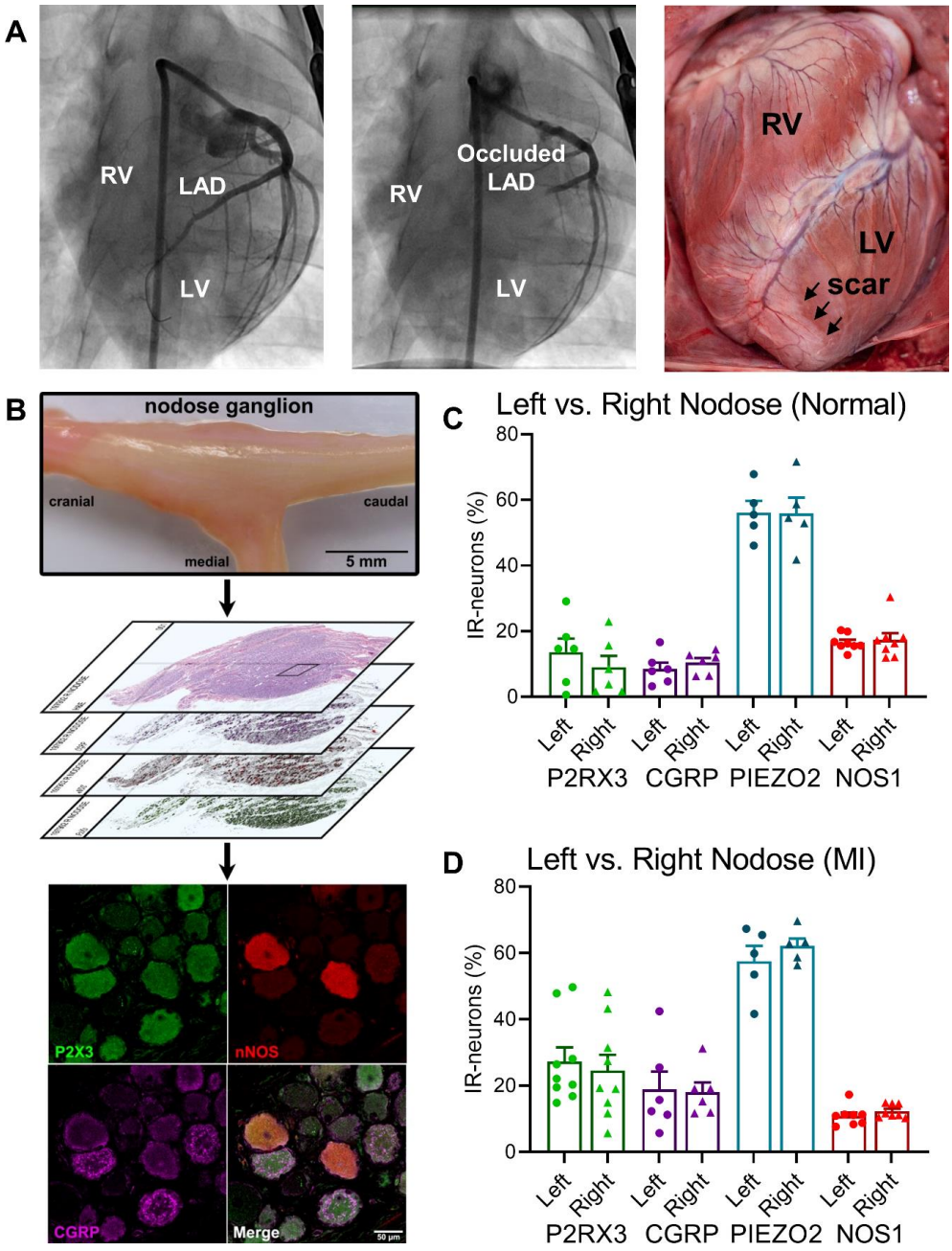

Figure 3-1. ***Assessment of expression profiles of left vs. right nodose ganglia neurons in normal and LAD-infarcted animals.*** (**A**) Creation of myocardial infarct in the LAD distribution. Left panel: representative coronary angiography. Middle panel: Coronary artery angiography after microsphere injection showing occlusion at the mid-LAD. Right panel: Representative gross image of an infarcted heart showing scar in the region vascularized by the LAD. (**B**) Nodose ganglia from normal and infarcted animals were removed and analyzed for immunohistochemical changes. Scale bars are 5 mm (top), 50 µm (bottom). (**C**) Percentages of nodose ganglia neurons from normal and (**D**) infarcted (MI) animals expressing P2RX3, CGRP, PIEZO2, and NOS1 were quantified. No difference in the expression profiles of neurons between the left and right nodose ganglia was found in either normal or infarcted animals for P2RX3 (normal left vs.

right nodose: P = 0.82; MI left vs. right nodose: P = 0.67), CGRP (normal left vs. right nodose: P = 0.82; MI left vs. right nodose: P = 0.89), PIEZO2 (a mechanosensitive ion channel; normal left vs. right nodose: P = 0.97; MI left vs. right nodose: P = 0.67), or NOS1 (normal left vs. right nodose: P = 0.82; MI left vs. right nodose: P = 0.67). n = 6 pairs of nodose for P2RX3 in normal animals and CGRP in both normal and MI animals. n = 5 pairs of nodose ganglia for PIEZO2 in normal and MI animals. n = 8 pairs of nodose ganglia for NOS1 in normal and MI animals. Data shown as mean ± SEM; paired, 2-tailed Student's t test with the false discovery rate corrected by the Benjamini-Hochberg method was used for analyses. CGRP, calcitonin gene-related peptide; LV, left ventricle; NOS1, nitric oxide synthase 1; P2RX3, P2X purinoceptor 3; RV, right ventricle.

remained significant whether data was analyzed by animal (Figure 2) or by individual nodose ganglia (Supplemental Figure 2).

Subsequently, we analyzed the effect of the location of the MI (LAD vs. RCA infarction) on phenotypical changes in nodose ganglia neurons. When comparing neural remodeling between LAD-infarcted (n = 10) and RCA-infarcted (n = 7) animals, no significant differences in protein expression profiles were noted. Nodose ganglia from RCA-infarcted animals also demonstrated a significant increase in CGRP and P2RX3 expression, a decrease in NOS1 expression, and no significant change in PIEZO2 expression (Supplemental Figure 3), suggesting that these pathological phenotypical changes occurred regardless of the location of infarction. Animals with RCA infarction showed a modestly greater increase in CGRP expression as compared with animals with LAD infarction (27.4% ± 2.7% in RCA- vs. 17.3% ± 2.0% in LAD-MI, P = 0.04, Supplemental Figure 3).

Phenotypical changes in left versus right nodose ganglia

To assess whether different territories of MI influenced laterality and degree of neural remodeling in the nodose ganglia, left versus right ganglion differences were compared in normal animals and in those with LAD and RCA infarcts. No discernable differences in expression of CGRP, P2RX3, NOS1, or PIEZO2 were observed between the left and right nodose ganglia in normal animals (Figure 1). Similarly, both the left and right nodose ganglia showed comparable

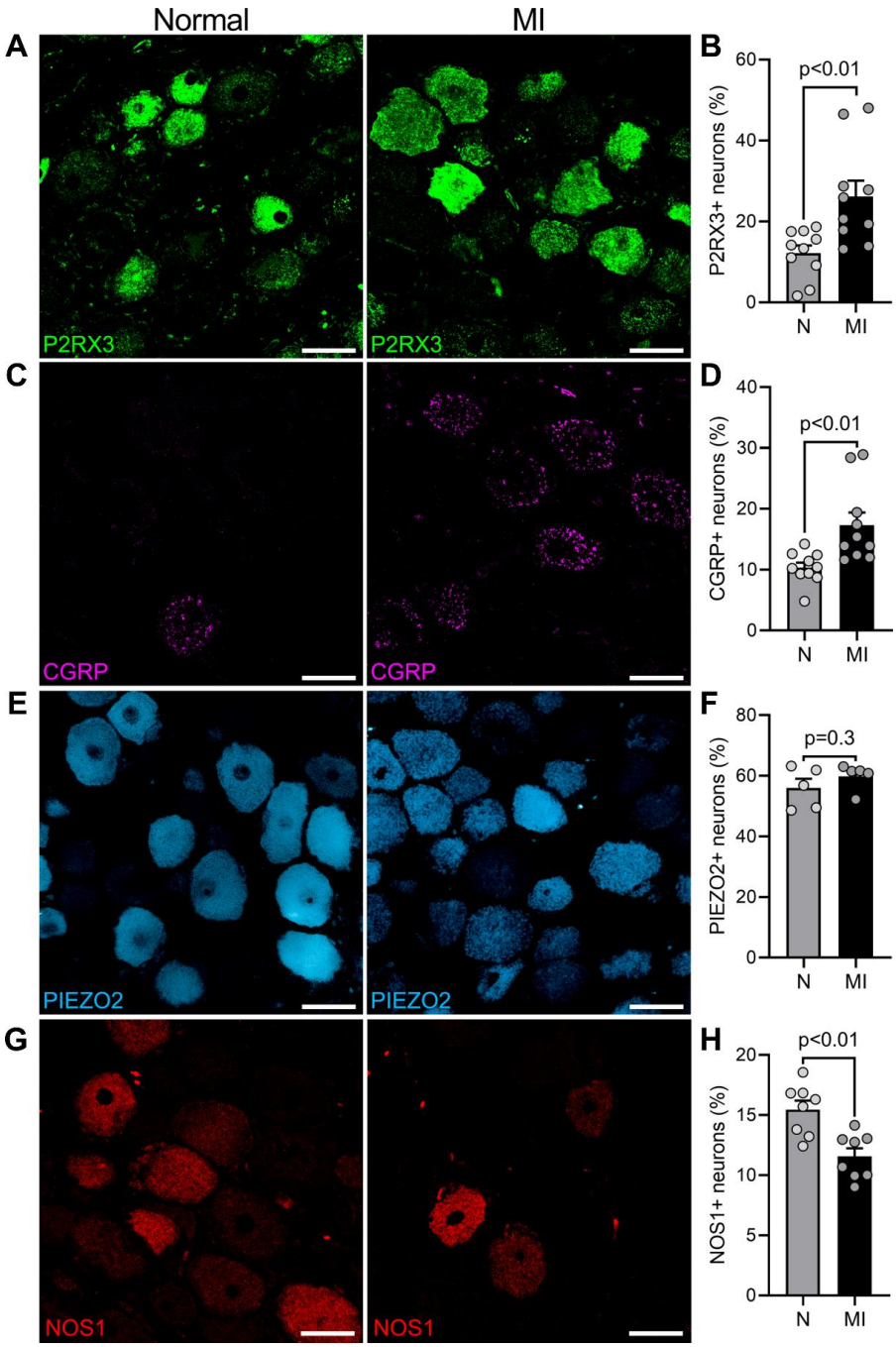

Figure 3-2. ***Immunohistochemical assessment of neurons in the porcine nodose ganglia.*** Representative images of nodose ganglia from normal (left) and LAD-infarcted (right) pig nodose ganglion stained and quantified for (**A** and **B**) P2RX3, (**C** and **D**) CGRP, (**E** and **F**) PIEZO2, and (**G** and **H**) NOS1. Expression of P2RX3 and CGRP were increased after chronic LAD infarction (P = 0.005 for normal vs. infarcted animals for P2RX3 and CGRP). PIEZO2 expression remained unchanged (P = 0.32). Expression of NOS1 in the nodose ganglia was reduced after LAD infarction (P = 0.002 for normal vs. infarcted animals). n = 10 pigs per group for P2RX3 and CGRP quantification, n = 5 pigs per group for PIEZO2, and

n = 8 pigs per group for NOS1; data are shown as mean ± SEM; unpaired, 2-tailed Student's *t* test was used for comparisons. Scale bars are 50 μm.

pathological changes in LAD- and RCA-infarcted animals, with a lack of laterality in the altered expression of CGRP, P2RX3, NOS1 (Figure 1 and Supplemental Figure 3).

Basal activity of nodose ganglia neurons in infarcted and healthy animals

To assess functional changes in cardiac vagal afferent signaling, the activity of neurons in the nodose ganglia in both normal and chronically infarcted animals (chronic RCA infarcts) were recorded in vivo using linear microelectrode arrays (Figure 3). To specifically identify cardiac related nodose neurons, the responses of nodose neurons to cardiac stressors/interventions, including epicardial application of chemical and mechanical stimuli, IVC occlusion, aortic occlusion, and ventricular pacing, were evaluated in all animals (normal: *n* = 11 pigs; RCA-MI: *n* = 11 pigs). Basal neural activity was also analyzed (prior to application of cardiac stressor). Of note, RCA-infarcted animals (which have posterior/dorsal ventricular scars) were used for functional neuronal recording studies to determine responses of vagal afferents to chemical stimuli on the anterior ventricles/viable regions, without the potential confounding effects of scar and denervation that may affect responses. Changes in hemodynamic parameters in response to the above cardiac stressors are shown in Supplemental Table 1. In 11 normal animals, 97 cardiac related neurons (8.8 ± 2.1 per animal), and in 11 infarcted animals, 133 cardiac related neurons (12.1 ± 4.5 per animal), were identified based on their significant responses (using the Skellam test)[14] to cardiovascular interventions (Figure 3).

No significant differences between basal firing rates of left versus right nodose cardiac related neurons in healthy animals were observed (left: 0.04 Hz [IQR 0.01–0.09 Hz], *n* = 37 neurons vs. right: 0.05 Hz [0.004–0.16 Hz], *n* = 56 neurons, *P* = 0.72). Similarly, no differences in the basal firing rates of left versus right nodose cardiac related neurons of infarcted animals

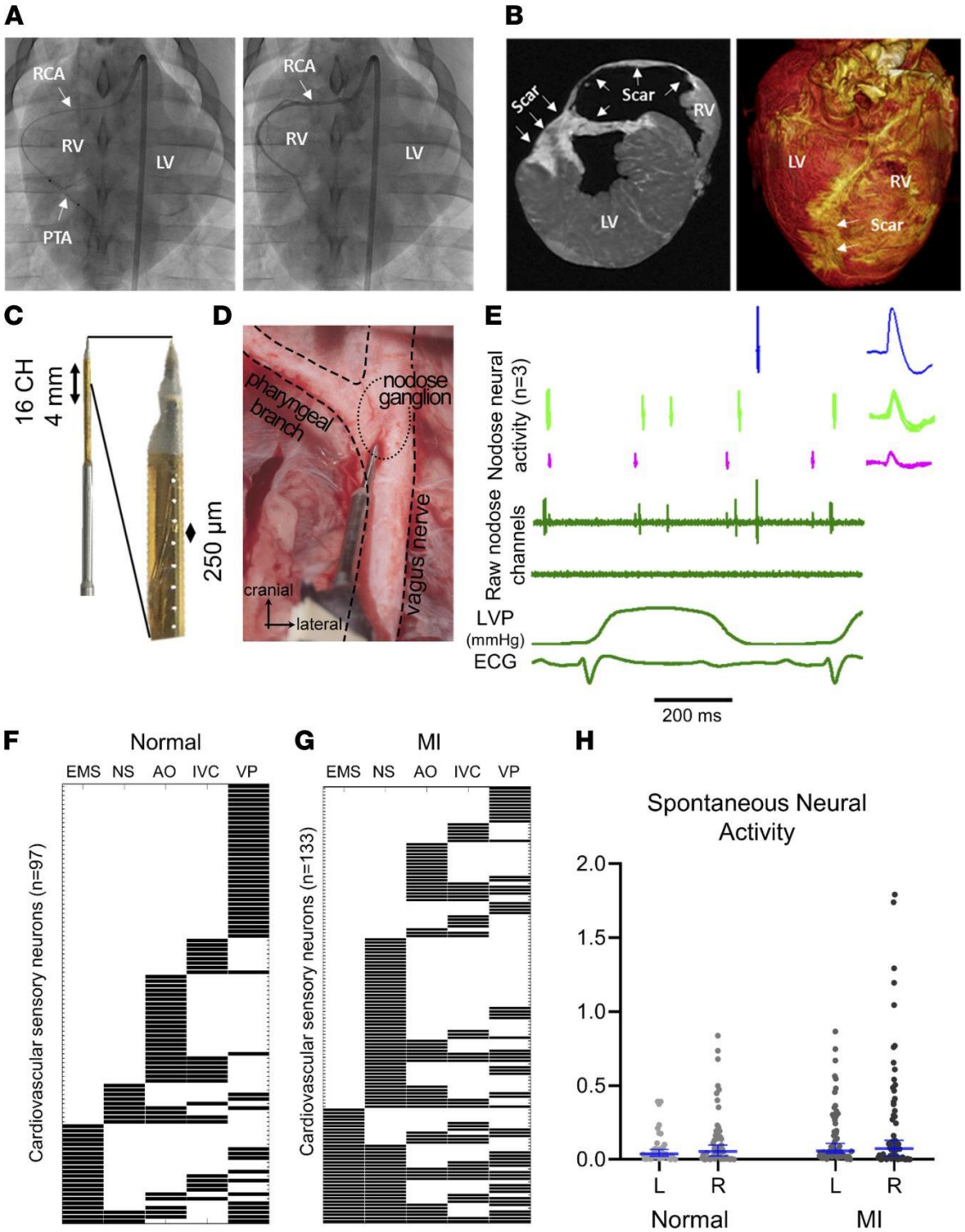

Figure 3-3. ***Functional analysis of nodose neuronal activity following MI.*** (**A**) Creation of right coronary artery myocardial infarct. Left panel: representative coronary angiography (RCA) while placing the percutaneous transluminal angioplasty catheter (PTA) in the RCA. The distal radiopaque marker indicates the distal end of the angioplasty catheters where microspheres are injected. Right panel: Coronary artery angiography after RCA infarct creation. Contrast dye was injected into the RCA to confirm the location of the occlusion. (**B**) Representative magnetic resonance imaging (MRI) images of the RCA-infarcted heart. Scar

tissues were confirmed by assessing the thickness and the color of the myocardial regions in the MRI image. (**C**) Customized 16-channel linear microelectrode array probes were used to record nodose neurons in vivo. (**D**) The neural probe was inserted in the nodose ganglion. (**E**) Representative sorted neuronal action potentials for 3 neurons from 1 animal. Action potentials from individual neurons are illustrated in the right panel. Left ventricular pressure (LVP) and electrocardiogram (ECG) were recorded simultaneously with neural recordings. (**F**) Responses of 97 cardiac nodose neurons from 11 normal animals (8.8 ± 2.1 per animal) to epicardial mechanical stimulation (EMS), epicardial nociceptive stimuli (NS), aortic occlusion (AO), inferior vena cava (IVC) occlusion, and ventricular pacing (VP). Only significant responses ($P < 0.05$) to each stressor based on the Skellam test are shown. (**G**) The response of 133 cardiac nodose neurons from 11 animals with MI involving the RCA to cardiac stressors are shown. (**H**) Nodose neuronal firing rate at baseline. There was no difference in the basal activity of nodose neurons in normal versus MI animals. There was no difference in the activity of neurons from the left versus right nodose ganglia. (n = 37, 56, 63, and 62 for normal-left nodose, normal-right nodose, MI-left nodose, and MI-right nodose ganglia, respectively.) Median and 95% confidence intervals are shown, and Mann-Whitney U statistical test was used for comparisons.

were observed (left: 0.06 Hz [0.02–0.27 Hz], n = 63 vs. right: 0.07 Hz [0.007–0.38 Hz], n = 62, P = 0.80) (Figure 3).

Neurons that responded to at least 1 ventricular chemical stimulus and none of the epicardial mechanical stimuli were categorized as chemosensitive cardiac neurons. Mechanosensitive neurons were defined as neurons that responded to epicardial mechanical stimuli and none of the chemical stimuli. If a neuron responded to both mechanical and chemical stimuli, it was defined as a multimodal neuron consistent with previously published criteria.[15,16] The basal activities of mechanosensitive, chemosensitive, and multimodal neurons were compared in normal and infarcted animals to assess any potential differences in basal firing rates of these neurons. No significant difference was found in the basal firing rates of mechanosensitive (MI: 0.12 Hz [0.008–0.49 Hz] vs. normal: 0.16 Hz [0.10–0.38 Hz], P = 0.62), chemosensitive (MI: 0.08 Hz [0.03–0.31 Hz] vs. normal: 0.22 Hz [0.08–0.23 Hz] P = 0.48), or multimodal (MI: 1.00 Hz [0.32–3.80 Hz] vs. normal: 0.84 Hz [0.74–1.20 Hz] $P > 0.99$) neurons.

Cardiac phase-related neural activity

To assess the preferential activation of nodose neurons during specific parts of the cardiac cycle, the timing of neuronal firing relative to the phase of the left ventricular pressure was

evaluated (Figure 4). The cardiac cycle was divided into the following 4 phases: diastole, isovolumetric contraction, systole, and isovolumetric relaxation (Figure 4). Although some nodose neurons showed cardiac phase–related activity in both normal and infarcted animals, there was no significant difference in the normalized firing rates of neurons in each phase of the cardiac cycle between normal and infarcted animals (diastole: 0.19 Hz [0.11–0.30 Hz] for normal vs. 0.18 Hz [0.11–0.25 Hz] for MI animals, $P = 0.98$; isovolumetric contraction: 0.20 Hz [0.12–0.25 Hz] for normal vs. 0.14 Hz [0.08–0.27 Hz] for MI animals, $P = 0.17$; systole: 0.28 Hz [0.24–0.43 Hz] for normal vs. 0.24 Hz [0.17–0.29 Hz] for MI animals, $P = 0.10$; isovolumetric relaxation: 0.22 Hz [0.13–0.34 Hz] for normal vs. 0.33 Hz [0.06–0.43 Hz] for MI animals, $P = 0.63$) (Figure 4), suggesting that mechanotransduction of cardiac cycle pressure changes through the nodose ganglia remained intact after MIs. These findings were consistent with the absence of differences in PIEZO2 channel expression in nodose ganglia of normal versus infarcted animals.

Neuronal responses to cardiac interventions

Chemicals were applied to the anterior/ventral surface of the RV and LV in normal and RCA-infarcted animals. In healthy animals, epicardial application of chemicals (e.g., capsaicin, bradykinin, and veratridine) evoked responses in 13% of neurons, while aortic occlusion, EMS, and IVC occlusion significantly changed firing rates in 34%, 23%, and 23% of neurons, respectively. Ventricular pacing showed the greatest response (52%) in normal animals. In chronically infarcted animals, epicardial application of chemicals engaged the greatest percentage of neurons (60%), followed by ventricular pacing (43%) and aortic occlusion (37%). IVC occlusion activated 33% of cardiac related neurons, and EMS affected the activity of 26% of neurons (Figure 5). When comparing the percentage of neurons responding to specific interventions between infarcted and normal animals, significant differences were only observed in responses to nociceptive chemicals (normal: 13% vs. MI: 60%; Fisher's exact test, $P < 0.0001$). In keeping with histological findings and cardiac phase synchronization data, no functional

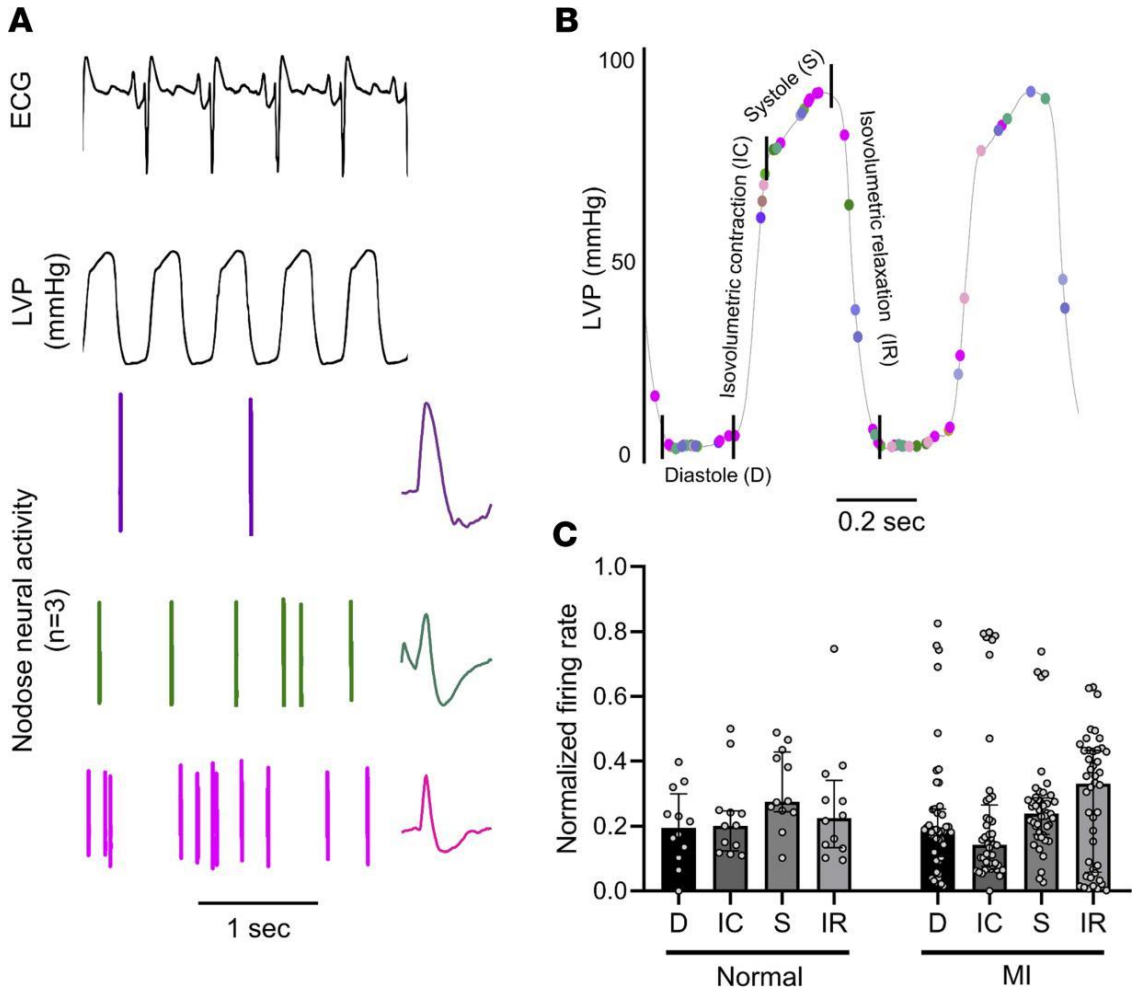

Figure 3-4. ***Cardiac phase-related neural activity.*** (**A**) Representative neural activity from 3 nodose neurons. The first neuron (top, purple) fires during isovolumetric relaxation, the one in the middle fires during systole, and the third (bottom, pink) fires stochastically. The characteristic extracellular action potential for each neuron is also shown on the right. (**B**) Cardiac phases were divided into the following 4 phases: diastole (D), isovolumetric contraction (IC), systole (S), and isovolumetric relaxation (IR). Each dot represents a neural spike, and dots with the same color represent the spiking activity from the same neuron. The position of each dot shows the LVP at each spike time. (**C**) Normalized firing rate of nodose neurons in each cardiac phase. There is no significant difference between normal and RCA-infarcted animals (n = 12 for normal and n = 44 for MI animals). Median with IQR is shown, and Mann-Whitney U statistical test was used.

differences in responses to LV or RV EMS, or to significant blood pressure changes during IVC and aortic occlusions, in normal versus infarcted animals were observed.

To further evaluate the response of cardiac nodose neurons to nociceptive stimuli, we assessed the percentage of neurons that responded to each nociceptive chemical (Figure 5).

Percentages of cardiac sensory neurons that responded to capsaicin (normal: 10% vs. MI: 30%, $P = 0.01$), bradykinin (normal: 10% vs. MI: 42%, $P < 0.001$), and veratridine (normal: 7% vs. MI: 22%, $P = 0.01$) were all increased in infarcted animals.

Excitatory and inhibitory cardiac sensory responses

Given the increased prevalence of chemosensitive neurons in infarcted animals, we further probed the magnitude of response and whether nociceptive chemicals had excitatory or inhibitory effects on cardiac vagal neurotransmission, as these responses after MI were unknown. In general, most cardiac stressors caused both excitatory and inhibitory effects on the activity of cardiac sensory neurons (Figure 5). In response to nociceptive stimuli, nodose neurons in healthy animals showed a higher incidence of excitatory responses (increase in firing rates). Although the magnitude of the absolute firing rates (regardless of activation or inhibition) was higher in response to nociceptive chemicals after MI (Supplemental Figure 4), surprisingly, the application of nociceptive chemicals in infarcted animals showed a predominantly inhibitory response (Figure 5). Unlike normal animals, the majority of the neurons in the MI animals decreased their firing rates in response to a chemical application (normal: 90% excitatory, 10% inhibitory vs. MI: 25% excitatory, 75% inhibitory, $P < 0.001$). No differences in excitatory or inhibitory responses were observed for other cardiac interventions, including aortic and IVC occlusions, where interventions caused similar excitatory and inhibitory responses in MI versus normal animals.

Since the responses to cardiac nociceptive stimuli seemed to be specifically affected after MI, additional detailed analyses of neural responses to epicardial application of each nociceptive chemical were undertaken. In normal animals, capsaicin and bradykinin both evoked purely excitatory responses from all recorded chemosensitive nociceptive neurons (i.e., an increase in firing rate was seen in these neurons in response to bradykinin and capsaicin, Figure 5). Surprisingly, in chronically infarcted animals, capsaicin evoked a significant decrease in the firing activity of 91% of recorded chemosensitive/nociceptive neurons, while bradykinin resulted in an inhibitory response in 72% of chemosensitive/nociceptive neurons ($P < 0.001$ vs. responses in

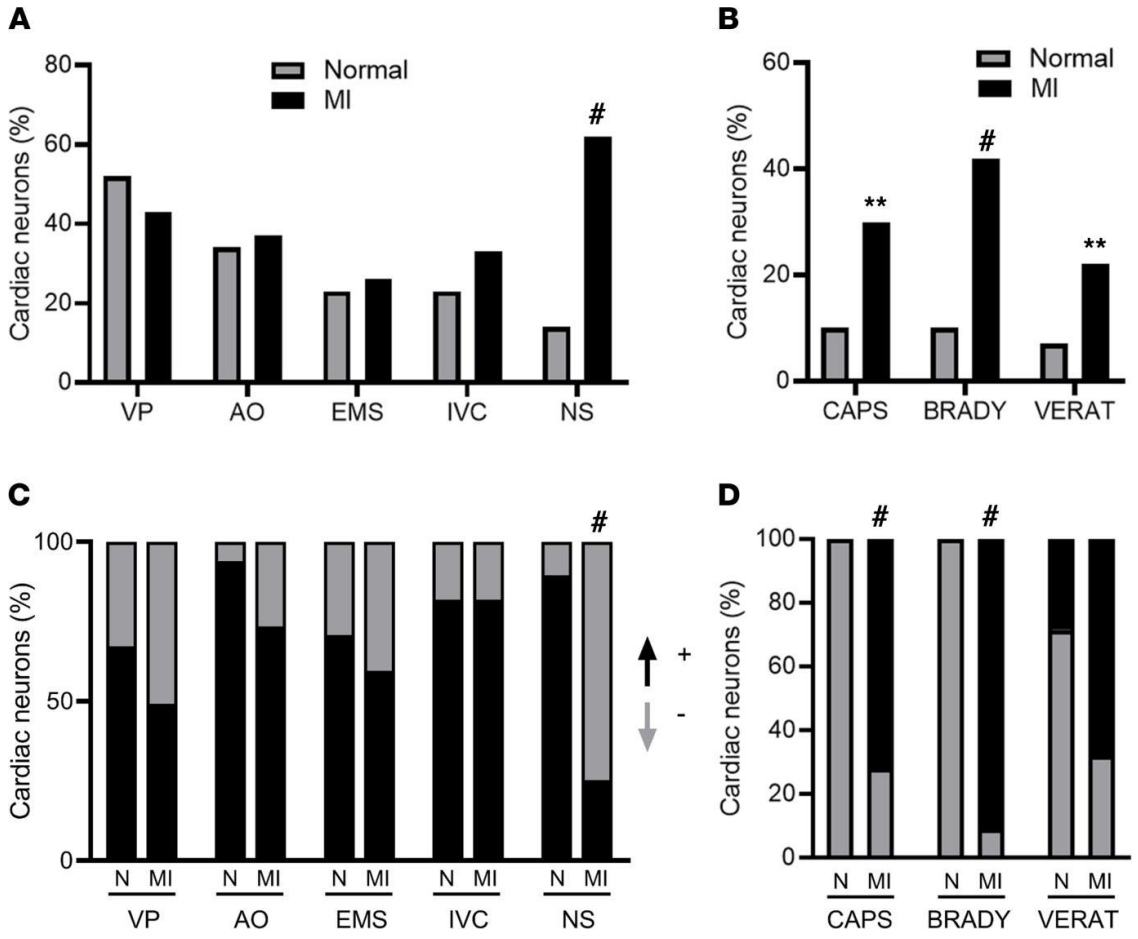

Figure 3-5. ***Nodose neural responses to specific cardiac interventions.*** (**A**) Percentages of neurons with significant changes in absolute firing rates in response to ventricular pacing (VP), aortic occlusion (AO), epicardial mechanical stimulation (EMS), inferior vena cava (IVC) occlusion, and nociceptive stimuli (NS) are shown. (**B**) Percentage of chemosensitive neurons that responded to each specific chemical stimulus is shown (capsaicin, CAPS; bradykinin, BRADY; veratridine, VERAT) in normal and MI animals. (**C**) Percentage of neurons that were excited or inhibited in response to each cardiac stressor is shown. The predominant response to nociceptive stimuli in normal animals was excitatory (an increase in firing rate: +) while the predominant response to nociceptive chemicals in RCA-infarcted animals was inhibitory (a decrease in firing rate: -). (**D**) The percentage of neurons that were excited or inhibited for each specific chemical in normal and RCA-infarcted animals is shown. Both capsaicin and bradykinin caused statistically significant decreases in firing rates. Fisher's exact test with Dunn's correction for multiple comparisons was used to compare the percentage of neurons in normal and MI animals. **$0.001 < P \leq 0.01$, $^{\#}P \leq 0.001$ compared with normal animals.

normal animals for bradykinin and capsaicin). Furthermore, cardiac sensory neurons that were inhibited by 1-minute application of nociceptive chemicals showed continued inhibition of firing

compared with baseline for up to 1 minute after removal of the chemical and cessation of stimuli (Figure 6). In normal animals, the temporal response of cardiac neurons that showed excitatory responses to nociceptive stimuli terminated after removal of the nociceptive stimulus (Supplemental Figure 5).

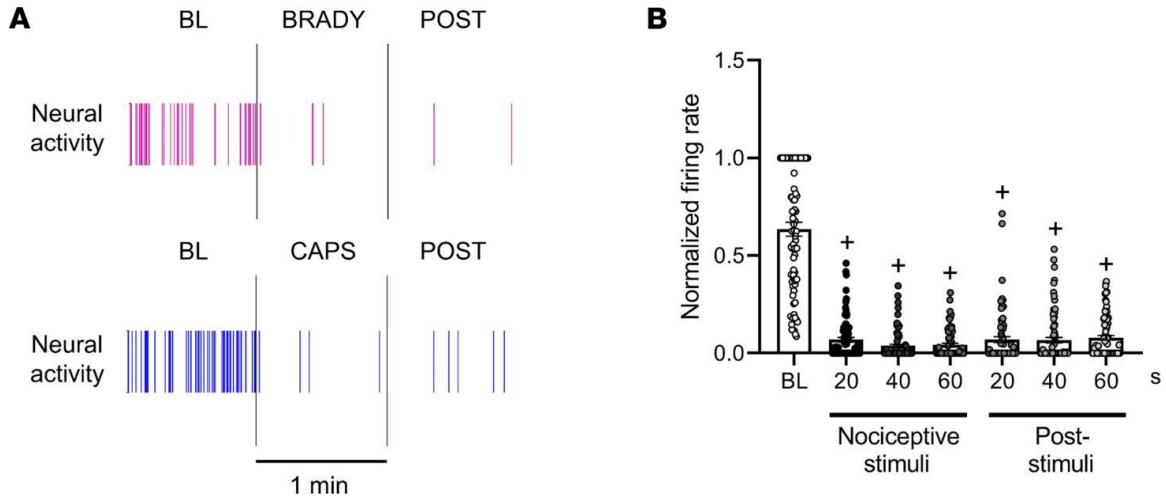

Figure 3-6. ***Temporal profile of nociceptive neural responses in infarcted animals demonstrates inhibition of firing during nociceptive chemical application of capsaicin and bradykinin, which persists after removal of the nociceptive chemical***. (**A**) Representative inhibitory response of 2 nodose neurons to bradykinin (BRADY) and capsaicin (CAPS) in a chronic RCA infarct. (**B**) Quantified temporal inhibitory responses of neurons (n = 80) to nociceptive stimuli in the RCA-infarcted animals show persistence of inhibition of neural firing rates even after removal of the stimulus/chemical. Data are shown as mean ± SEM. Dunn's multiple-comparison tests were used to compare the normalized firing rate versus baseline (BL). $^{+}P \leq 0.001$ compared with BL.

Modulation of nociceptive neurons via GABAergic expression, glial activation, and neuronal nitric oxide synthase

To determine potential alterations in neuronal phenotype that may explain why nodose nociceptive neurons from chronically infarcted animals may display an inhibitory response, we analyzed additional neurochemical changes in CGRP-positive neurons, as these neurons are involved in nociception and release CGRP upon activation of transient receptor potential cation channel subfamily V member 1 (TRPV1). Several potential neuromodulatory factors have been shown to affect the activity of nociceptive neurons in other sensory ganglia (i.e., dorsal root

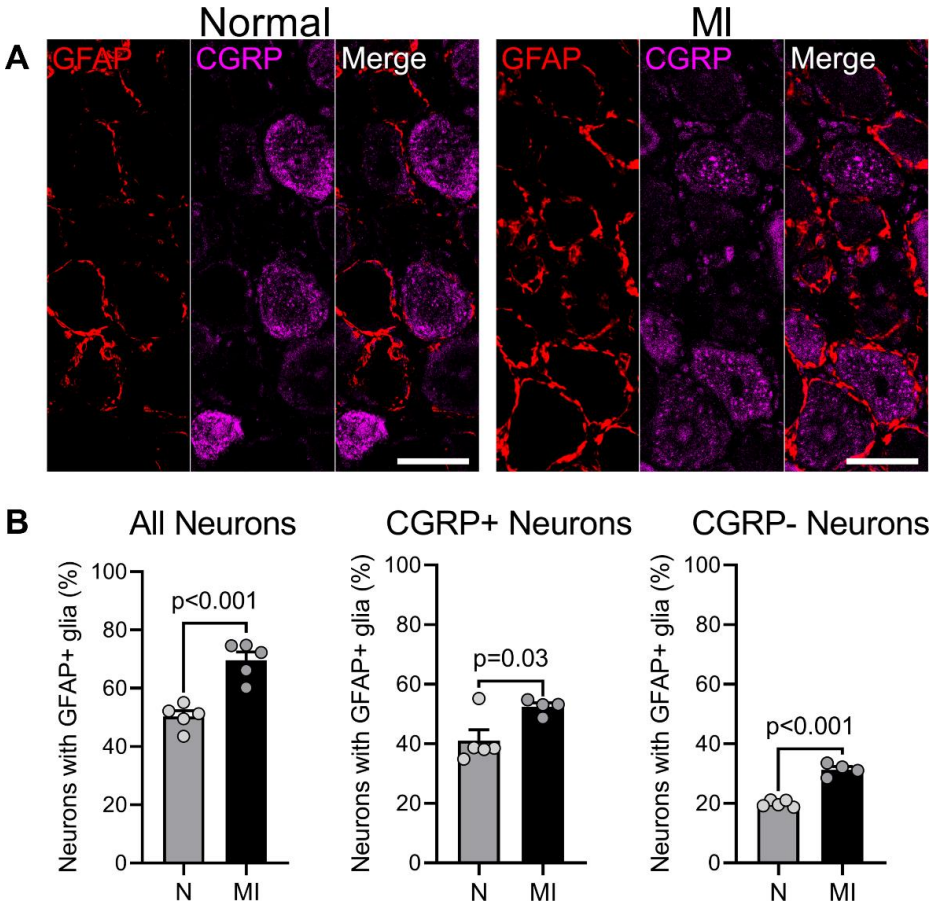

Figure 3-7. ***Non-selective augmentation of satellite glial cell activation following myocardial infarction in the nodose ganglia.*** (**A**) Representative images of nodose ganglia from normal (N; left) and LAD-infarcted (MI; right) pigs stained for GFAP (red) and CGRP (purple). (**B**) Summary of the percentage of neurons surrounded by GFAP$^+$ satellite glial cells as a subset of all neurons, CGRP$^+$ neurons, and CGRP$^-$ neurons is shown. There was a statistically significant increase in GFAP expression after MI ($P < 0.001$ for infarcted vs. normal animals). This was, however, true for both CGRP-positive ($P = 0.03$ for infarcted vs. normal animals) and CGRP-negative neurons ($P < 0.001$ for infarcted vs. normal animals). $n = 5$ pigs per group in all neurons. $n = 5$ normal pigs and $n = 4$ for MI animals for coexpression. Data are shown as mean ± SEM; unpaired, 2-tailed Student's *t* test was used for comparisons. Scale bars are 50 μm.

ganglia). These include glial activation, changes in GABA expression, and reduction in NOS1.[17-19] We first determined the expression of glial fibrillary acidic protein (GFAP) in nodose ganglia and then its expression in satellite glia cells that encircled CGRP-expressing nodose neurons in normal versus infarcted animals. GFAP expression was significantly increased in the ganglia from infarcted animals (MI animals 69.6% ± 2.8% vs. 50.3% ± 1.9% in normal animals, $P < 0.001$), but these differences were observed for both CGRP-expressing and CGRP-negative neurons,

suggesting a more global phenotype after MI (Figure 7 and Supplemental Figure 6). Given that nociceptive signaling was largely altered after MI, the global changes in observed GFAP expression, thus, were unlikely to be a primary reason for alterations in nociceptive neurotransmission.

GABA is another known neuromodulator in peripheral sensory autonomic ganglia seen to be expressed by neurons of the trigeminal, nodose, and dorsal root ganglia (DRG).[19,20] In DRG, GABA has been reported to produce a net inhibitory effect on peripheral nociceptive neurotransmission.[19] In nodose neurons, these effects of GABA have further been shown to be nonsynaptically mediated, spreading between neurons and glia.[21] Given previous findings that GABA may perhaps induce global vagal silencing and our in vivo functional findings, changes in GABAergic expression in the nodose ganglia after MI were evaluated. No differences in expression of GABA or glutamic acid decarboxylase (GAD2), the enzyme required for GABA synthesis, were noted in the nodose ganglion globally (Figure 8 and Supplemental Figure 7). However, a significant increase in the percentage of CGRP-positive neurons that coexpress GABA (34.0% ± 3.9% in MI vs. 20.2% ± 3.1% in normal, $P = 0.02$) and GAD2 was observed (41.6% ± 3.4% in MI vs. 31.6% ± 2.3% in normal, $P = 0.04$) after MI. Interestingly, CGRP-negative neurons demonstrated decreased expression of GAD2 (17.2% ± 1.2% in MI vs. 26.2% ± 2.1% in normal, $P = 0.006$) in infarcted compared with normal animals. suggesting that GABA may be a factor in the greater inhibitory responses observed to nociceptive chemicals. In addition, as the presence of GABA type B receptors, and especially the GABBR1 subunit, had not been previously described in the nodose ganglia of larger mammals to our knowledge, we confirmed the presence of GABBR1 in these ganglia and found that approximately 70%–80% of CGRP-expressing neurons also expressed GABBR1 in both normal and infarcted pigs (Figure 8 and Supplemental Figure 7).

Finally, NOS1, another known autonomic and afferent neuromodulator, was globally decreased following MI (Figure 1), and we evaluated whether these alterations were specific to CGRP-expressing neurons and may explain the differences in observed functional responses.

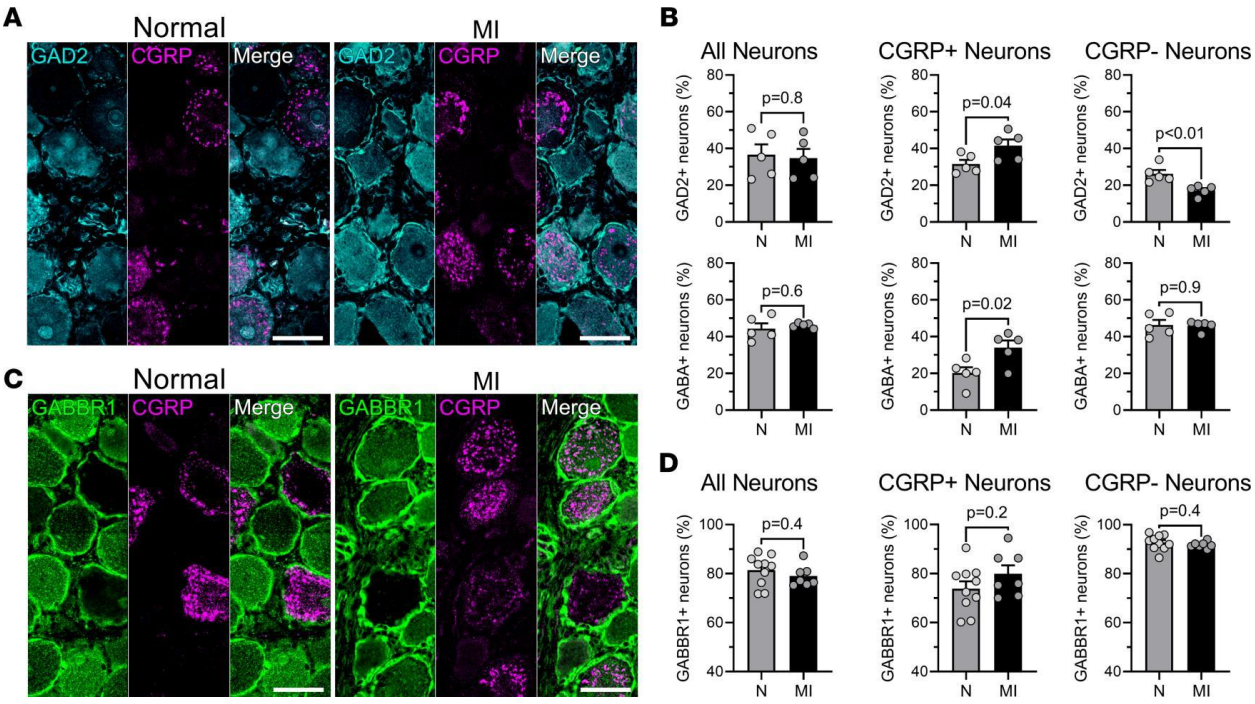

Figure 3-8. ***Upregulation of inhibitory GABAergic neurotransmission specifically in CGRP-expressing nodose ganglia neurons involved in nociceptive neurotransmission***. (**A**) Representative images of nodose ganglia from normal (N; left) and LAD-infarcted (MI; right) animals stained for GAD2 (blue) and CGRP (purple). (**B**) *Top,* summary of the percentage of $GAD2^+$ neurons as a subset of all neurons, $CGRP^+$ neurons, and $CGRP^-$ neurons is shown. Although overall expression of GAD2 was unchanged between normal and LAD-infarcted animals ($P = 0.80$), the percentage of neurons that coexpress both GAD2 and CGRP was increased after MI ($P = 0.04$ for LAD-infarcted vs. normal animals). Coexpression of GAD2 was decreased in neurons that do not express CGRP ($P = 0.006$ for normal vs. LAD-infarcted animals). $n = 5$ pigs per group. *Bottom,* summary of the percentage of $GABA^+$ neurons as a subset of all neurons, $CGRP^+$ neurons, and $CGRP^-$ neurons is shown. Similar to GAD2, GABA showed no overall difference ($P = 0.57$) while its expression in $CGRP^+$ neurons was increased ($P = 0.02$) in MI animals. However, expression of GABA in $CGRP^-$ neurons was similar between normal and MI animals ($P = 0.89$). (**C**) Representative images of nodose ganglia from normal (left) and LAD-infarcted (right) pigs stained for GABA type B receptor subunit 1 (GABBR1) (green) and CGRP (purple). There was no difference in the expression of GABBR1. $n = 5$ pigs per group. (**D**) Summary of the percentage of $CGRP^+$ neurons with $GABBR1^+$ expression ($P = 0.21$). $n = 10$ for normal and $n = 7$ for MI animals. Data are shown as mean ± SEM; unpaired, 2-tailed Student's *t* test. Scale bars are 50 μm.

Despite an overall decrease in NOS1 expression after MI, nociceptive CGRP neurons were not selectively affected (19.7% ± 1.6% in normal vs. 25.5% ± 2.4% in MI; $P = 0.07$, Supplemental Figure 8).

DISCUSSION

To our knowledge, this is the first study to evaluate the effects of chronic MI on vagal afferent neurotransmission using both functional (direct in vivo neural recordings) and immunohistochemical data. A major finding of this study is that, while the percentage of nociceptive neurons was increased after MI, as assessed by histological and functional responses, the predominant response observed in infarcted animals was significant inhibition ($P < 0.01$) of neural activity with application of nociceptive chemicals. This was significantly different from normal animals, in whom the predominant response was excitatory. This potentially novel finding has important implications for vagal dysfunction. In addition, for the first time to our knowledge, we show that both LAD and RCA myocardial infarcts caused pathological changes in the expression profiles of neurons of the right and left nodose ganglia. No differences between the right versus left nodose ganglia (i.e., no laterality) were observed with respect to neuronal receptors, peptides, or functional responses to cardiac interventions, suggesting that infarction of a particular region of the heart has global effects on both ganglia. This study also demonstrates that the proportion of PIEZO2-expressing neurons was unchanged after MI; consistent with these findings, the functional neuronal responses to EMS, IVC occlusion, and aortic occlusion were comparable between normal and infarcted animals. Similarly, specific differences were not found in cardiac phase–related neuronal activity between infarcted and normal pigs. Finally, the percentage of CGRP-positive neurons that express GABA was significantly increased ($P = 0.02$) after MI, which may suggest that GABA may play a role in the functional differences in nociception observed after MI.

The autonomic nervous system controls every aspect of cardiac function. Sensory pseudounipolar neurons in DRG and nodose ganglia contain a diverse population of chemosensitive and mechanosensitive neurons that sense the cardiac milieu and transmit this information to the spinal cord and brainstem, respectively.[1,5,22-24] Activation of nociceptive neurons

in DRG increases sympathetic tone, while activation of nociceptive neurons in nodose ganglia increases the central vagal drive to the heart.[25-28] Therefore, the effects of cardiac nociceptive stimuli in normal animals are determined by the balance between sympathetic and vagal output. It is established that chronic MI leads to reduced vagal drive, increasing the risk of ventricular arrhythmias and heart failure. Augmenting vagal drive via vagal nerve stimulation has been shown to be antiarrhythmic in animal models.[5,6,29,30] Yet, mechanisms behind central vagal dysfunction after MI are unknown. We hypothesized that MI, as a form of chronic injury, similar to chronic pain conditions that cause remodeling in DRG, may cause alterations in nodose ganglia signaling that then drive reduced vagal function. Toward this goal, an investigation was undertaken in a large-animal (porcine) model to assess both structural and functional changes after chronic MI. This animal model has been established to undergo neural, electrical, and cardiac remodeling that is very similar to humans after MI.[5,31,32]

Different markers for mechano- and chemotransduction were utilized in this study. PIEZO2 receptors on neurons in the nodose ganglia are thought to sense visceral and cardiovascular mechanical stretch,[33,34] and expression of PIEZO2 was used as a marker for mechanosensitive neurons. In this study, no histological differences or functional changes, as assessed by cardiac phase–related activity or transduction of pressure-associated interventions, in mechanosensitivity of vagal afferents were observed. Of note, in our model of MI, hypertension and significant LV hypertrophy do not occur, and it is possible that in the setting of hypertensive heart disease, PIEZO2-sensitive neurons in the nodose ganglia may remodel, as suggested by a mouse model of aortic constriction.[35]

In this study, in healthy animals, nociceptive stimuli engaged the lowest number of neurons (10% of all identified cardiac neurons), suggesting a high threshold for activation of these neurons in the setting of a normal heart. The responses observed were predominantly excitatory. In animals after MI, however, the same application of nociceptive chemicals affected the activity of a greater proportion (48%) of all cardiac neurons, and the predominant responses observed

were inhibitory. It has also been previously shown that acute application of nociceptive chemicals, such as capsaicin, bradykinin,[36,37] and veratridine,[38] causes neuronal depolarization and predominantly increases in activity and firing rates of the majority of nociceptive neurons in the peripheral autonomic ganglia when evaluated either in vivo or using whole-cell voltage-clamp recordings.[39,40] In vivo nodose recordings from guinea pigs with healthy hearts, which were consistent with the healthy porcine animal data in this study, showed that epicardial application of bradykinin activated the majority (74%) of identified cardiac nociceptive neurons, with a decrease in firing rate observed in only 26% of recorded neurons.[22] Unexpectedly, neuronal analyses of cardiac sensory nodose neuronal activity after chronic MI showed that application of nociceptive chemicals caused a predominantly inhibitory response in the vast majority of recorded chemosensitive neurons. For all other cardiac stressors except nociceptive stimuli, the percentages of inhibitory and excitatory responses were not different in normal versus infarcted animals. This was despite the application of these chemicals to viable, noninfarcted regions of the heart and has significant implications for vagal neurotransmission, given that excitatory responses by nociceptive chemicals are known to increase vagal tone. For example, a nociceptive stimulus, such as a second ischemic insult, in an already diseased heart would lead to a reduction in vagal tone (as opposed to an increase), further increasing the risk of ventricular arrhythmias. Although the effect of ischemia was not assessed in this study, given the complex responses to ischemia that involve activation of both mechano- and chemosensitive neurons, the neuropeptides and receptors evaluated, including CGRP and P2RX3, are known to be released and activated during ischemia, respectively.[41] In addition to ischemia-induced release of ATP, which activates P2RX3 receptors, release of CGRP is known to occur with activation of TRPV1 receptors because of the low pH ischemia causes. Finally, ischemia also leads to release of bradykinin.[42] Thus, it’s reasonable to assume that given altered responses to nociceptive chemicals, vagal afferent responses due to ischemia would be altered in infarcted animals.

The reason for the inhibitory neural response observed in chronically infarcted animals requires further investigation, but greater expression of GABA may play a role.[19,20,43,44] GABA is known to reduce nociceptive neurotransmission through DRG, where activation of TRPV1 nociceptive neurons releases not only CGRP but also GABA upon binding of chemicals such as capsaicin.[45] GABA was reported to act on TRPV1-coupled GABBR1 of these neurons, reducing further activation, not only of the same neuron but also of nearby nociceptive neurons, in a negative feedback fashion.[43] In this study, a greater percentage of CGRP-positive neurons in the nodose after MI expressed GABA compared with controls. Therefore, it is possible that remodeling of nodose neurons after chronic MI that leads to greater expression and release of GABA by CGRP-expressing nodose neurons may inhibit surrounding TRPV1 receptors/CGRP-positive neurons, resulting in more inhibitory functional responses.[19] In this study, we further show that nodose neurons also express the GABBR1, with a large percentage (approximately 70%–80%) of CGRP-expressing neurons coexpressing GABBR1 in this large-animal model.

In this study, we investigated several other immunohistochemical changes that are thought to modulate peripheral neurotransmission to see if they were responsible for functional changes that were observed in nociceptive neurons. Activation of satellite glial cells in response to injury, as reflected by increased GFAP (a reactive cytoskeletal protein), has been shown to modulate neuronal excitability and function in other peripheral ganglia.[17,46] In this study, although an increase in GFAP globally in the nodose ganglia after MI was also observed, this increase was not selective for CGRP-expressing neurons. Finally, nitric oxide is an important neuromodulatory molecule, and a decrease in neuronal nitric oxide synthase can alter neuronal signaling.[47] Nitric oxide in the nodose ganglia is thought to enhance cholinergic neurotransmission[18,48] and improve baroreceptor sensitivity.[49] Reduction in release of NOS1, therefore, could potentially decrease sensory afferent transduction. However, NOS1 expression, although reduced globally, did not selectively affect CGRP-expressing neurons and tended to affect CGRP-negative neurons.

In summary, this is the first study to our knowledge to show that chronic MI causes both structural and functional changes in vagal afferent nociceptive signaling that can exacerbate parasympathetic dysfunction and reduce vagal tone. Responses to nociceptive stimuli were overall inhibitory, rather than excitatory, a change that may be mediated by increased GABAergic expression in nociceptive neurons. Inhibitory responses in vagal afferent signaling would result in decreased central vagal efferent drive and may explain why patients after MI experience parasympathetic dysfunction, increased risk of ventricular arrhythmias, and associated sudden death. Future studies following up on specific alterations reported herein will likely shed further light on the effects of MI on the activity of specific types of vagal neurons and modulation of a specific pathway.

Our study has limitations. General anesthesia is known to suppress neuronal activity. In this study, after completion of surgical procedures, isoflurane was discontinued and α-chloralose used as an alternative anesthetic agent to minimize the effects of isoflurane. Nevertheless, it is possible that the neuronal responses in this study are a conservative estimate of those that would be observed in conscious animals. For neural recordings, an RCA infarct model was used in order to allow for epicardial application of mechanical/chemical stimuli on the viable, accessible ventral regions of the ventricles. It is possible that the application of chemicals to infarcted regions would lead to different responses. Given the lack of previous data on post-MI alterations in nodose signaling, viable regions were studied in order to avoid effects that may be caused by denervation and fibrosis. Acute effects of stimuli were evaluated. Cardiac neural responses to chronic stimuli may be different due to neuronal memory or remodeling of receptors. Direct staining for TRPV1 expression was not performed, given the lack of specific antibodies in the porcine model, and CGRP expression was used as a surrogate for TRPV1. It is, however, established that the large majority of TRPV1-expressing neurons express and release CGRP.[50,51] In this study, assessment of efferent vagal tone using direct vagal efferent nerve recordings was not performed, and given the short duration (1 minute) of interventions, heart rate variability analysis during stimuli was not

appropriate. However, using the same infarct model and direct intrinsic cardiac neural recordings from postganglionic intrinsic cardiac parasympathetic neurons, our laboratory has shown previously that central vagal tone and inputs to intrinsic cardiac ganglia neurons are altered, consistent with decreased central vagal drive.[5] In a canine infarct model, lower central vagal drive during ischemia is associated with the occurrence of ventricular fibrillation.[52] Finally, direct application of GABA agonists or antagonists was not performed to confirm restoration of nociceptive neurotransmission in infarcted animals. Therefore, although the findings of this study are suggestive, the role of GABA in nociceptive neurotransmission within the vagal ganglia requires confirmation in future studies.

METHODS

Yorkshire pigs (Premier BioSource) were used for histological evaluation and in vivo nodose neural recording. For histological assessment, normal Yorkshire pigs (*n* = 22, 52.1 ± 2.5 kg, 20 males) and Yorkshire pigs with healed anterior/apical (ventral) MI involving the LAD (*n* = 24, 58.6 ± 2.9 kg, 22 males) or inferior/dorsal MI involving the RCA (*n* = 7, 56.9 ± 3.0 kg, 7 males) were used (Supplemental Table 2). For extracellular nodose neural recordings, normal Yorkshire pigs (*n* = 11, 58.2 ± 3.2 kg, 9 males) and Yorkshire pigs with healed RCA myocardial infarcts (*n* = 11, 59.5 ± 1.7 kg, 9 males) were used.

Creation of myocardial infarcts

Percutaneous MI in the region of RCA was created in 42 pigs (30–35 kg) as previously described.[5,12] Briefly, animals were sedated (tiletamine-zolazepam, 4–8 mg/kg IM), intubated, and placed under general anesthesia with isoflurane (1%–5% inhaled). For RCA infarcts, under fluoroscopic guidance, an 8F AL2 guide catheter (Boston Scientific) was advanced from the femoral artery to the ostium of the RCA. A 2.5 to 3.5 mm percutaneous transluminal angioplasty balloon catheter (Abbott) was advanced over a balance middleweight universal guidewire (Abbott) into the RCA and positioned after the takeoff of the atrioventricular nodal artery (Figure 1). The

balloon was inflated, and 3–5 mL of polystyrene microspheres (Polybead 90.0 μm, Polysciences) followed by 5 mL normal saline were injected through the lumen of the catheter. The balloon was then deflated and removed. MI was confirmed by the presence of ST elevation or T wave inversion on ECG and coronary angiography showing a lack of flow in the artery (Figure 1). After the procedure, ECG and blood pressure were monitored for 20 minutes before extubation. Immediate external defibrillation was performed if the animal developed VT or fibrillation. After extubation, animals were monitored until they could ambulate.

For LAD infarcts, a similar procedure was performed, but the AL2 was used to cannulate the ostium of the left main coronary artery and a balance middleweight universal wire advanced into the LAD, instead of the RCA. The percutaneous transluminal angioplasty balloon catheter was inflated after the first diagonal branch, followed by microsphere injection.[5,12] Six to eight weeks were allowed for maturation of MI in all infarcted animals prior to terminal studies.

Immunohistochemical analysis

Animals were sedated, intubated, and placed under anesthesia as described above. Lateral neck dissections were performed, and the vagus nerve was isolated bilaterally. The nerve was followed superiorly, and the inferior vagal (nodose) ganglia were identified (Figure 1). Bilateral nodose ganglia from infarcted animals 6–8 weeks post-MI and from normal animals of similar weight were removed. Ganglia were fixed in 4% paraformaldehyde for 24 hours at 4°C and then embedded in paraffin. Tissue was sectioned (5 μm) longitudinally, and midsections of each ganglion with the largest cross-sectional area were used for staining. Sections were deparaffinized in 2 xylene washes followed by rehydration in 3 ethanol washes and water. Antigen retrieval was performed using EDTA buffer, pH 8.0 (90°C for 20 minutes; ab64216; Abcam). Slides were blocked for 1 hour in 3% BSA-TBS-0.2% Triton X-100 with 5% donkey serum and incubated overnight at 4 °C with primary antibody (Supplemental Table 2). Slides were subsequently incubated for 1 hour at room temperature with the appropriate affinity-purified $F(ab')_2$ fragment secondary antibody (Supplemental Table 2). Subsequent steps varied depending on the method of detection. For

immunofluorescence, slides were counterstained and mounted using Vectashield with DAPI (Vector Laboratories; H-1200). Slides were imaged at ×100 original magnification (×10 objective, ×10 eyepiece) using a Zeiss LSM 880 with Airyscan. For bright-field detection, the avidin-biotin complex method (PK-6100; Vector Laboratories) of signal amplification followed by 3,3′-diaminobenzidine to induce chromogenic color development was used. Slides were then counterstained with Harris's hematoxylin, dehydrated, and mounted with Permount (Fisher Chemical, Thermo Fisher Scientific; SP15-100). Slides were imaged at ×400 magnification (×40 objective, ×10 eyepiece) using an Aperio ScanScope AT (Leica Biosystems). The number of nodose neurons or glia expressing a particular antigen was quantified (NIH ImageJ 1.8.0) by 2 independent researchers. Data from left and right nodose were analyzed both by individual ganglia and by animal. All scale bars shown in figures are 50 μm.

Surgical preparation for neural recording experiments

Animals were sedated, intubated, and placed under anesthesia as described above. Isoflurane was used for surgical procedures/sternotomy and transitioned to α-chloralose (MilliporeSigma; 50 mg/kg initial bolus, after that 20–35 mg/kg/h IV) for the neural recording portion of experiments. Depth of anesthesia was adjusted based on corneal reflex, jaw tone, and hemodynamics indices. Peripheral capillary oxygen saturation (SpO_2), end-tidal CO_2, and arterial blood gases were monitored throughout the experiments; tidal volume and/or respiratory rate were adjusted or sodium bicarbonate (HCO_3) was administered to maintain a normal pH. Body temperature was monitored and adjusted using a water heating pad (Gaymar T/Pump, Gaymar Inc.). The CardioLab System (GE Healthcare) was used to record continuous 12-lead ECGs. Ventral precordial leads were placed posteriorly given sternotomy. The femoral and carotid arteries were cannulated to measure blood pressure and obtain access to the LV for pressure recordings, respectively. Sheaths were placed in the femoral veins for delivery of medications and saline. ECG, arterial pressure, and LVP were digitized (Power 1401, Cambridge Electronic Design); stored; and analyzed off-line (Spike2, Cambridge Electronic Design). Fentanyl boluses

(20–30 mcg/kg) were used during sternotomy to reduce discomfort. Sodium pentobarbital (Med-Pharmex Inc.; 100 mg/kg IV) followed by saturated KCl (MilliporeSigma; 1–2 mg/kg IV) was used for euthanasia.

Nodose neuronal activity recordings

For in vivo extracellular neural recordings of the nodose ganglia, vagi were kept intact during neural recordings. Custom-made 16-channel linear microelectrode arrays (MicroProbes; 25 μm diameter platinum/iridium electrodes, 16 electrodes/probe, 250 μm interelectrode spacing) were gently advanced into the nodose ganglia and connected to a 16-channel preamplifier (NeuroNexus). Neural signals were sampled at 20 kHz, amplified, and digitized (SmartBox acquisition system, NeuroNexus). The signals were filtered (300 Hz to 10 kHz). In vivo soma activity of individual neurons was assessed at baseline and during each cardiovascular intervention. Activity from axons of passage was not recorded, as with high-impedance neural probes, it is not possible to record axonal action potentials.[10] Linear microelectrode arrays position was adjusted if no cardiac-related neuronal activity was observed.

Cardiovascular interventions

To characterize and identify cardiovascular nodose neurons, the following cardiovascular stimuli were applied: ventricular epicardial i) mechanical and ii) nociceptive (capsaicin, bradykinin, veratridine) stimuli, iii) ventricular pacing, iv) IVC occlusion, and v) descending aortic occlusion. Interventions were performed in a random order in all animals; however, application of chemical stimuli was performed last, and in particular, the application of capsaicin was performed as the last intervention in each experiment, given previous data suggesting that capsaicin may alter afferent transduction to subsequent stimuli. A 15- to 30-minute waiting period was allowed for hemodynamic indices to return to baseline between interventions.

Ventricular epicardial mechanical stimuli

To identify nodose ganglia neurons that respond to mechanical stimuli, gentle pressure (~10 g/cm^2) was applied to the right and left anterior ventricular epicardium for 15 seconds via a saline-soaked cotton-tipped applicator.

Ventricular epicardial nociceptive stimuli

Nociceptive neurons were identified by assessing the response of nodose neurons to a 1-minute application of gauze soaked in bradykinin (1.06 mg/mL), capsaicin (0.03 mg/mL), or veratridine (0.67 mg/mL), placed on the ventral (anterior) aspect of the left and right ventricular epicardium.

Ventricular pacing

The right ventricle was paced endocardially for 1 minute at 15% above the baseline heart rate and intermittently every 4–7 beats with random/variable coupling intervals (300–600 ms) via a quadripolar catheter (Abbott) placed from the femoral vein and attached to a cardiac stimulator (EPS320, MicroPace).

Great vessel occlusions

The IVC and then descending aorta were occluded for 30 seconds via 2 umbilical tapes placed around the IVC and descending aorta. Afferent neural responses to changes in preload and afterload were evaluated.

Neural signal processing and analysis

Neural signals were processed using Spike2 software (Cambridge Electronic Design, Cambridge, England).[5,15,16] Artifacts were identified and removed by detecting similar and simultaneous waveforms on all neural channels. Neural spikes were identified using a threshold of 3× signal-to-noise ratio. Spike classification was performed using principal component, cluster on measurements, and K-means clustering analysis. The spiking activity of each individual neuron was obtained for the entire experiment and transferred to MATLAB (MathWorks) for post hoc neural analysis.

Neuronal responses to each intervention were assessed by comparing the neural activity at baseline (1 minute) to “during the intervention” using the Skellam statistical test.[14] Cardiac related neurons were identified as those that significantly responded to at least 1 cardiovascular stressor. All non–cardiac related neurons were excluded from post hoc analysis. Neurons that responded to at least 1 ventricular epicardial chemical stimuli and none of the epicardial mechanical stimuli were labeled as chemosensitive cardiac neurons. Neurons that responded to nociceptive chemicals (capsaicin, bradykinin, and veratridine) were classified as nociceptive chemosensitive neurons. Mechanosensitive neurons were defined as neurons that responded to the epicardial mechanical stimuli and none of the chemical/nociceptive stimuli. If a neuron responded to both ventricular epicardial mechanical and chemical stimuli, it was classified as a multimodal neuron.

Statistics

Neuronal responses to interventions were assessed by Skellam’s significant test, which has been validated for neural activity in nodose and other peripheral ganglia,[5,15,16] as well as the central nervous system.[14] Neural responses to different cardiovascular stressors were compared using Fisher’s exact test. Anderson-Darling test was used to check data for normality of distribution. Paired data were compared using 2-tailed Student’s paired *t* test or Wilcoxon’s signed-rank test, depending on the distribution. Unpaired data (normal vs. MI) were compared using unpaired *t* test or Mann-Whitney *U* test, depending on Gaussian distribution. For histological data, comparison of molecular expression profiles between normal and infarcted animals was performed using unpaired, 2-tailed Student’s *t* test. Phenotypic comparisons within an animal (e.g., left vs. right) were performed using paired, 2-tailed Student’s *t* test. Benjamini-Hochberg method was used to correct for the false discovery rate. Dunn’s multiple-comparison test was used to compare neural firing rates at baseline with multiple time points. Prism (GraphPad) was used for all statistical analyses. Data are presented as mean ± SEM or median and IQR [25th, 75th percentiles]. A $P \leq 0.05$ was considered significant.

Study approval

Animal experiments were performed in accordance with the NIH *Guide for the Care and Use of Laboratory Animals* (National Academies Press, 2011) and approved by the UCLA Chancellor's Animal Research Committee.

ACKNOWLEDGMENTS

We would like to thank Dr. Koji Yoshie and Ms. Janki Mistry for their technical assistance with experiments. We would like to thank Dr. Kalyanam Shivkumar for his guidance and support.

FUNDING SUPPORT AND AUTHOR DISCLOSURES

This work was supported by NIH DP2HL132356, NIH R01HL148190, and SPARC OT2OD023848 to MV and JAA; Uehara Memorial Foundation postdoctoral fellowship and Nihon University Graduate School of Medicine international research fellowship to NY; and Quebec Nature and Technology Research Fund postdoctoral scholarship to SS.

REFERENCES

1 Jänig, W. The integrative action of the autonomic nervous system: neurobiology of homeostasis. 2006. The integrative action of the autonomic nervous system: neurobiology of homeostasis, 1-610.

2 Shen, M. J. & Zipes, D. P. Role of the autonomic nervous system in modulating cardiac arrhythmias. Circ Res 114, 1004-1021, doi:10.1161/CIRCRESAHA.113.302549 (2014).

3 Vaseghi, M. & Shivkumar, K. The role of the autonomic nervous system in sudden cardiac death. Prog Cardiovasc Dis 50, 404-419, doi:10.1016/j.pcad.2008.01.003 (2008).

4 Wu, P. & Vaseghi, M. The autonomic nervous system and ventricular arrhythmias in myocardial infarction and heart failure. Pacing Clin Electrophysiol 43, 172-180, doi:10.1111/pace.13856 (2020).

5 Vaseghi, M. et al. Parasympathetic dysfunction and antiarrhythmic effect of vagal nerve stimulation following myocardial infarction. JCI Insight 2, doi:10.1172/jci.insight.86715 (2017).

6 Yamakawa, K. et al. Electrophysiological effects of right and left vagal nerve stimulation on the ventricular myocardium. Am J Physiol Heart Circ Physiol 307, H722-731, doi:10.1152/ajpheart.00279.2014 (2014).

7 Kleiger, R. E., Miller, J. P., Bigger Jr, J. T. & Moss, A. J. Decreased heart rate variability and its association with increased mortality after acute myocardial infarction. The American journal of cardiology 59, 256-262 (1987).

8 La Rovere, M. T. et al. Baroreflex sensitivity and heart-rate variability in prediction of total cardiac mortality after myocardial infarction. The Lancet 351, 478-484 (1998).

9 Fallen, E. L. Vagal afferent stimulation as a cardioprotective strategy? Introducing the concept. Annals of Noninvasive Electrocardiology 10, 441-446 (2005).

10 Salavatian, S. et al. Premature ventricular contractions activate vagal afferents and alter autonomic tone: implications for premature ventricular contraction-induced cardiomyopathy. Am J Physiol Heart Circ Physiol 317, H607-H616, doi:10.1152/ajpheart.00286.2019 (2019).

11 Armour, J. A. Cardiac neuronal hierarchy in health and disease. Am J Physiol Regul Integr Comp Physiol 287, R262-271, doi:10.1152/ajpregu.00183.2004 (2004).

12 Irie, T. et al. Cardiac sympathetic innervation via middle cervical and stellate ganglia and antiarrhythmic mechanism of bilateral stellectomy. Am J Physiol Heart Circ Physiol 312, H392-H405, doi:10.1152/ajpheart.00644.2016 (2017).

13 Bagriantsev, S. N., Gracheva, E. O. & Gallagher, P. G. Piezo proteins: regulators of mechanosensation and other cellular processes. J Biol Chem 289, 31673-31681, doi:10.1074/jbc.R114.612697 (2014).

14 Shin, H. C., Aggarwal, V., Acharya, S., Schieber, M. H. & Thakor, N. V. Neural decoding of finger movements using Skellam-based maximum-likelihood decoding. IEEE Trans Biomed Eng 57, 754-760, doi:10.1109/TBME.2009.2020791 (2010).

15 Beaumont, E. et al. Network interactions within the canine intrinsic cardiac nervous system: implications for reflex control of regional cardiac function. J Physiol 591, 4515-4533, doi:10.1113/jphysiol.2013.259382 (2013).

16 Rajendran, P. S. et al. Myocardial infarction induces structural and functional remodelling of the intrinsic cardiac nervous system. J Physiol 594, 321-341, doi:10.1113/JP271165 (2016).

17 Hanani, M. & Spray, D. C. Emerging importance of satellite glia in nervous system function and dysfunction. Nat Rev Neurosci 21, 485-498, doi:10.1038/s41583-020-0333-z (2020).

18 Danson, E. J., Choate, J. K. & Paterson, D. J. Cardiac nitric oxide: emerging role for nNOS in regulating physiological function. Pharmacology & therapeutics 106, 57-74, doi:10.1016/j.pharmthera.2004.11.003 (2005).

19 Du, X. et al. Local GABAergic signaling within sensory ganglia controls peripheral nociceptive transmission. J Clin Invest 127, 1741-1756, doi:10.1172/JCI86812 (2017).

20 Stoyanova, II. Gamma-aminobutiric acid immunostaining in trigeminal, nodose and spinal ganglia of the cat. Acta Histochem 106, 309-314, doi:10.1016/j.acthis.2004.05.001 (2004).

21 Shoji, Y., Yamaguchi-Yamada, M. & Yamamoto, Y. Glutamate- and GABA-mediated neuron-satellite cell interaction in nodose ganglia as revealed by intracellular calcium imaging. Histochem Cell Biol 134, 13-22, doi:10.1007/s00418-010-0711-0 (2010).

22 Thompson, G. W., Horackova, M. & Armour, J. A. Chemotransduction properties of nodose ganglion cardiac afferent neurons in guinea pigs. Am J Physiol Regul Integr Comp Physiol 279, R433-439 (2000).

23 Hoover, D. B., Shepherd, A. V., Southerland, E. M., Armour, J. A. & Ardell, J. L. Neurochemical diversity of afferent neurons that transduce sensory signals from dog ventricular myocardium. Auton Neurosci 141, 38-45, doi:10.1016/j.autneu.2008.04.010 (2008).

24 Kupari, J., Haring, M., Agirre, E., Castelo-Branco, G. & Ernfors, P. An Atlas of Vagal Sensory Neurons and Their Molecular Specialization. Cell Rep 27, 2508-2523 e2504, doi:10.1016/j.celrep.2019.04.096 (2019).

25 Lombardi, F., Patton, C. P., Della Bella, P. D., Pagani, M. & Malliani, A. Cardiovascular and sympathetic responses reflexly elicited through the excitation with bradykinin of sympathetic and vagal cardiac sensory endings in the cat. Cardiovasc Res 16, 57-65 (1982).

26 Malliani, A., Lombardi, F., Pagani, M., Recordati, G. & Schwartz, P. J. Spinal sympathetic reflexes in the cat and the pathogenesis of arterial hypertension. Clin Sci Mol Med Suppl 2, 259s-260s (1975).

27 Recordati, G., Lombardi, F., Bishop, V. S. & Malliani, A. Mechanical stimuli exciting type A atrial vagal receptors in the cat. Circ Res 38, 397-403 (1976).

28 Wang, H. J., Rozanski, G. J. & Zucker, I. H. Cardiac sympathetic afferent reflex control of cardiac function in normal and chronic heart failure states. J Physiol 595, 2519-2534, doi:10.1113/JP273764 (2017).

29 De Ferrari, G. M., Mantica, M., Vanoli, E., Hull, S. S., Jr. & Schwartz, P. J. Scopolamine increases vagal tone and vagal reflexes in patients after myocardial infarction. J Am Coll Cardiol 22, 1327-1334 (1993).

30 Vanoli, E. et al. Vagal stimulation and prevention of sudden death in conscious dogs with a healed myocardial infarction. Circ Res 68, 1471-1481 (1991).

31 Nakahara, S. et al. Characterization of myocardial scars: electrophysiological imaging correlates in a porcine infarct model. Heart Rhythm 8, 1060-1067, doi:10.1016/j.hrthm.2011.02.029 (2011).

32 Weaver, M. E., Pantely, G. A., Bristow, J. D. & Ladley, H. D. A quantitative study of the anatomy and distribution of coronary arteries in swine in comparison with other animals and man. Cardiovasc Res 20, 907-917, doi:10.1093/cvr/20.12.907 (1986).

33 Nonomura, K. et al. Piezo2 senses airway stretch and mediates lung inflation-induced apnoea. Nature 541, 176-181, doi:10.1038/nature20793 (2017).

34 Zeng, W. Z. et al. PIEZOs mediate neuronal sensing of blood pressure and the baroreceptor reflex. Science 362, 464-467, doi:10.1126/science.aau6324 (2018).

35 Huo, L. et al. Piezo2 channel in nodose ganglia neurons is essential in controlling hypertension in a pathway regulated directly by Nedd4-2. Pharmacol Res, 105391, doi:10.1016/j.phrs.2020.105391 (2020).

36 Staszewka-Barczak, J., Ferreira, S. H. & Vane, J. R. An excitatory nociceptive cardiac reflex elicited by bradykinin and potentiated by prostaglandins and myocardial ischaemia. Cardiovasc Res 10, 314-327, doi:10.1093/cvr/10.3.314 (1976).

37 Goncalves, E. C. D. et al. Bradykinin Receptors Play a Critical Role in the Chronic Post-ischaemia Pain Model. Cell Mol Neurobiol, doi:10.1007/s10571-020-00832-3 (2020).

38 Mohammed, Z. A., Kaloyanova, K. & Nassar, M. A. An unbiased and efficient assessment of excitability of sensory neurons for analgesic drug discovery. Pain 161, 1100-1108, doi:10.1097/j.pain.0000000000001802 (2020).

39 Caterina, M. J. et al. The capsaicin receptor: a heat-activated ion channel in the pain pathway. Nature 389, 816-824, doi:10.1038/39807 (1997).

40 Armour, J. A., Huang, M. H., Pelleg, A. & Sylven, C. Responsiveness of in situ canine nodose ganglion afferent neurones to epicardial mechanical or chemical stimuli. Cardiovasc Res 28, 1218-1225 (1994).

41 Kumar, A., Potts, J. D. & DiPette, D. J. Protective Role of alpha-Calcitonin Gene-Related Peptide in Cardiovascular Diseases. Front Physiol 10, 821, doi:10.3389/fphys.2019.00821 (2019).

42 Pan, H. L., Chen, S. R., Scicli, G. M. & Carretero, O. A. Cardiac interstitial bradykinin release during ischemia is enhanced by ischemic preconditioning. Am J Physiol Heart Circ Physiol 279, H116-121, doi:10.1152/ajpheart.2000.279.1.H116 (2000).

43 Hanack, C. et al. GABA blocks pathological but not acute TRPV1 pain signals. Cell 160, 759-770, doi:10.1016/j.cell.2015.01.022 (2015).

44 Stoyanova, I., Dandov, A., Lazarov, N. & Chouchkov, C. GABA- and glutamate-immunoreactivity in sensory ganglia of cat: a quantitative analysis. Arch Physiol Biochem 106, 362-369, doi:10.1076/apab.106.5.362.4360 (1998).

45 McCoy, E. S., Taylor-Blake, B. & Zylka, M. J. CGRPalpha-expressing sensory neurons respond to stimuli that evoke sensations of pain and itch. PLoS One 7, e36355, doi:10.1371/journal.pone.0036355 (2012).

46 Suadicani, S. O. et al. Bidirectional calcium signaling between satellite glial cells and neurons in cultured mouse trigeminal ganglia. Neuron Glia Biol 6, 43-51, doi:10.1017/S1740925X09990408 (2010).

47 Esplugues, J. V. NO as a signalling molecule in the nervous system. Br J Pharmacol 135, 1079-1095, doi:10.1038/sj.bjp.0704569 (2002).

48 Choate, J. K., Danson, E. J., Morris, J. F. & Paterson, D. J. Peripheral vagal control of heart rate is impaired in neuronal NOS knockout mice. Am J Physiol Heart Circ Physiol 281, H2310-2317 (2001).

49 Mohan, R. M., Golding, S., Heaton, D. A., Danson, E. J. & Paterson, D. J. Targeting neuronal nitric oxide synthase with gene transfer to modulate cardiac autonomic function. Progress in biophysics and molecular biology 84, 321-344, doi:10.1016/j.pbiomolbio.2003.11.013 (2004).

50 Assas, B. M., Pennock, J. I. & Miyan, J. A. Calcitonin gene-related peptide is a key neurotransmitter in the neuro-immune axis. Front Neurosci 8, 23, doi:10.3389/fnins.2014.00023 (2014).

51 Meng, J. et al. Activation of TRPV1 mediates calcitonin gene-related peptide release, which excites trigeminal sensory neurons and is attenuated by a retargeted botulinum toxin with anti-nociceptive potential. J Neurosci 29, 4981-4992, doi:10.1523/JNEUROSCI.5490-08.2009 (2009).

52 De Ferrari, G. M. et al. Vagal reflexes and survival during acute myocardial ischemia in conscious dogs with healed myocardial infarction. Am J Physiol 261, H63-69, doi:10.1152/ajpheart.1991.261.1.H63 (1991).

SUPPLEMENTAL TABLES AND FIGURES

		Δ HR (bpm)	Δ LVSP (mmHg)	Δ dP/dt_{max} (mmHg/s)	Δ dP/dt_{min} (mmHg/s)
EMS	**normal**	0.1±0.1	**-3.4±1.4***	-4.0±10.7	50.6±42.8
	MI	-0.5±0.2	**-3.0±0.9***	-8.7±9.7	58.0±19.8*
BRADY	**normal**	-2.0±1.5	-8.5±4.3	-99.9±57.0	**667.3±240.1***
	MI	**4.6±1.6***	**-24.5±5.6***	-81.3±47.7	**661.9±189.8***
CAPS	**normal**	-1.8±0.8	-2.4±0.8	-11.1±23.1	81.8±92.8
	MI	-0.1±2.6	**10.2±3.1***	-49.7±27.7	-79.0±40.5
VERAT	**normal**	**-0.4±0.1***	-0.2±2.8	18.1±22.5	-53.3±94.6
	MI	**-1.9±1.1***	-1.2±1.8	-11.3±17.6	34.6±25.0
VP	**normal**	**10.9±2.6***	**-16.0±4.3***	**-147.4±64.2***	**316.5±95.9***
	MI	**7.4±2.2***	**-16.5±4.7***	**-179.4±85.4***	**294.6±95.1***
IVC	**normal**	**1.9±1.0***	**-57.9±8.3***	**-612.5±123.0***	**1180.0±187.0***
	MI	**6.0±2.9***	**-75.2±6.9***	**-946.2±102.4***	**1522.0±192.8***
AO	**normal**	**-8.3±2.6***	**73.0±6.2***	29.9±117.8	-235.9±218.0
	MI	**-13.9±3.6***	**66.6±7.7***	102.4±77.3	-54.5±131.9

Supplemental Table 3-1. ***Hemodynamic responses to cardiac interventions.*** Values are shown as mean ± SE for change from baseline in heart rate (HR), left ventricular end-systolic pressure (LVSP), as well as the maximum and minimum first derivatives of LV pressure (dP/dt). AO = aortic occlusion; EMS = epicardial mechanical stimulation; IVC = inferior vena cava occlusion; VP = ventricular pacing; CAPS = capsaicin; VERAT = veratridine; BRADY = bradykinin; *represents statistically significant changes in parameters from baseline.

Primary Antibody	Host	Dilution	Vendor	Catalog #
Anti-PIEZO2	Rabbit Polyclonal	1:200	Neuromics	RA10109
Anti-P2X3	Rabbit Polyclonal	1:200	Thermo Fisher Scientific	PA5-72975
Anti-GAD65	Rabbit Polyclonal	1:2500	Sigma	G5038
Anti-GABA	Rabbit Polyclonal	1:1000	Immunostar	20094
Anti-GABA B Receptor 1	Mouse Monoclonal	1:300	Abcam	ab55051
Anti-NOS1	Mouse Monoclonal	1:100	Santa Cruz Biotechnology	sc-5302
Anti-GFAP	Mouse Monoclonal	1:1000	Thermo Fisher Scientific	MA5-12023
Anti-CGRP	Goat Polyclonal	1:1000	Abcam	ab36001

Secondary Antibody	Host	Dilution	Vendor	Catalog #
Anti-Mouse IgG - Alexa Fluor 488	Donkey Polyclonal	1:200	Jackson Immunoresearch	715-546-150
Anti-Rabbit IgG - Cy3	Donkey Polyclonal	1:200	Jackson Immunoresearch	711-166-152
Anti-Goat IgG - Alexa Fluor 647	Donkey Polyclonal	1:200	Jackson Immunoresearch	705-606-147
Anti-Mouse IgG - HRP	Donkey Polyclonal	1:200	Jackson Immunoresearch	715-036-151
Anti-Rabbit IgG - HRP	Donkey Polyclonal	1:200	Jackson Immunoresearch	711-036-152
Anti-Goat IgG - HRP	Donkey Polyclonal	1:200	Jackson Immunoresearch	705-036-147

Supplemental Table 3-2. ***Primary and secondary antibodies used for histological analysis.***

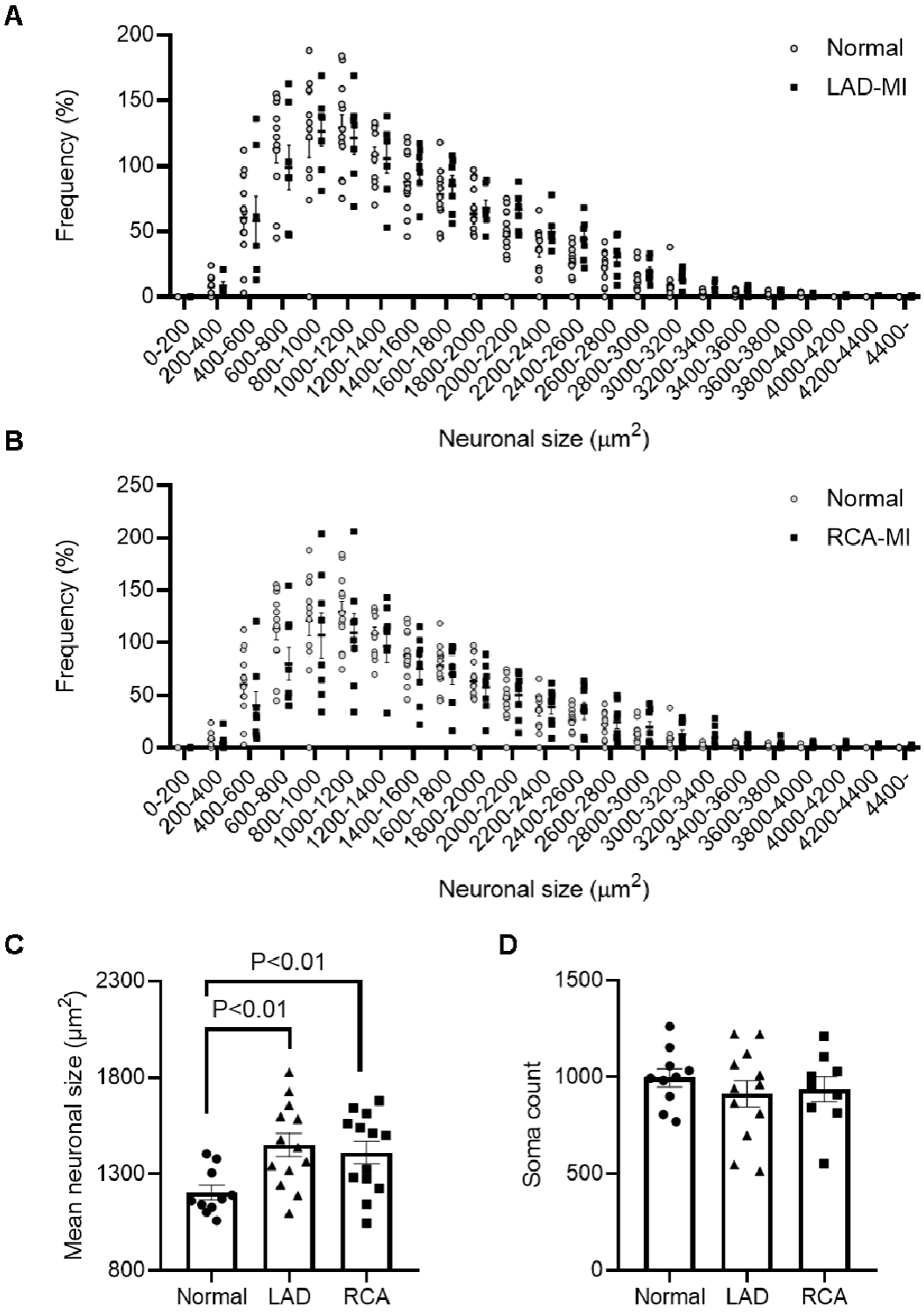

Supplemental Figure 3-1. ***Effect of myocardial infarction and the infarct region on nodose neuronal size.*** (**A**) Analysis of the distribution of neuronal sizes shows that the number of neurons with larger sizes is increased in LAD-MI pigs (*n* = 7 ganglia) compared to normal pigs (*n* = 12 ganglia). (**B**) Neuronal size distribution in normal and RCA infarcted animals is shown. The number of neurons with larger sizes is higher in the RCA-MI pigs (*n* = 8 ganglia) than normal pigs (*n* = 12 ganglia). (**C**) Compiled data across all sizes shows

that the mean nodose neuronal size is higher in infarcted animals (LAD: $P = 0.004$, $n = 13$ ganglia, vs. normal, $n = 10$ ganglia; RCA: $P = 0.014$, $n = 13$ ganglia, vs. normal, $n = 10$ ganglia). (**D**) There was no significant difference in the number of cells in normal animals ($n = 10$ ganglia) vs. LAD ($n = 12$ ganglia) or RCA ($n = 9$ ganglia) chronically infarcted animals. Data is shown as mean ± SE. Unpaired two-tailed Student's *t*-tests with the false discovery rate corrected by the Benjamini-Hochberg method was used for comparisons of ganglia from normal vs. infarcted animals.

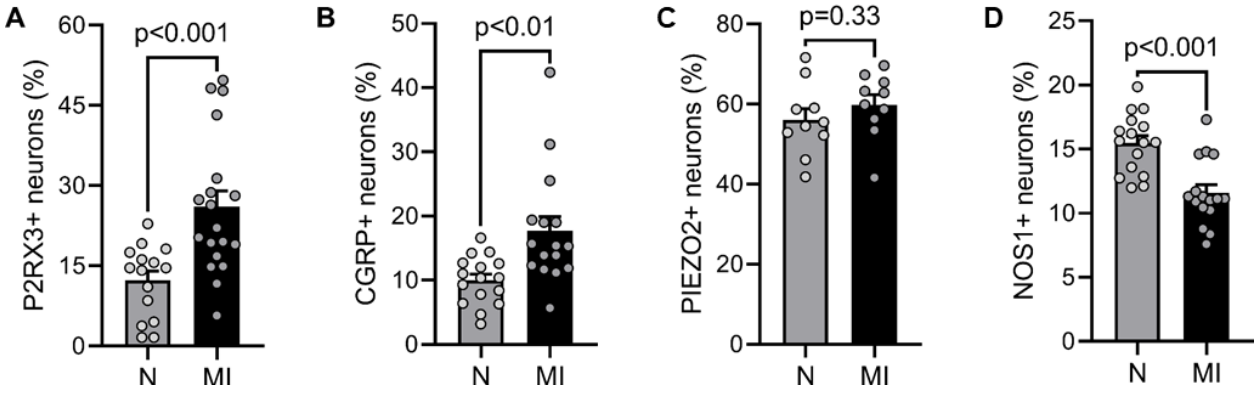

Supplemental Figure 3-2. ***Immunohistochemical assessment of neural remodeling after MI (analysis by nodose ganglion).*** Percentage of neurons in normal and MI nodose ganglia which express (**A**) P2RX3 ($P < 0.001$) and (**B**) CGRP ($P = 0.003$) is increased, while the expression of (**C**) PIEZO2 ($P = 0.33$) is unchanged, and (**D**) NOS1 expression is reduced ($P < 0.001$). $n = 15$ nodose ganglia from normal animals and $n = 19$ nodose ganglia from LAD-infarcted animals for P2RX3; $n = 16$ nodose ganglia from normal and MI animals for CGRP and NOS1; $n = 10$ nodose ganglia per group for PIEZO2. Data are shown as mean ± SE; unpaired, two-tailed Student's *t*-test used for comparison of MI and normal animals. N = normal animals, MI = animals with chronic LAD myocardial infarction.

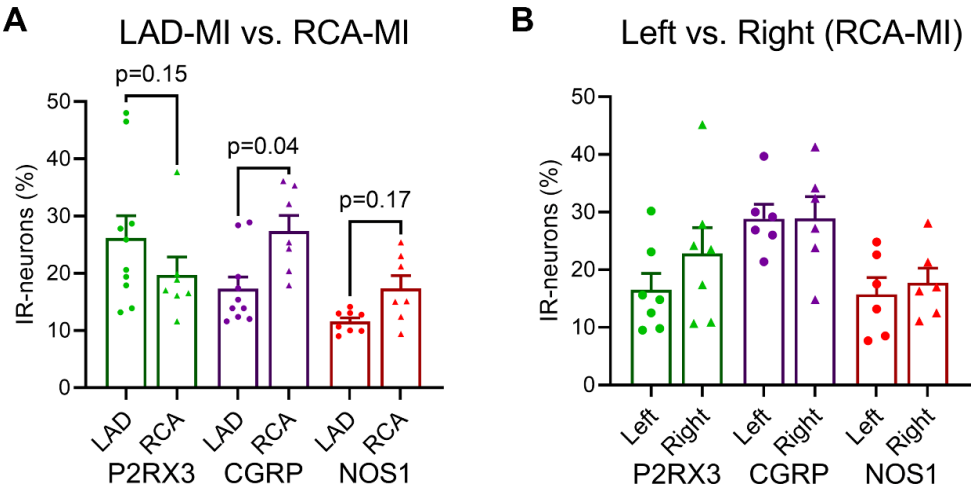

Supplemental Figure 3-3. ***Effect of infarcted region on remodeling of the nodose ganglia following myocardial infarction.*** (**A**) Percentage of nodose ganglia neurons from LAD and RCA infarcted animals

which express P2RX3 (*N* = 10 LAD infarcted pigs, *N* = 7 RCA infarcted pigs), CGRP (*N* = 10 LAD infarcted pigs, *N* = 7 RCA infarcted pigs), and NOS1 (*N* = 8 LAD infarcted pigs and *N* = 7 RCA infarcted pigs) is shown. There was no difference in the expression profiles of nodose ganglia neurons from LAD infarcted vs. RCA infarcted animals with regards to increases in P2RX3 (*P* = 0.15) or decreases in NOS1 (*P* = 0.17) expression. RCA infarcted animals showed modestly higher expression of CGRP (*P* = 0.04) compared to LAD infarcted animals. (**B**) A comparison of right vs. left nodose ganglia neural expression profiles for P2RX3 (*P* = 0.52; *n* = 7 pairs of nodose), CGRP (*P* = 0.98; *n* = 6 pairs of nodose) and NOS1 (*P* = 0.57; *n* = 6 pairs of nodose) showed no significant differences in the expression profiles of right vs. left nodose ganglia, indicating that both the left and right-sided ganglia are affected by myocardial infarction. Data is shown as mean ± SE. (**A**) Unpaired or (**B**) paired, two-tailed Student's *t*-tests with the false discovery rate corrected by the Benjamini-Hochberg method were used for analysis.

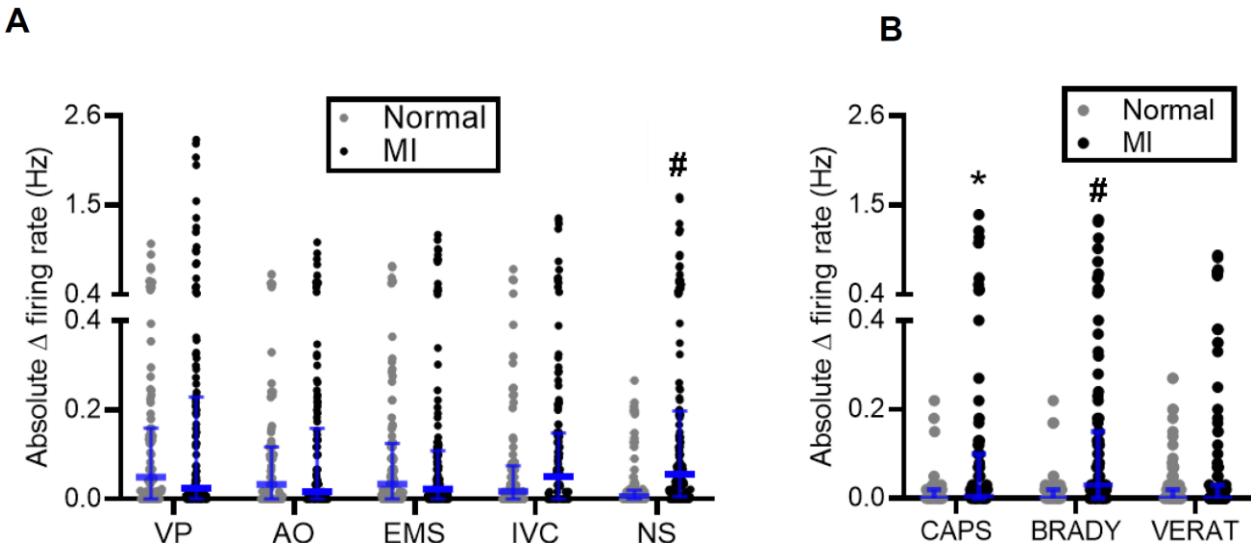

Supplemental Figure 3-4. ***Nodose neural responses to specific cardiac interventions.*** (**A**) Absolute changes in the firing rates of neurons (normal: 97 neurons, RCA-MI: 133 neurons) to each cardiac stressor and (**B**) to each specific chemical are also shown (number of neurons for normal animals: VP = 93, AO = 91, EMS = 94, IVC: 93, NS: 93, CAPS: 58, BRADY: 58, VERAT: 93; number of neurons for infarcted animals: VP = 129, AO = 122, EMS = 121, IVC = 128, NS = 120, CAPS = 72 BRADY = 117, VERAT = 117 neurons). Wilcoxon signed-rank test with correction for multiple comparisons was used to compare firing rates of neurons in normal vs. MI animal. *0.01< *P* ≤ 0.05, #*P* ≤ 0.001 compared to normal animals.

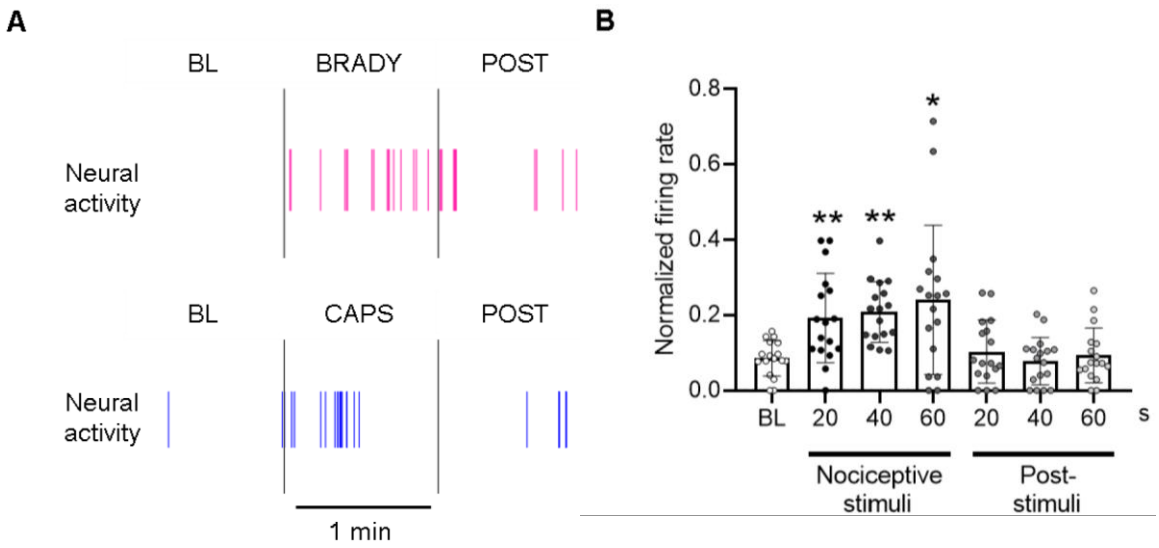

Supplemental Figure 3-5. ***Temporal profile of neuronal responses in normal animals demonstrates excitatory responses during application of nociceptive chemicals.*** (**A**) Representative excitatory responses to bradykinin (BRADY) and capsaicin (CAPS) of two nodose neurons from a normal animal is shown. (**B**) Quantified temporal responses in firing rates of neurons (n = 17) from normal animals showed an increase in firing rates upon epicardial application of nociceptive chemicals that subsided after removal of the stimulus. Data is shown as mean ± SE. Dunn's multiple comparison tests were used to compare the normalized firing rate vs. baseline (BL). $^{**}P \leq 0.001$ and $^{*}P \leq 0.05$ vs. baseline.

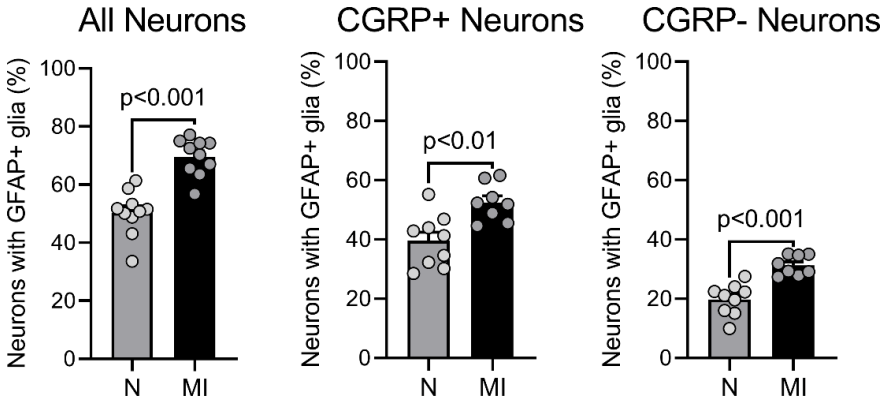

Supplemental Figure 3-6. ***Non-selective augmentation of nodose ganglia satellite glial cell activation following myocardial infarction involving the LAD coronary artery (analysis by nodose ganglion).*** Percentage of neurons surrounded by GFAP+ satellite glial cells in normal and MI nodose ganglia as a subset of all neurons ($P < 0.001$), CGRP+ neurons ($P = 0.004$) and CGRP- neurons ($P < 0.001$) shows that although glial activation occurs throughout the nodose ganglia of the animals after myocardial infarction, this response is not specific to CGRP expressing/nociceptive neurons. n = 10 nodose ganglia per group for all neurons (normal and LAD-MI), n = 9 nodose ganglia for CGRP+ neurons and CGRP- neurons in normal animals, n = 8 nodose ganglia for CGRP+ neurons and CGRP- neurons in LAD-MI animals. Data is shown as mean ± SE. Unpaired, two-tailed Student's t-test was used for MI vs. normal group comparisons.

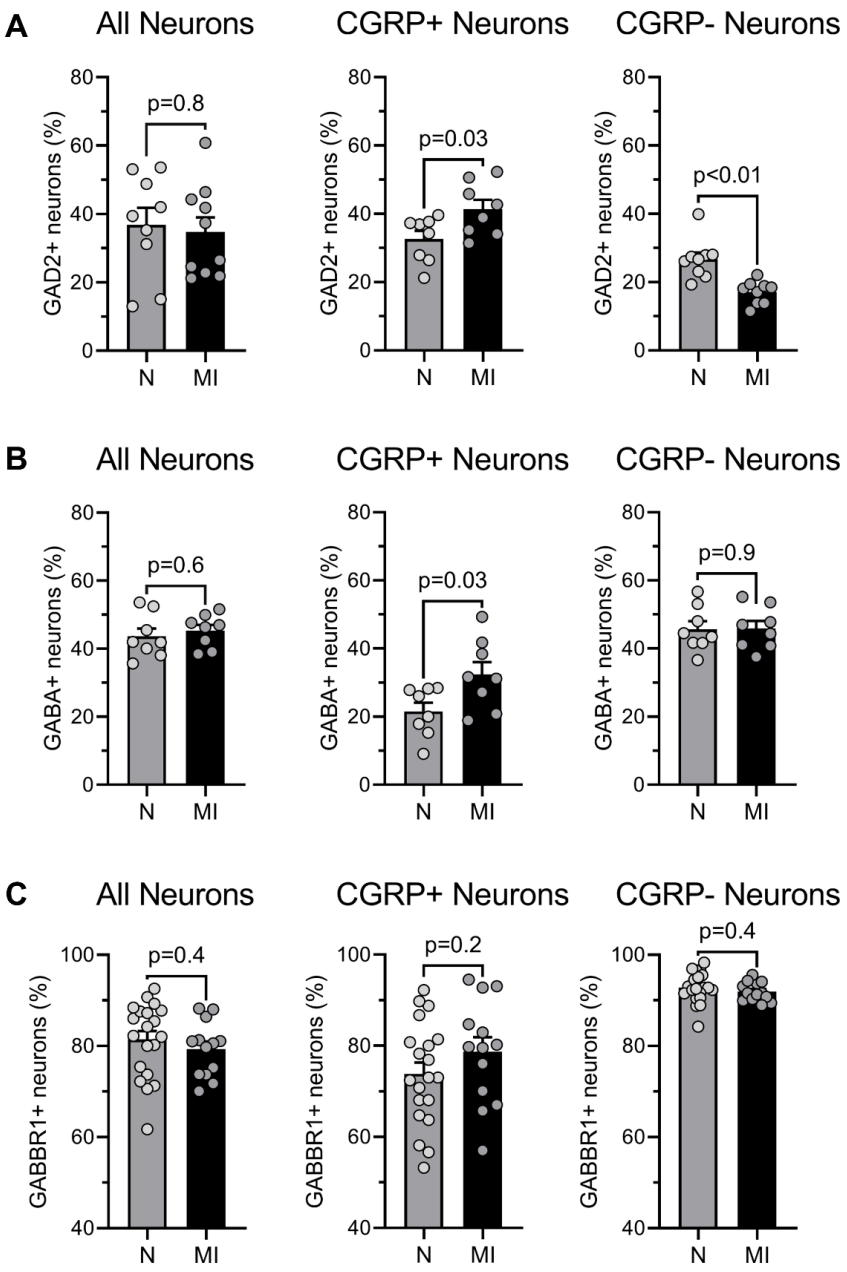

Supplemental Figure 3-7. ***Upregulation of inhibitory, GABAergic expression in nodose ganglia neurons co-expressing CGRP after myocardial infarction involving the coronary LAD artery(analysis by nodose)***. (**A**) Percentage of GAD2+ neurons in normal and MI nodose ganglia as a subset of all neurons as well as those co-expressing CGRP and not expressing CGRP (CGRP-). The percentage of neurons that co-express CGRP and GAD2 are increased after MI. (**B**) Percentage of all neurons expressing GABA in normal and MI animals as well as the percentage co-expressing CGRP is shown, as analyzed both by animal and by ganglion. The percentage of neurons co-expressing CGRP and GABA is increased after MI. (**C**) Percentage of neurons with GABBR1+ expression in normal and MI nodose ganglia as a subset of all neurons, CGRP+ neurons, and CGRP- neurons shows no difference in the expression of GABA type B receptors after MI. *n* = 9 normal nodose and 10 MI nodose ganglia for GAD2 in all neurons. *n* = 8 normal nodose and MI

nodose ganglia for GAD2+ CGRP+ neurons. *n* = 9 normal nodose and MI nodose ganglia for GAD2+ CGRP- neurons. *n* = 8 normal nodose and MI nodose ganglia for GABA. *n* = 20 normal nodose and *n* = 13 MI nodose ganglia for GABBR1. Data is shown as mean ± SE. Unpaired, two-tailed Student's *t*-test was used for comparison of normal and MI animals and ganglia.

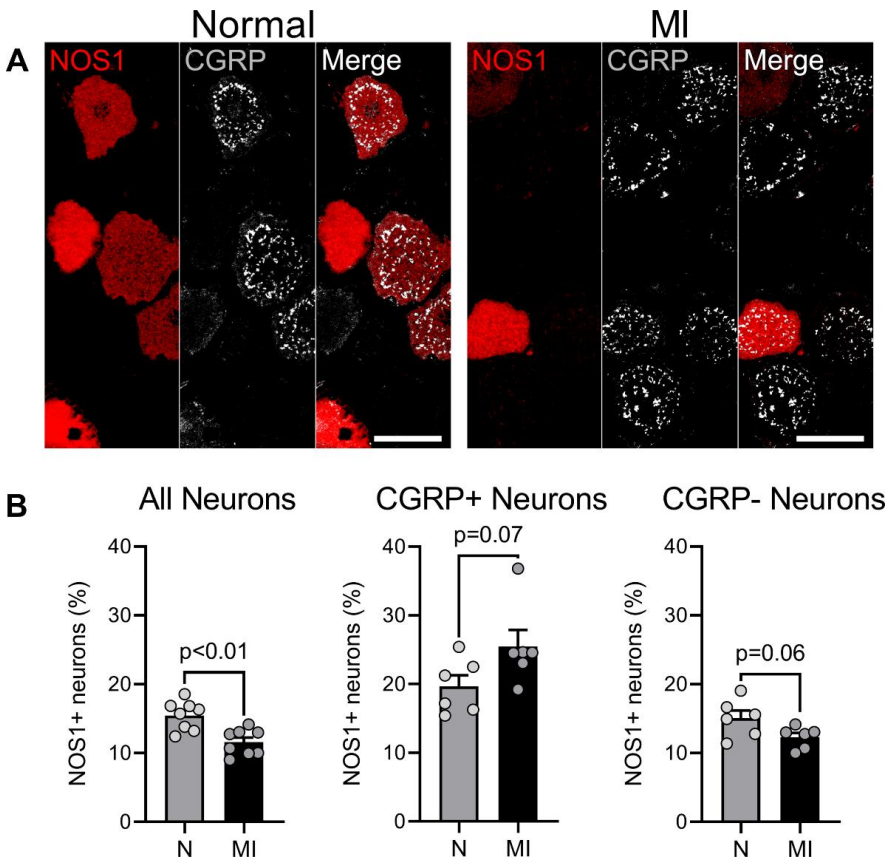

Supplemental Figure 3-8. ***Non-selective loss of neuronal nitric oxide synthase expression in the porcine nodose ganglia.*** (**A**) Representative images of nodose ganglia from normal (N; left) and LAD-infarcted (MI; right) animals stained for NOS1 (red) and CGRP (white) are shown in the upper panels. (**B**) Quantified expression of NOS1 in normal and MI animals (*N* = 8 pigs per group) and co-expression with CGRP+ neurons (*P* = 0.07) and CGRP- neurons (*P* = 0.06) (*N* = 6 pigs per group for co-expression) are shown. Although global expression of NOS1 is significantly reduced, the reduction is not specific to CGRP-expressing neurons. Data is shown as mean ± SE. Unpaired, two-tailed Student's *t*-test was used for comparison of normal and MI groups. Scale bars are 50 µm.

Chapter 4

Autonomic and Electrophysiological Effects of Thoracic Epidural Anesthesia on Infarcted Porcine Hearts

Jonathan D Hoang, Mohammed Amer Swid, Ki-Woon Kang, Christopher A Chan, Neil R Jani, Marmar Vaseghi

In submission.

ABSTRACT

Background: Thoracic epidural anesthesia (TEA) reduces burden of ventricular tachyarrhythmias (VT/VF) in case-series of patients with refractory arrhythmias and cardiomyopathy. However, its electrophysiological and autonomic effects in diseased hearts remain unclear and its use after myocardial infarction (MI) is limited by concerns for RV dysfunction.

Methods: MI was created in Yorkshire pigs (*n* = 10) by LAD occlusion. Six weeks post-MI, an epidural catheter was placed at the C7-T1 vertebral level for injection of 2% lidocaine. RV and LV hemodynamics were recorded using Millar pressure-conductance catheters, and ventricular activation-recovery intervals (ARIs), a surrogate of action potential durations, by a 56-electrode sock. Hemodynamics and ARIs, baroreflex sensitivity (BRS), atrial and ventricular effective refractory periods (ERP), and atrioventricular delay (AH interval) were assessed before and after TEA. VT/VF inducibility was assessed by programmed electrical stimulation.

Results: TEA reduced inducibility of VT/VF by 67%, comparable to results reported in case series. Though sufficient for anti-arrhythmic benefit, TEA did not affect RV-systolic pressure or contractility, although LV-systolic pressure and contractility decreased modestly. Atrial and ventricular ERPs, and AH interval were significantly prolonged. Global and regional ventricular ARIs increased, including in scar and border zone regions post-TEA. Notably, TEA significantly improved parasympathetic function as measured by BRS.

Conclusion: TEA does not compromise RV function in infarcted hearts and its anti-arrhythmic mechanisms are mediated by increases in ventricular ERP and ARIs. TEA improves parasympathetic function, which may be independently anti-arrhythmic. This study provides novel insight into the anti-arrhythmic mechanisms of TEA while highlighting its applicability to the clinical setting.

INTRODUCTION

The sympathetic nervous system plays an important role in the occurrence of ventricular tachyarrhythmias (VT/VF).[1] Cardiac sympathetic activation promotes triggered activity[2] and increases spatial heterogeneity and dispersion of ventricular repolarization,[3] creating the trigger and substrate for VT/VF, leading to sudden cardiac death.[4]

Thoracic epidural anesthesia (TEA) acts at the dorsal and ventral horns of the spinal cord as a specific, but reversible, blockade of cardiac sympathetic neurotransmission. Case reports and small case series of patients have shown that TEA is effective in acutely decreasing the burden of VT/VF in patients with structural heart disease.[5] These retrospective case series have suggested that TEA may be more effective than cardiac sympathetic denervation at decreasing arrhythmia burden,[6] effects which are likely mediated by decreases in ventricular excitability and shifts in autonomic tone.[7] However, the widespread adoption of TEA as an antiarrhythmic treatment has been limited partially by concerns of right ventricular (RV) dysfunction, particularly in the setting of chronic left ventricular myocardial infarction (MI), where concerns for hemodynamic deterioration and preload dependence of the RV have limited the use of TEA in the treatment of VT/VF.[8]

Moreover, previous experimental studies investigating efficacy of TEA have been limited in scope and clinical relevancy by their application in normal hearts.[8, 9] To date, electrophysiological and autonomic effects of TEA in diseased/infarcted hearts remain to be evaluated and the mechanisms underlying the potential anti-arrhythmic effects of TEA, beyond simply “sympathetic efferent blockade,” remain to be elucidated. Thus, the purpose of this study was to assess the biventricular hemodynamic, electrophysiological, and autonomic effects of TEA in the setting of chronic MI in a porcine model.

METHODS

Ethical approval

Ten Yorkshire pigs were used in this study. Care of animals conformed to the National Institutes of Health Guide for the Care and Use of Laboratory Animals. The protocol was approved by the University of California, Los Angeles, Institutional Animal Care and Use Committee.

Creation of myocardial infarction

MI was created percutaneously under fluoroscopic guidance as previously described.[10, 11] Briefly, animals (39.6 ± 0.7 kg) were sedated with tiletamine-zolazepam (4-8 mg/kg, intramuscular), intubated, and general anesthesia maintained by isoflurane (1-2%, inhaled). Next, a balloon-tipped coronary angioplasty catheter was advanced through a coronary guide catheter and over an angioplasty wire to the middle of the left anterior descending coronary artery (LAD) from the femoral artery. The balloon was inflated after the first diagonal branch of the LAD in each animal and 3 ml polystyrene microspheres (Polybead, 90 μm, Polysciences, Warrington, PA) were slowly injected via the lumen of the angioplasty catheter. The balloon was then deflated, and infarction was confirmed by lack of flow to the distal LAD on coronary angiogram coupled with ST-segment elevation. Catheters and sheaths were then removed, the animal weaned from anesthesia, and monitored until ambulating.

Animal preparation

Four to six weeks following MI, animals (53.3 ± 1.2 kg) were sedated with tiletamine-zolazepam (4-8 mg/kg, intramuscular) and general anesthesia maintained by isoflurane (1-2%, inhaled) throughout surgical preparation. 8 Fr introducer sheaths were placed in the bilateral femoral veins for infusion of normal saline and supportive medications and arteries for pressure monitoring. Animals were transitioned to α-chloralose (50 mg/kg initial bolus, then 20-30 mg/kg/hr infusion, IV) for electrophysiological and autonomic assessment.

High thoracic epidural anesthesia

Pigs were placed in the left lateral decubitus position. A 17-gauge Tuohy needle was inserted via the paramedian approach into the T5-T6 epidural interspace via standard loss-of-resistance approach and under fluoroscopic guidance (Figure 1). A 19-gauge open-end epidural

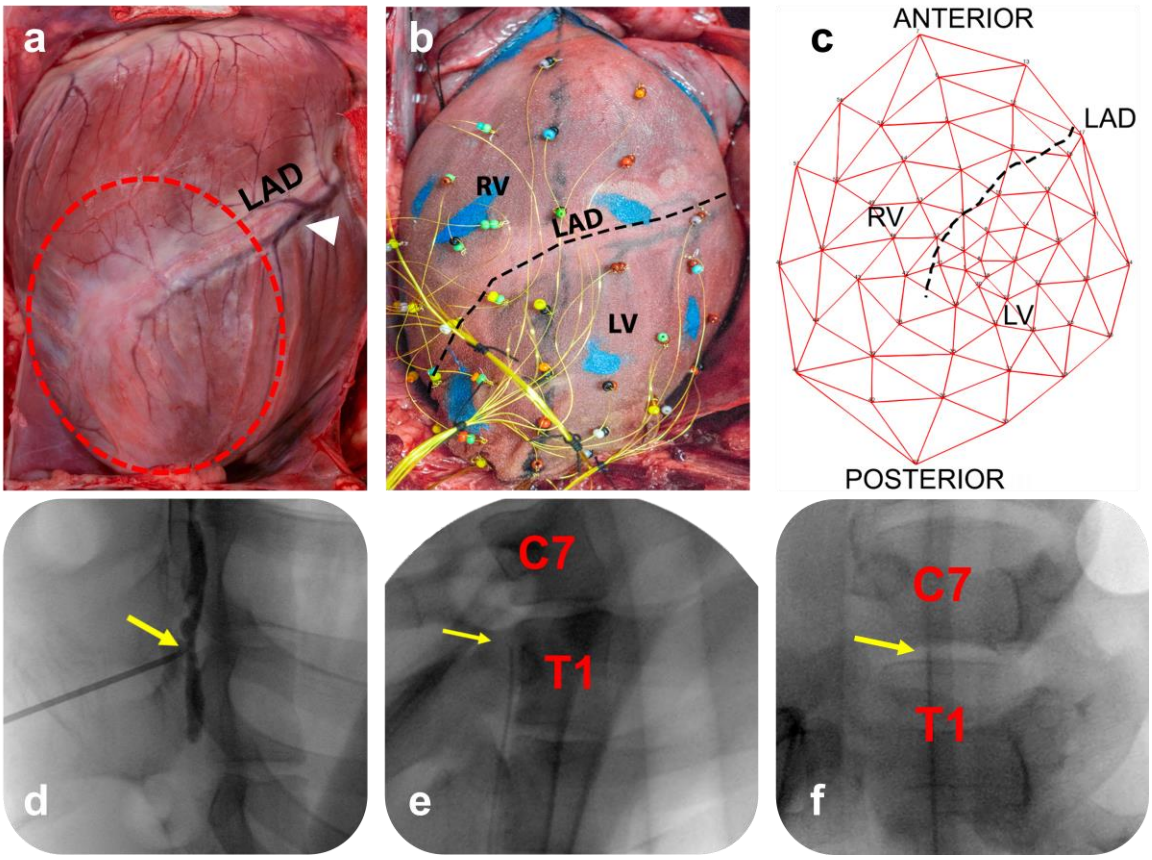

Figure 4-1. ***Infarct creation and experimental design.*** (**a**) Myocardial infarcts were created by occlusion of the left anterior descending coronary artery (LAD) immediately after the first diagonal branch (white arrowhead). The infarcted region 6 weeks post-MI of the left and right ventricles is indicated by the red dashed line. (**b**) A 56-electrode sock is placed over the ventricles to acquire local, unipolar electrograms from the epicardium which can be mapped (**c**) onto a 2D polar map to assess regional differences. (**d**) A 17-gauge Tuohy needle is advanced into the epidural space from the T5-T6 or T6-T7 interspace and contrast is injected to confirm the initial placement of the needle tip (arrow). (**e**) An open-tip epidural catheter (arrow) is placed with the animal in the lateral decubitus position and advanced to the C7-T1 vertebral level under fluoroscopic guidance. (**f**) Final catheter placement (arrow) is confirmed in the supine position (antero-posterior view).

catheter (Teleflex Inc, Wayne, PA) was advanced beyond the needle tip into the epidural space. The catheter tip was advanced to the C7-T1 vertebral space and contrast injected to confirm appropriate placement under fluoroscopy. Lack of aspiration of blood and cerebrospinal fluid was used to exclude intravascular or intrathecal catheter placement. 0.2-0.4 ml/kg lidocaine (2%) was administered epidurally at a rate of 4 ml/min. The direct effects of TEA were assessed immediately before (pre-TEA) and 10 minutes after infusion of lidocaine (post-TEA).

Ventricular hemodynamic measurements

A 5-Fr Millar pressure-conductance pressure catheter was placed in the RV and left ventricle (LV) via the femoral vein and artery, respectively, for continuous pressure measurements throughout the experiment. Raw signals were digitized and recorded by CED Power1401 and subsequently analyzed using Spike2.

Evaluation of cardiac autonomic function

Animals underwent median sternotomy to expose the heart. Bilateral stellate ganglia were isolated behind the parietal pleura and stimulated via bipolar needle electrodes (Grass).[11, 12] After lateral neck cutdown, the cervical vagi were isolated and stimulated via bipolar spiral cuff electrodes (LivaNova, PLC). Threshold was defined unilaterally for the stellate ganglia as the current causing a 10% increase in heart rate or systolic pressure at 4 Hz, 4 msec. Vagi thresholds were defined unilaterally at 10 Hz, 1 msec as the current causing a 10% decrease in heart rate.[11, 12] Bilateral stellate stimulation (BSS) was performed pre- and post-TEA at 4 Hz, 4 msec and 1.5× threshold current for 1 minute, to assess the effects on stellate-mediated sympathetic efferent activation. Right and left vagal nerve stimulation (VNS) was performed pre- and post-TEA at 10 Hz, 1 msec and 1.2× threshold current for 10 seconds to assess effects of TEA on VNS-mediated electrical effects.

Baroreflex sensitivity was tested by bolus of phenylephrine (3-5 μg/kg, intravenous) to evoke a 30-40 mmHg increase in systolic pressure. The same dose of phenylephrine was use before and after TEA in all animals. Sensitivity of the parasympathetic component of the baroreflex was determined as the beat-to-beat relationship between the prolongation of the RR interval and increases in systolic blood pressure, as described previously.[13]

Cardiac electrophysiological recordings and analysis

Quadripolar pacing catheters were placed in the RV and right atrium (RA) to determine effective refractory periods (ERP) and measure atrio-His (AH) and His-ventricular (HV) conduction time. AH and HV intervals were measured pre- and post-TEA during atrial pacing at a drive cycle length (CL) of 450 msec.

A 56-electrode sock was placed over the ventricles to continuously record unipolar epicardial electrograms using a GE CardioLab System (Boston, MA). Activation recovery intervals (ARIs) were analyzed to estimate regional action potential durations, using customized software, iScaldyn (University of Utah, Salt Lake City, UT).[14] ARIs were then mapped onto 2D-schematic polar maps with relative positions of the LV, RV and LAD delineated to assess regional differences. Bipolar voltage mapping was performed to delineate scar, border zone, and viable regions using a standard electrophysiology catheter (2-2-2 duodecapolar catheter Abbot, Minneapolis, MN). The location of each sock electrode with respect to its underlying bipolar voltage was noted. Using standard voltage criteria utilized in patients undergoing clinical electrophysiological procedures, regions were defined as either scar (0.05 mV < voltage < 0.5 mV), border zone (0.5 mV < voltage < 1.5 mV), or viable (voltage > 1.5 mV).[15] Of note, if an electrode was overlaying an area of very dense scar (voltage < 0.05 mV) that did not give rise to a discernable or analyzable signal, data from this electrode was removed from ARI analysis.

Atrial and ventricular effective refractory period and VT/VF inducibility

Atrial and ventricular ERP were measured by extra-stimulus pacing at a drive CL of 400-500 msec using an epicardial pacing catheter. An extra-stimulus was decremented by 5 msec down to ERP. The same drive CL and locations were chosen pre- and post-TEA.

VT inducibility was tested using programmed electrical stimulation as is commonly performed in patients undergoing electrophysiological studies for VT. Programmed stimulation was performed using an 8-beat drive train stimulus (S1) at 450 msec or 500 msec (depending on intrinsic sinus rate), followed by an S2 extra-stimulus. The extra-stimulus was decremented by 10 msec down to a CL of 200 msec or ERP. The same CL was used pre- and post-TEA to minimize effects on drive CL on inducibility of VT. The next extra-stimulus (S2, S3, or S4) was set at 75% of S1 CL. If the extra-stimulus reached ERP without causing sustained VT, a CL 10-20 msec above ERP was chosen for S2 to assure ventricular capture, and the next extra-stimulus (S3 and up to S4) was added. Ventricular extra-stimulus testing was performed using Micropace (EP320) and Prucka

CardioLab System (GE Healthcare) from the RV endocardium or LV anterior epicardium. If VT was induced pre-TEA, the same site was used post-TEA. Inducible animals were cardioverted if VT did not terminate after 30 seconds. If sustained VT was inducible at baseline, a minimum wait period of 60 minutes was allowed after cardioversion and before TEA and repeat inducibility testing.

Statistical analysis

Data are reported as mean ± SEM. Global ventricular ARIs were calculated as the mean ARI across all 56 electrodes and regional ARIs as the mean ARI of the electrodes classified by bipolar voltage mapping. After confirmation of normality, paired two-tailed Student's *t*-test was used to compare parameters pre- and post-TEA. Student's *t*-test was used for comparison of AERP, VERP, AH interval, HV interval and hemodynamic parameters pre- vs. post-TEA. For responses to BSS and VNS, percent changes in parameters from baseline were calculated first; then paired two-tailed Student's *t*-test was used to compare BSS- and VNS-induced ARI changes from baseline, before and after TEA. Baroreflex sensitivity before and after TEA was compared by paired, Wilcoxon signed rank test. Comparison of VT inducibility before and after TEA was performed using the exact binomial test. $P < 0.05$ was considered statistically significant.

RESULTS

TEA mitigates inducibility of ventricular arrhythmias

VT inducibility was assessed by ventricular extra-stimulus pacing before and after TEA ($n = 10$), Figure 2. Epicardial activation mapping performed during pacing from within the scar-border zone region revealed more homogenous impulse conduction after TEA, suggesting increased stability of cardiac electrical propagation (Figure 2b). All ten infarcted animals tested (100%) were inducible for VT requiring defibrillation pre-TEA. After TEA, only 3 of 10 (30%) infarcted animals were inducible for VT ($P < 0.001$). Overall, TEA decreased inducibility of ventricular tachyarrhythmias by 70% ($P < 0.05$). The antiarrhythmic benefit of TEA seen herein is comparable to that observed in clinical case series.[5]

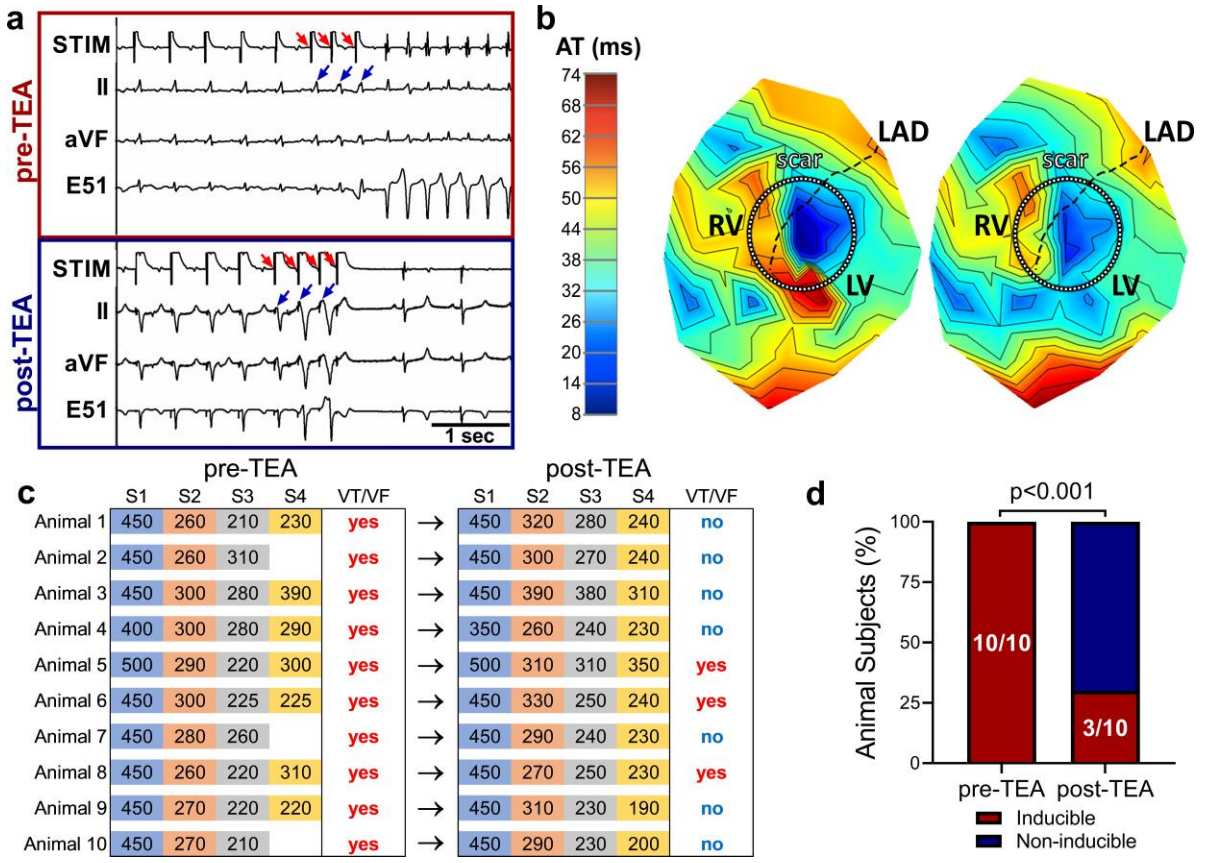

Figure 4-2. ***Thoracic epidural anesthesia stabilizes electrical substrate and reduces inducibility of ventricular tachycardia.*** (**a**) Example of VT/VF induction using programmed ventricular stimulation. Prior to TEA, this animal was inducible for VT with double extra-stimuli. After TEA, VT/VF was no longer inducible with triple extra-stimuli and ventricular ERP was reached (red arrows indicate pacing artifact and blue arrows indicate ventricular capture). (**b**) Isochronal activation map comparing paced impulse propagation from a scar-border zone region, before and after TEA, showing improvements in regions of late activation. (**c**) Before TEA, all ten animals were inducible for VT, but after TEA, only 3 animals were inducible. (**d**) TEA led to an overall reduction in VT inducibility by nearly 70%. E51 = cardiac electrogram from sock electrode #51; STIM = channel used for ventricular stimulation pacing. VT inducibility pre-TEA *vs* post-TEA was compared by the exact binomial test, *n* = 10 animals.

Hemodynamic changes resulting from high thoracic epidural blockade

To assess the effects of TEA on biventricular function, RV and LV function were continuously measured in infarcted animals before and after infusion of TEA (*n* = 10). Despite sufficient epidural blockade to achieve antiarrhythmic benefit, TEA modestly decreased LV systolic pressure (LVSP; 112 ± 5 to 98 ± 4 mmHg, P < 0.01), inotropy (LV-d*P*/dt_{max}; 1472 ± 102 to 1124 ± 142 mmHg/s, P < 0.01) and heart rate (HR; 90.9 ± 3.2 to 85.1 ± 3.5 bpm, P = 0.01), Figure 3b-e.

However, while TEA depressed heart rate and LV function, it had no effect on RV systolic pressure (43 ± 4 to 43 ± 4 mmHg; P = 0.7) or RV inotropy (301 ± 36 to 287 ± 28 mmHg/s; P = 0.2), Figure 3f-h. Importantly, both RV inotropic and lusitropic function were unaffected despite its preload dependence, Fig 3f-h.

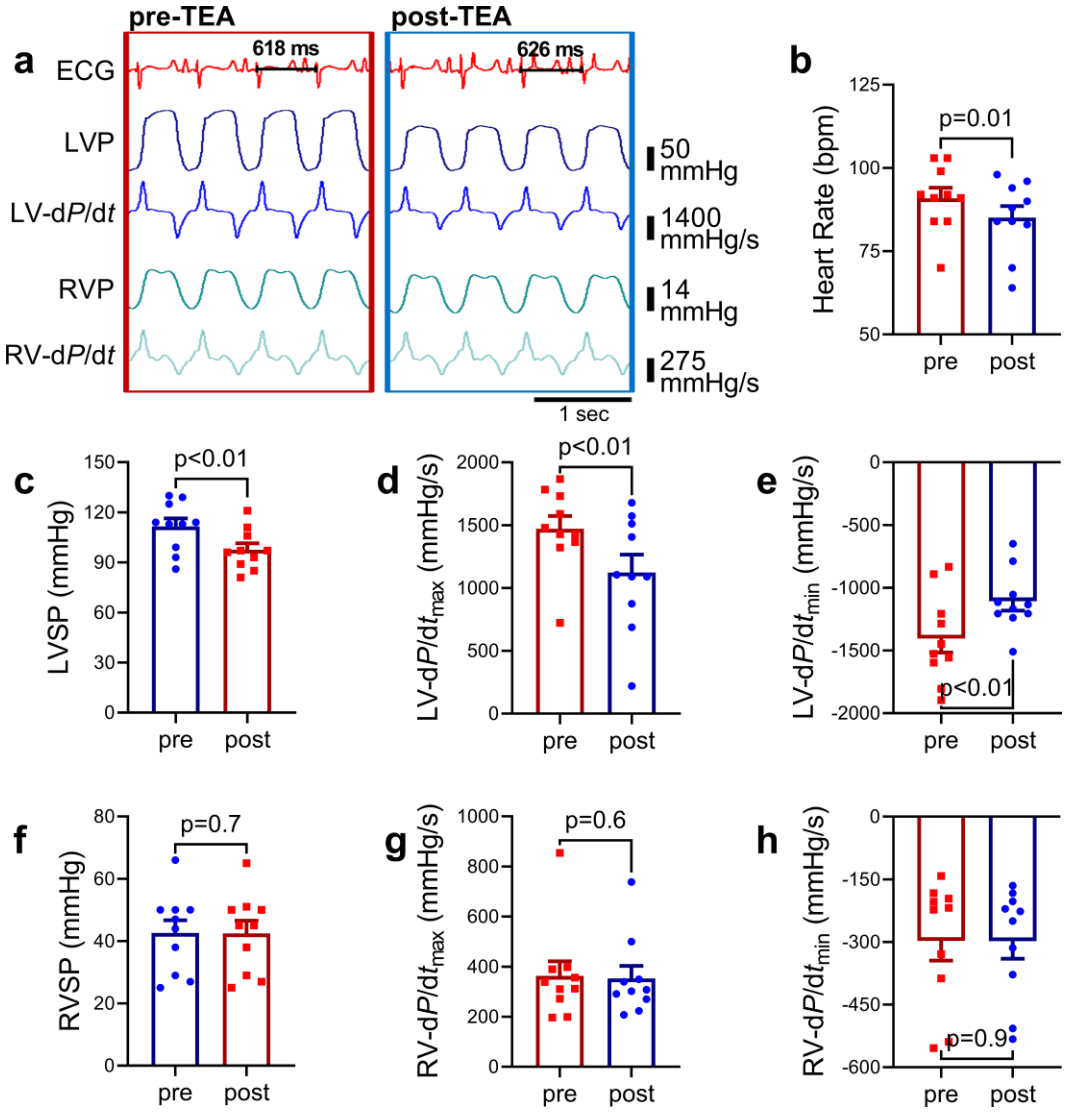

Figure 4-3. ***Biventricular mechanical effects of thoracic epidural anesthesia.*** (**a**) Representative raw traces of the effects of TEA on RV and LV function. TEA significantly decreased (**b**) heart rate (**c**) LVSP, (**d**) LV-dP/dt_{max} and (**e**) LV-dP/dt_{min}. TEA did not have any effects on (**f**) RVSP, (**g**) RV-dP/dt_{max} or (**h**) RV-dP/dt_{min}. Pre-TEA *vs* post-TEA were compared by Student's paired *t*-test, *n* = 10 animals.

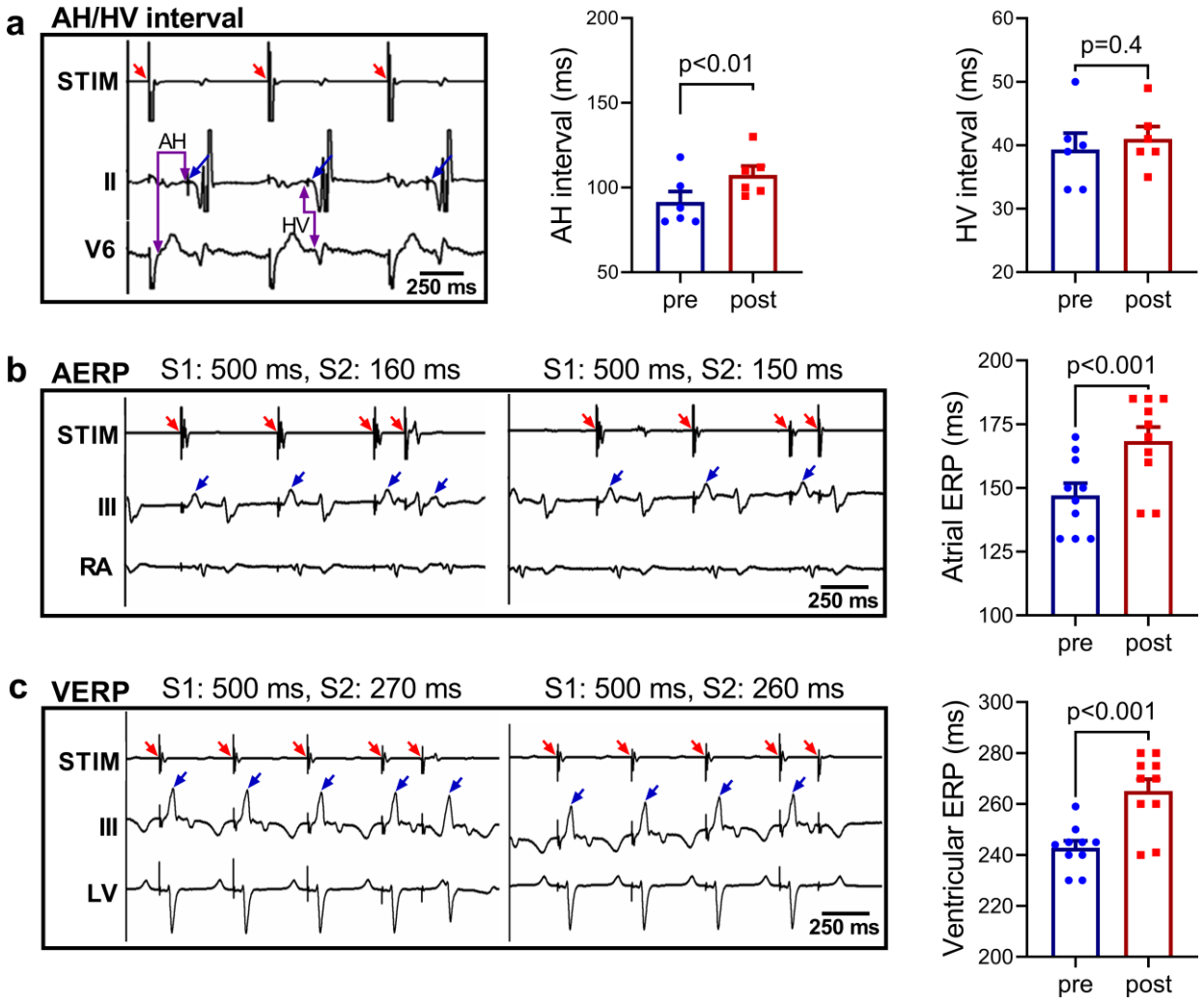

Figure 4-4. ***Effects of thoracic epidural anesthesia on cardiac electrical parameters.*** (**a**) Example and quantified data of AH and HV interval showing atrio-ventricular conduction before (pre-TEA) and after administration of lidocaine (post-TEA) are shown (red arrow indicates pacing and blue arrow indicates His signal). (**b**) Example of atrial ERP measurements in one animal pre-TEA (red arrow indicates pacing and blue arrow indicates atrial capture) with quantified data pre- and post-TEA. (**c**) Example of ventricular ERP measurements (red arrow indicates pacing and blue arrow indicates ventricular capture) and quantified data pre- and post-TEA. AERP = atrial effective refractory period, VERP = ventricular effective refractory period, STIM = channel used for atrial stimulation/pacing. Pre-TEA *vs* post-TEA were compared by Student's paired *t*-test, $n = 6$ for AH/HV interval and $n = 10$ for AERP and VERP.

Supraventricular electrophysiological effects of TEA

Given applications of TEA for treating post-operative atrial fibrillation, the supraventricular electrophysiological effects of TEA were further evaluated in our model. Atrioventricular conduction was assessed by measuring the atrial to His bundle conduction time (AH interval; $n =$

7). TEA significantly prolonged the AH interval (98 ± 9 to 114 ± 8 msec; P = 0.001) without affecting the HV interval, despite pacing at the same cycle length pre- and post-TEA (Figure 4a). Next, the effects of TEA on atrial refractoriness were assessed by extra-stimulus pacing of the left atrium (*n* = 10). Importantly, TEA significantly prolonged atrial ERP (147 ± 5 to 168 ± 5 msec; P < 0.001), suggesting the persistence of its benefits for supraventricular arrhythmias in the setting of MI-induced autonomic remodeling (Figure 4b).

Effects of TEA on ventricular refractoriness and action potential duration

While supraventricular effects of TEA were observed, we sought to determine whether these effects would persist in the ventricles (*n* = 10) despite autonomic and ventricular myocardial remodeling. However, ventricular ERP was also significantly prolonged by TEA (243 ± 3 to 265 ± 5 msec; P < 0.001), suggesting that the benefits of TEA may not be restricted to the atria, an important anti-arrhythmic mechanism.

Moreover, in a similar fashion, TEA significantly prolonged global ventricular ARIs by 15 ± 5 msec (331 ± 16 to 347 ± 18 msec; P = 0.02), Figure 4c. Importantly, bipolar voltage mapping to delineate regions of viable myocardium from scar and border zone regions revealed that this effect was not restricted to just the viable myocardium. While ARIs from viable regions of myocardium were prolonged by 13 ± 3 msec (340 ± 16 to 353 ± 17 msec; P < 0.01), ARIs of both scar (332 ± 19 to 348 ± 20 msec; P < 0.01) and border zones (337 ± 16 to 355 ± 18 msec; P = 0.02) also significantly prolonged, Figure 4. There were no significant differences between regions.

Effects of TEA on cardiac autonomic function

Responses to electrical nerve stimulation

To assess whether TEA had effects on efferent function of either the stellate or vagal nerve, the stellate ganglia and cervical vagi were electrically stimulated pre- and post-TEA (*n* = 6). There were no significant differences in either the threshold of stimulation as determined at 4 Hz for stellate ganglia (Figure 5b) or 10 Hz for vagal nerves (Figure 5d). Similarly, or the amplitude of effect on ventricular ARIs with BSS or VNS before *vs* after TEA Figure 5.

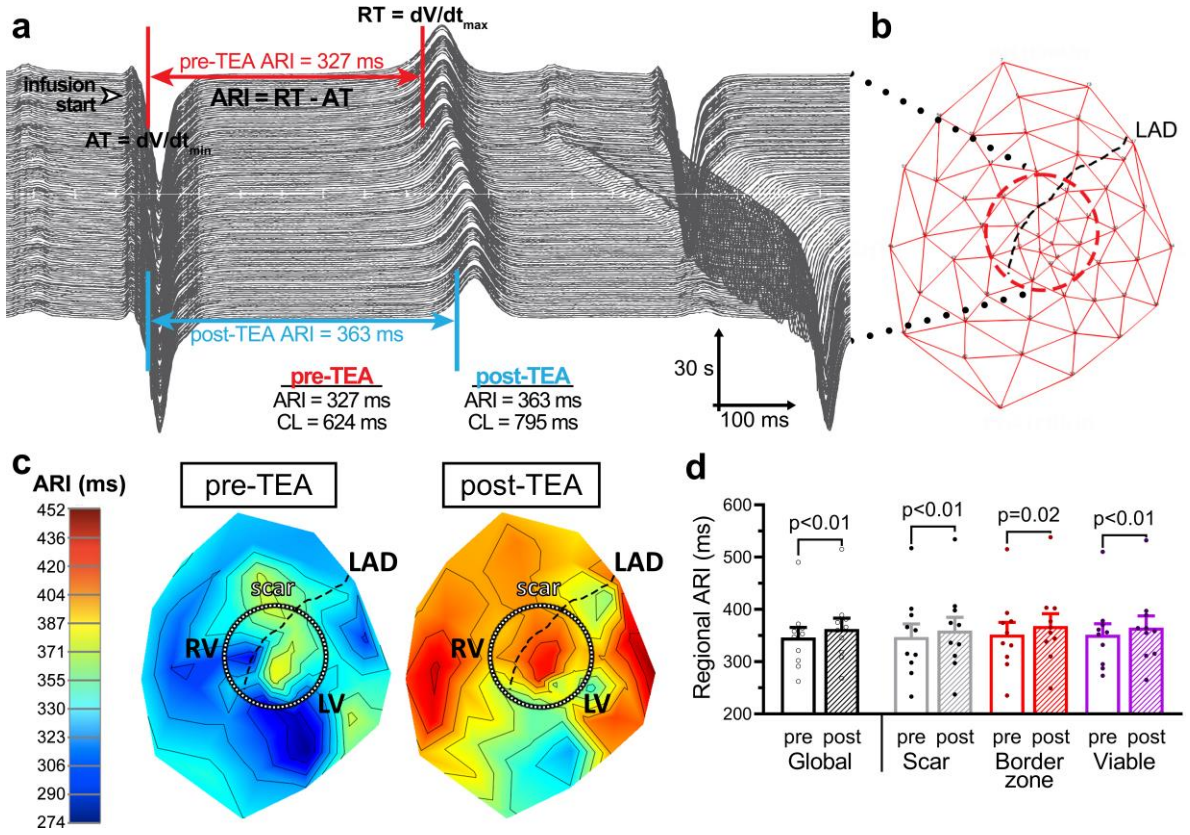

Figure 4-5. ***Ventricular action potential duration is prolonged by epidural blockade.*** (**a**) Representative unipolar electrograms spanning the duration of lidocaine administration. Activation recovery interval (ARI), a surrogate for local action potential duration, is calculated as the time from AT (dV/dt_{min} of activation wavefront) to RT (dV/dt_{max} of repolarization wavefront) from each electrogram. The ARI before and after TEA can then be compared both globally and regionally. (**b, c**) The general area of infarction is indicated by the red dashed line. ARIs calculated from unipolar EGMs of the 56-electrode sock are mapped onto this surface and show global prolongation in ARI, without any differences between physical regions. (**d**) Functional, electrical regions are parsed out and validated by bipolar voltage mapping. Scar, border zone, and viable regions were affected equally. Pre-TEA *vs* post-TEA were compared by Student's paired *t*-test, $n = 10$ animals.

Evaluation of baroreflex sensitivity

Given the lack of effects of TEA on efferent autonomic stimulation via the stellate ganglia or vagal nerve, we additionally investigated whether TEA would have any effect on afferent-mediated autonomic function ($n = 10$). After TEA, phenylephrine-induced increases in systolic blood pressure were significantly blunted with the same dose (44.8 ± 1.1 mmHg before TEA *vs* 39.7 ± 1.7 mmHg after TEA, p = 0.03), Figure 6c. Despite a smaller increase in blood pressure, the chronotropic response was significantly greater after TEA (-2.8 ± 1.8 bpm *vs* -6.6 ± 2.5 bpm),

Figure 6d. Assessing the beat-to-beat relationship of systolic pressure to chronotropy further revealed that TEA significantly increased the baroreflex sensitivity from 0.49 mmHg/ms to 1.48 mmHg/ms (P < 0.01), Figure 6e.

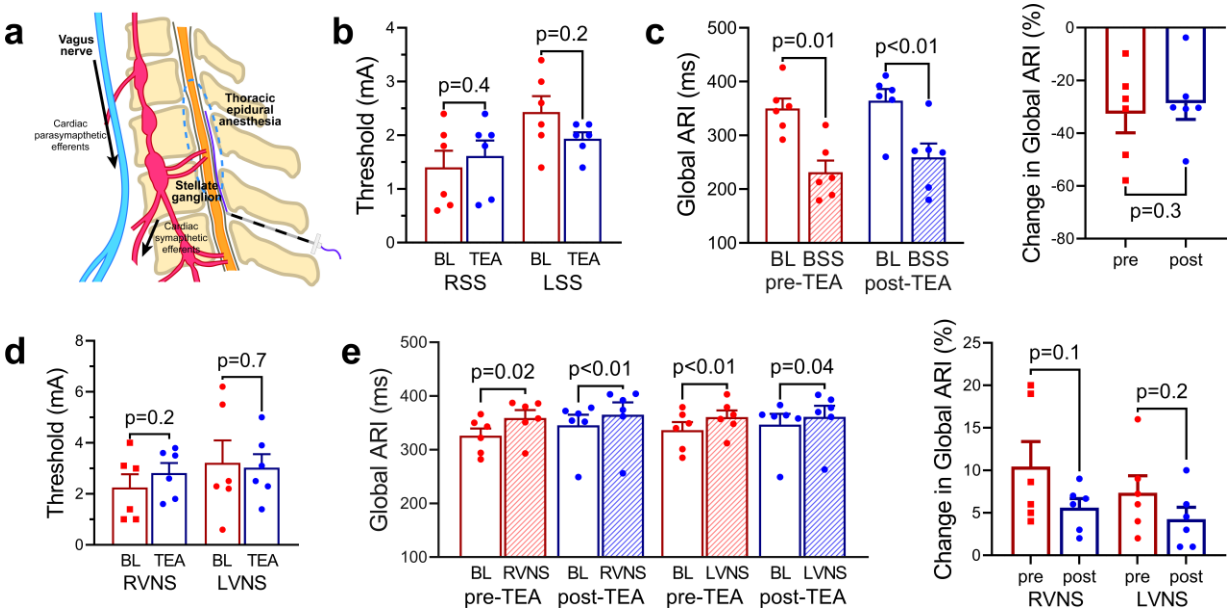

Figure 4-6. ***Thoracic epidural anesthesia does not disrupt efferent autonomic function.*** (**a**) Schematic indicating sites of stimulation (cervical vagus, stellate ganglion) relative to the site of blockade at the spinal cord. (**b**) TEA did not affect the current of stimulation required to reach sympathetic thresholds (defined unilaterally as a 10% increase in heart rate or systolic pressure). (**c**) BSS significantly shortened ventricular before TEA without notable differences after TEA. (**d**) Similarly, TEA did not affect the current of stimulation required to reach parasympathetic thresholds (defined unilaterally as a 10% decrease in heart rate). (**e**) VNS significantly prolonged ventricular ARI both before and after TEA but these effects were somewhat attenuated. BL = baseline, RVNS = right vagal nerve stimulation, LVNS = left vagal nerve stimulation. BL *vs* stimulation and pre-TEA *vs* post-TEA were compared by Student's paired *t*-test, *n* = 6 animals.

DISCUSSION

Major findings

In the present study, the effects of TEA on cardiac function and the mechanisms underlying the anti-arrhythmic benefits of TEA were investigated by detailed electrophysiological mapping, hemodynamic recordings, and autonomic testing in chronically infarcted pigs. This study demonstrates that the therapeutic effects of TEA in infarcted hearts may be due to relief of spinal afferent-mediated suppression of vagal efferent outflow and improvement in BRS, a novel finding

of this study. Improved parasympathetic function in addition to sympathetic efferent blockade can lead to the increased electrical stability and reduction in the incidence of ventricular arrhythmias by increasing ventricular ERP and ARI. Finally, TEA increases atrial ERP and AH interval in infarcted hearts and, importantly, does not have significant detrimental effects on RV function, as previously postulated.

Safety of TEA after myocardial infarction

While a mild decrease in LV contractility has been previously reported with TEA,[16] these effects on LV function are well-tolerated in patients.[17] However, data examining the effects of TEA in diseased hearts are lacking, resulting in hesitation to use TEA in patients with MI; in this study of chronically infarcted pigs, only a modest reduction in LV inotropy and lusitropy was observed without overt hemodynamic collapse or compromise.

Moreover, previous studies in healthy hearts and in patients with pulmonary hypertension had suggested a potential decrease in RV preload after TEA that may compromise basal RV function or its adaptations to increased afterload noted in pulmonary hypertension.[8, 18, 19] Data on the effects of TEA on RV function in the setting of LV dysfunction due to MI are lacking. Our study demonstrates that TEA did not affect RV systolic pressure or inotropy and suggest that in the setting of MI, the use of TEA as an anti-arrhythmic therapy may be both effective and safe.

Electrophysiological effects of TEA

Present studies investigating the electrophysiological effects of TEA in infarcted hearts are limited in both scope and quantity. Electrophysiological data from prior studies show mixed effects on surface parameters including RR and QT intervals where they report no effect or even shortening of these parameters.[20-22] Rodent studies investigating the cardiac sympathetic afferent reflex similarly suggest a role for cardiovascular disease-induced, state-dependent effects,[23] thereby impeding the extrapolation of results from normal animals which lack autonomic imbalances. Importantly, in our translational, large animal study with disease-induced autonomic imbalances, the benefits of TEA were clearly revealed.

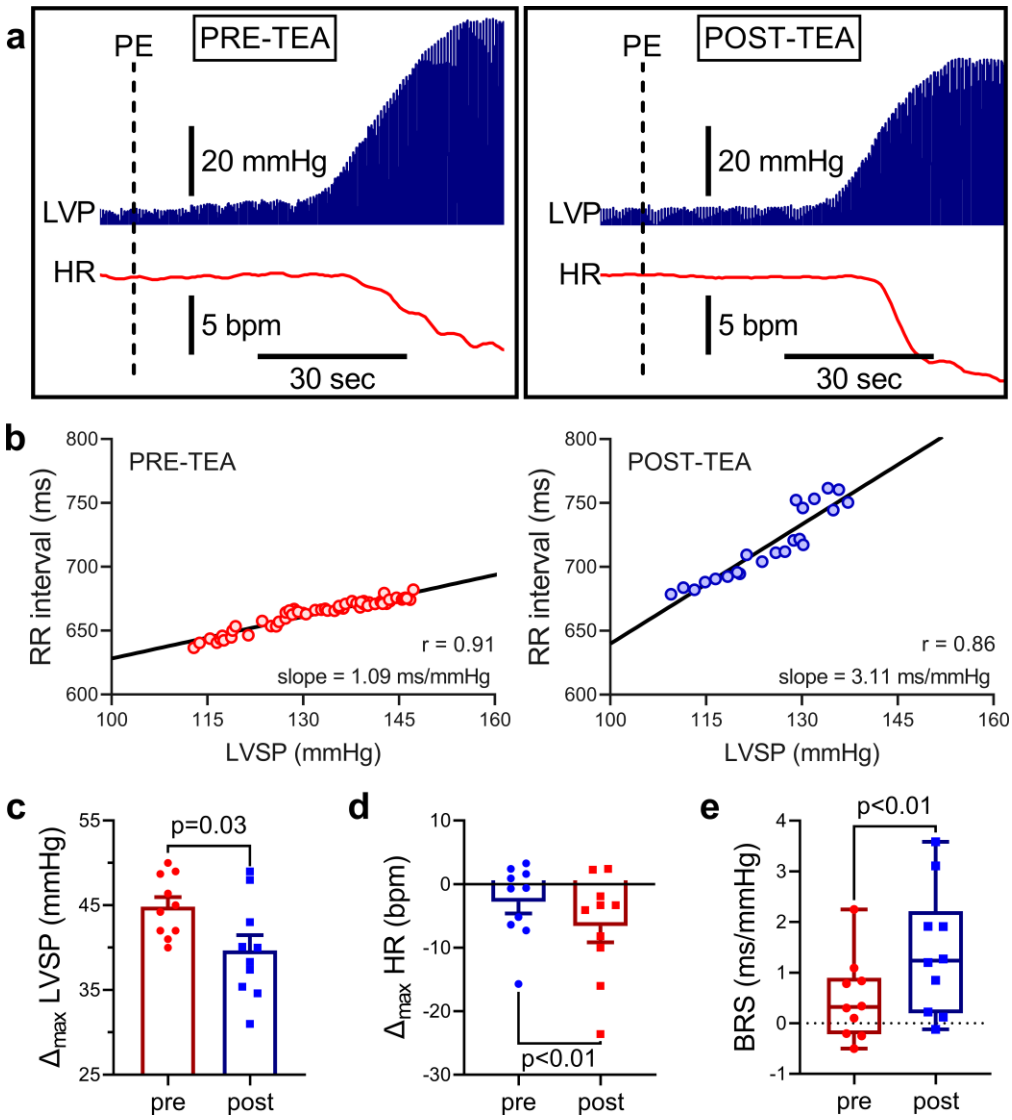

Figure 4-7. ***Baroreflex sensitivity is augmented by thoracic epidural anesthesia.*** (**a**) Representative raw trace depicting changes in heart rate upon phenylephrine challenge before and after TEA. The same dose of phenylephrine was used before and after TEA. (**b**) Beat-to-beat changes in LVSP and RR interval were plotted to assess BRS before and after TEA. The same dose of phenylephrine caused (**c**) a lesser increase in peak systolic pressure but (**d**) a greater slowing of heart rate after TEA. (**e**) BRS, the beat-to-beat relationship between systolic pressure and RR interval, was also significantly increased after TEA. PE = phenylephrine. Peak change in LVSP and HR was compared by paired Student's *t*-test and BRS was compared by paired Wilcoxon signed ranked test, *n* = 10 animals.

Our study herein demonstrated that TEA prolonged the AH interval without altering the HV interval. The observed increase in AH interval can be driven by both blockade of sympathetic efferent neurotransmission as well as improvement in vagal tone. We also found that atrial ERP

significantly increased after epidural anesthesia with lidocaine. Although the goal of this study was not to test the value of this therapy in the setting of atrial fibrillation (AF) inducibility, these data suggest that TEA may also be effective in settings where occurrence of AF is common, such as post-cardiac surgery.

Moreover, this is the first study to examine, in addition to ventricular refractoriness, the effects of TEA on action potential duration as measured by detailed electrophysiological mapping in structurally diseased hearts. In addition to prolonging ventricular refractoriness, TEA also prolonged ventricular action potential duration. Importantly, these effects spanned viable, scar, and border zone regions of the ventricles. Prolongation of action potential duration in the scar-border zone regions, established tinderboxes for ventricular arrhythmogenesis,[1] suggests that in chronically diseased hearts, TEA may act at these sites of myocardial and neural heterogeneity and suppress arrhythmogenesis. Furthermore, prior studies have shown that these benefits may be greater at higher heart rates,[24] suggesting that the effects seen here at rest may be an underestimation of its antiarrhythmic benefits when stressed. Interestingly, given that central sympathetic outflow is already inhibited in the setting of TEA, these prior findings hint at a role for reflexive activation of the parasympathetic nervous system.

Combined, these electrophysiological effects of TEA led to an overall reduction in inducibility of ventricular tachyarrhythmias by nearly 70%. Interestingly, this reduction in inducibility of VT/VF is comparable to the antiarrhythmic benefit reported in case series of patients receiving TEA.[5] These benefits likely result from a combination of increased ventricular electrical stability driven simultaneously by sympathetic blockade and augmentation of parasympathetic drive.

Effects of TEA on parasympathetic function

MI leads to significant parasympathetic dysfunction which manifests as decreased BRS.[25] Reduced BRS is an independent predictor of sudden cardiac death and ventricular arrhythmias in patients with MI and heart failure.[25, 26] Previous studies have suggested that the effects of TEA are predominantly due to blockade of sympathetic efferents.[27] However, the residual chronotropic

and inotropic effects of TEA and reductions in ventricular arrhythmia burden in the setting of high dose beta-blockers as seen in prior studies suggests that other anti-arrhythmic mechanisms of TEA exist. This study demonstrates that at least a portion of the anti-arrhythmic benefit of TEA may be due to enhanced vagal function.[21]

BRS in infarcted pigs at baseline was low, as was expected in the setting of chronic MI. However, the effects of TEA on BRS in patients or animals with MI are unknown. Studies in healthy hearts, where BRS is normal, had suggested that TEA may not change or even mildly reduce responses to phenylephrine.[28, 29] These data may suggest that in healthy hearts, a portion of the baroreflex response is mediated via sympathetic withdrawal. However, our data in infarcted hearts where parasympathetic dysfunction acts in tandem with sympathetic hyperactivity, shows that BRS significantly improves after TEA.

Previous studies in animals have shown that cardiac sympathetic afferent activation occurs in the setting of MI and that this chronic activation increases sympathetic outflow.[23] Moreover, in healthy animals, stimulation of sympathetic afferents can suppress vagal outflow.[30, 31] Although overlooked in studies-to-date, these prior data suggest that the benefits of TEA, in part, may be mediated via augmentation of the parasympathetic nervous system. Our study demonstrates for the first time, that in the setting of chronic MI where both sympathetic efferent and afferent activation occurs, epidural anesthesia may enhance parasympathetic function.

This data provides important mechanistic support for the sympathetic afferent-mediated reduction of parasympathetic tone following MI. In this regard, it is possible that some of the anti-arrhythmic, electrophysiological effects of TEA, including increases in ventricular ERP and ARI, are mediated through improved central vagal tone. This data also suggests a therapeutic role for sympathetic afferent blockade in improving parasympathetic function. Interestingly, while parasympathetic activation is generally perceived as cardioinhibitory, prior studies by Kock *et al*. have shown that TEA may improve LV function in the setting of coronary artery disease, despite maximal beta-blockade.[32] Thus, these data combine suggest a role for TEA-mediated relief of

central parasympathetic in 1) being anti-arrhythmic and 2) improving cardiac function, perhaps through a combination of improved coronary perfusion, more balanced cardiometabolic demand, and enhanced diastolic function.

In addition to a decrease in systolic blood pressure, likely due to withdrawal of central sympathetic outflow, we observed a decreased sensitivity to alpha-adrenergic stimulation after TEA. Although not explored in detail in the present study, this may be due to the baroreflex-triggered changes in autonomic control of the left ventricular inotropy and/or systemic vasculature.[33] This data further suggests that TEA may be a promising adjunct therapy to traditional antihypertensive pharmacological regimen as a novel parasympathetic neuromodulatory approach for treatment of resistant hypertension.

Lastly, TEA did not reduce the electrophysiological effects of peripheral VNS, where efferent fibers at the level of the cervical vagus are stimulated. However, there was a modest, but non-significant decrease in the ventricular effects of VNS. In line with prior studies,[34, 35] these data hint towards the benefits of vagal nerve stimulation being driven, at least in part, by afferent-mediated sympathetic withdrawal. Importantly, despite this modest reduction, VNS continued to prolong ventricular ARI by 15 to 20 msec. Thus, as ventricular electrical effects of VNS persisted, these data suggest that efferent parasympathetic activation alone via VNS may still provide additional cardioprotection and be employed synergistically with TEA.

Effects of TEA on stellate ganglia sympathetic function

In this study, TEA did not reduce effects of stellate stimulation. This is not unexpected as the stellate ganglion, which is part of the sympathetic chain, contains post-ganglionic sympathetic neurons that provide direct innervation to the heart. However, the fact that TEA reduced VT inducibility while increasing ERP and ARIs suggests that interruption of central sympathetic inputs to the stellate ganglia, and subsequently the heart, is anti-arrhythmic.

Importantly, the stellate ganglia contain a mixed population of nerves including afferents, efferents and local circuit neurons and are capable of maintaining reflex control of cardiac

function.[36, 37] Sympathetic blockade by TEA circumvents the interruption of intrathoracic cardiac reflexes which are critical for normal cardiovascular adaptation. Conversely, other neuromodulatory approaches targeted at disease-induced sympathoexcitation such as beta blockade, stellate ganglion blockade, and cardiac sympathetic denervation may hinder the maintenance of cardiac homeostasis. Neuromodulatory techniques such as TEA may thus benefit from reductions in central sympathetic outflow while leaving intact cardio-cardiac reflexes through the paravertebral ganglia.

Limitations

General anesthesia with isoflurane is known to blunt autonomic responses. To limit this effect, once surgical procedures had been completed, anesthesia was switched to α-chloralose.

Lidocaine has been shown to shorten action potential duration.[38, 39] Lidocaine absorbed into the systemic circulation may thus underestimate the effects of TEA. Moreover, the effects of TEA may be underestimated by potentially incomplete blockade of all cardiac spinal nerves. However, the blockade herein was sufficient to achieve a decrease in VT inducibility.

CONCLUSIONS

This study demonstrates that TEA is effective post-MI without compromising RV function. TEA increases atrial and ventricular ERPs and ARIs, the likely mechanism behind TEA's anti-arrhythmic effects. Notably, while TEA has been long purported to suppress cardiac sympathetic outflow and thereby reduce the damaging effects of sympathoexcitation, TEA also improves parasympathetic function, which can independently improve electrophysiological parameters and be anti-arrhythmic. The effects of TEA on BRS provides insight into parasympathetic dysfunction post-MI, demonstrating the role of sympathetic spinal afferents in reducing central vagal drive. TEA uniquely benefits from blockade at an anatomic and autonomic nexus point, achieving bilateral blockade of cardiac-projecting sympathetic efferents along with sympathetic afferents which may reduce further sympathoexcitation and simultaneously relieve afferent-mediated suppression of parasympathetic outflow.

ACKNOWLEDGMENTS

We would like to thank Zulfiqar Lokhandwala and Neil Jani for their technical assistance with experiments. We would like to thank Drs. Kalyanam Shivkumar and Jeffrey Ardell for their guidance and support.

FUNDING SUPPORT AND AUTHOR DISCLOSURES

The authors have no competing interests to report. This study was funded by NIHDP2HL132356 and SPARC OT2OD023848 to MV.

REFERENCES

1 Vaseghi M, Shivkumar K. The role of the autonomic nervous system in sudden cardiac death. Prog Cardiovasc Dis. 2008;50:404-419

2 Priori SG, Mantica M, Schwartz PJ. Delayed afterdepolarizations elicited in vivo by left stellate ganglion stimulation. Circulation. 1988;78:178-185

3 Opthof T, Misier AR, Coronel R, Vermeulen JT, Verberne HJ, Frank RG, Moulijn AC, van Capelle FJ, Janse MJ. Dispersion of refractoriness in canine ventricular myocardium. Effects of sympathetic stimulation. Circ Res. 1991;68:1204-1215

4 Shivkumar K, Ajijola OA, Anand I, Armour JA, Chen PS, Esler M, De Ferrari GM, Fishbein MC, Goldberger JJ, Harper RM, Joyner MJ, Khalsa SS, Kumar R, Lane R, Mahajan A, Po S, Schwartz PJ, Somers VK, Valderrabano M, Vaseghi M, Zipes DP. Clinical neurocardiology defining the value of neuroscience-based cardiovascular therapeutics. J Physiol. 2016;594:3911-3954

5 Do DH, Bradfield J, Ajijola OA, Vaseghi M, Le J, Rahman S, Mahajan A, Nogami A, Boyle NG, Shivkumar K. Thoracic epidural anesthesia can be effective for the short-term management of ventricular tachycardia storm. J Am Heart Assoc. 2017;6

6 Bourke T, Vaseghi M, Michowitz Y, Sankhla V, Shah M, Swapna N, Boyle NG, Mahajan A, Narasimhan C, Lokhandwala Y, Shivkumar K. Neuraxial modulation for refractory ventricular arrhythmias: Value of thoracic epidural anesthesia and surgical left cardiac sympathetic denervation. Circulation. 2010;121:2255-2262

7 Mahajan A, Takamiya T, Benharash P, Zhou W. Effect of thoracic epidural anesthesia on heart rate variability in a porcine model. Physiol Rep. 2017;5

8 Wink J, de Wilde RB, Wouters PF, van Dorp EL, Veering BT, Versteegh MI, Aarts LP, Steendijk P. Thoracic epidural anesthesia reduces right ventricular systolic function with maintained ventricular-pulmonary coupling. Circulation. 2016;134:1163-1175

9 Blomberg S, Ricksten SE. Thoracic epidural anaesthesia decreases the incidence of ventricular arrhythmias during acute myocardial ischaemia in the anaesthetized rat. Acta Anaesthesiol Scand. 1988;32:173-178

10 Nakahara S, Vaseghi M, Ramirez RJ, Fonseca CG, Lai CK, Finn JP, Mahajan A, Boyle NG, Shivkumar K. Characterization of myocardial scars: Electrophysiological imaging correlates in a porcine infarct model. Heart Rhythm. 2011;8:1060-1067

11 Hoang JD, Yamakawa K, Rajendran PS, Chan CA, Yagishita D, Nakamura K, Lux RL, Vaseghi M. Proarrhythmic effects of sympathetic activation are mitigated by vagal nerve stimulation in infarcted hearts. JACC Clin Electrophysiol. 2022;8:513-525

12 Irie T, Yamakawa K, Hamon D, Nakamura K, Shivkumar K, Vaseghi M. Cardiac sympathetic innervation via middle cervical and stellate ganglia and antiarrhythmic mechanism of bilateral stellectomy. Am J Physiol Heart Circ Physiol. 2017;312:H392-H405

13 Smyth HS, Sleight P, Pickering GW. Reflex regulation of arterial pressure during sleep in man. A quantitative method of assessing baroreflex sensitivity. Circ Res. 1969;24:109-121

14 Haws CW, Lux RL. Correlation between in vivo transmembrane action potential durations and activation-recovery intervals from electrograms. Effects of interventions that alter repolarization time. Circulation. 1990;81:281-288

15 Marchlinski FE, Callans DJ, Gottlieb CD, Zado E. Linear ablation lesions for control of unmappable ventricular tachycardia in patients with ischemic and nonischemic cardiomyopathy. Circulation. 2000;101:1288-1296

16 Goertz AW, Seeling W, Heinrich H, Lindner KH, Schirmer U. Influence of high thoracic epidural anesthesia on left ventricular contractility assessed using the end-systolic pressure-length relationship. Acta Anaesthesiol Scand. 1993;37:38-44

17 Wink J, Veering BT, Aarts L, Wouters PF. Effects of thoracic epidural anesthesia on neuronal cardiac regulation and cardiac function. Anesthesiology. 2019;130:472-491

18 Rex S, Missant C, Segers P, Wouters PF. Thoracic epidural anesthesia impairs the hemodynamic response to acute pulmonary hypertension by deteriorating right ventricular-pulmonary arterial coupling. Crit Care Med. 2007;35:222-229

19 Missant C, Claus P, Rex S, Wouters PF. Differential effects of lumbar and thoracic epidural anaesthesia on the haemodynamic response to acute right ventricular pressure overload. Br J Anaesth. 2010;104:143-149

20 Komatsuzaki M, Takasusuki T, Yamaguchi S. Impact of thoracic epidural sympathetic block on cardiac repolarization. Local Reg Anesth. 2018;11:81-85

21 Hotvedt R, Refsum H, Platou ES. Cardiac electrophysiological and hemodynamic effects of beta-adrenoceptor blockade and thoracic epidural analgesia in the dog. Anesth Analg. 1984;63:817-824

22 Owczuk R, Steffek M, Wujtewicz MA, Szymanowicz W, Twardowski P, Marjanski T, Wojciechowski J, Zienciuk A, Rzyman W, Wujtewicz M. Effects of thoracic epidural anaesthesia on cardiac repolarization. Clin Exp Pharmacol Physiol. 2009;36:880-883

23 Wang HJ, Rozanski GJ, Zucker IH. Cardiac sympathetic afferent reflex control of cardiac function in normal and chronic heart failure states. J Physiol. 2017;595:2519-2534

24 Meissner A, Eckardt L, Kirchhof P, Weber T, Rolf N, Breithardt G, Van Aken H, Haverkamp W. Effects of thoracic epidural anesthesia with and without autonomic nervous system blockade on cardiac monophasic action potentials and effective refractoriness in awake dogs. Anesthesiology. 2001;95:132-138; discussion 136A

25 Schwartz PJ, Vanoli E, Stramba-Badiale M, De Ferrari GM, Billman GE, Foreman RD. Autonomic mechanisms and sudden death. New insights from analysis of baroreceptor reflexes in conscious dogs with and without a myocardial infarction. Circulation. 1988;78:969-979

26 La Rovere MT, Bigger JT, Jr., Marcus FI, Mortara A, Schwartz PJ. Baroreflex sensitivity and heart-rate variability in prediction of total cardiac mortality after myocardial infarction. Atrami (autonomic tone and reflexes after myocardial infarction) investigators. Lancet. 1998;351:478-484

27 Lee SC, Lee C, Kim YC. Epinephrine-induced arrhythmias: Effects of thoracic epidural anesthesia and vagotomy during enflurane anesthesia in rabbits. J Korean Med Sci. 1999;14:133-137

28 Takeshima R, Dohi S. Circulatory responses to baroreflexes, valsalva maneuver, coughing, swallowing, and nasal stimulation during acute cardiac sympathectomy by epidural blockade in awake humans. Anesthesiology. 1985;63:500-508

29 Dohi S, Tsuchida H, Mayumi T. Baroreflex control of heart rate during cardiac sympathectomy by epidural anesthesia in lightly anesthetized humans. Anesth Analg. 1983;62:815-820

30 Schwartz PJ, Pagani M, Lombardi F, Malliani A, Brown AM. A cardiocardiac sympathovagal reflex in the cat. Circ Res. 1973;32:215-220

31 Gao L, Schultz HD, Patel KP, Zucker IH, Wang W. Augmented input from cardiac sympathetic afferents inhibits baroreflex in rats with heart failure. Hypertension. 2005;45:1173-1181

32 Kock M, Blomberg S, Emanuelsson H, Lomsky M, Stromblad SO, Ricksten SE. Thoracic epidural anesthesia improves global and regional left ventricular function during stress-induced myocardial ischemia in patients with coronary artery disease. Anesth Analg. 1990;71:625-630

33 Jordan J, Tank J, Shannon JR, Diedrich A, Lipp A, Schroder C, Arnold G, Sharma AM, Biaggioni I, Robertson D, Luft FC. Baroreflex buffering and susceptibility to vasoactive drugs. Circulation. 2002;105:1459-1464

34 Shen MJ, Shinohara T, Park HW, Frick K, Ice DS, Choi EK, Han S, Maruyama M, Sharma R, Shen C, Fishbein MC, Chen LS, Lopshire JC, Zipes DP, Lin SF, Chen PS. Continuous low-level vagus nerve stimulation reduces stellate ganglion nerve activity and paroxysmal atrial tachyarrhythmias in ambulatory canines. Circulation. 2011;123:2204-2212

35 Shen MJ, Hao-Che C, Park HW, George Akingba A, Chang PC, Zheng Z, Lin SF, Shen C, Chen LS, Chen Z, Fishbein MC, Chiamvimonvat N, Chen PS. Low-level vagus nerve stimulation upregulates small conductance calcium-activated potassium channels in the stellate ganglion. Heart Rhythm. 2013;10:910-915

36 Ardell JL, Nier H, Hammer M, Southerland EM, Ardell CL, Beaumont E, KenKnight BH, Armour JA. Defining the neural fulcrum for chronic vagus nerve stimulation: Implications for integrated cardiac control. J Physiol. 2017;595:6887-6903

37 Ardell JL, Shivkumar K. Foundational concepts for cardiac neuromodulation. Bioelectroincs in Medicine. 2017;1

38 Endresen K, Amlie JP. Acute effects of lidocaine on repolarization and conduction in patients with coronary-artery disease. Clin Pharmacol Ther. 1989;45:387-395

39 Ujhelyi MR, Schur M, Frede T, Bottorff MB, Gabel M, Markel ML. Hypertonic saline does not reverse the sodium channel blocking actions of lidocaine: Evidence from electrophysiologic and defibrillation studies. J Cardiovasc Pharm. 1997;29:61-68

Chapter 5

Cardiac Sympathetic Activation Circumvents High Dose Beta-blocker Therapy in Part Through Release of Neuropeptide-Y

Jonathan D Hoang*, Siamak Salavatian*, Naoko Yamaguchi*, Mohammed Amer Swid, David Hamon, Marmar Vaseghi

*These authors share first author position.

Hoang JD, Salavatian S, Yamaguchi N, Swid MA, David H, Vaseghi M. Cardiac sympathetic activation circumvents high-dose beta blocker therapy in part through release of neuropeptide Y. JCI Insight. 2020;5(11). Epub 2020/06/05. doi: 10.1172/jci.insight.135519.

ABSTRACT

The sympathetic nervous system plays an important role in occurrence of ventricular tachycardia (VT). Many patients, however, experience VT despite maximal doses of beta-blocker therapy, possibly due to the effects of sympathetic co-transmitters such as neuropeptide Y (NPY). The purpose of this study was to determine whether propranolol, at higher than clinically recommended doses, could block ventricular electrophysiological effects of sympatho-excitation via stellate ganglia stimulation, and if any residual effects were mediated by NPY, in a porcine model. Greater release of cardiac NPY was observed at higher frequencies of sympathetic stimulation (10 and 20 vs. 4Hz). Despite treatment with even higher doses of propranolol (1.0 mg/kg), electrophysiological effects of sympathetic stimulation remained with residual shortening of activation-recovery interval (ARI), a surrogate of action potential duration. Adjuvant treatment with NPY Y_1 receptor antagonist, BIBO 3304, however, reduced these electrophysiological effects, while augmenting inotropy. These data demonstrate that high dose beta-blocker therapy is insufficient to block electrophysiological effects of sympatho-excitation, and a portion of these electrical effects in-vivo are mediated by NPY. Y_1 receptor blockade may represent a promising adjuvant therapy to beta-adrenergic receptor blockade.

GRAPHICAL ABSTRACT

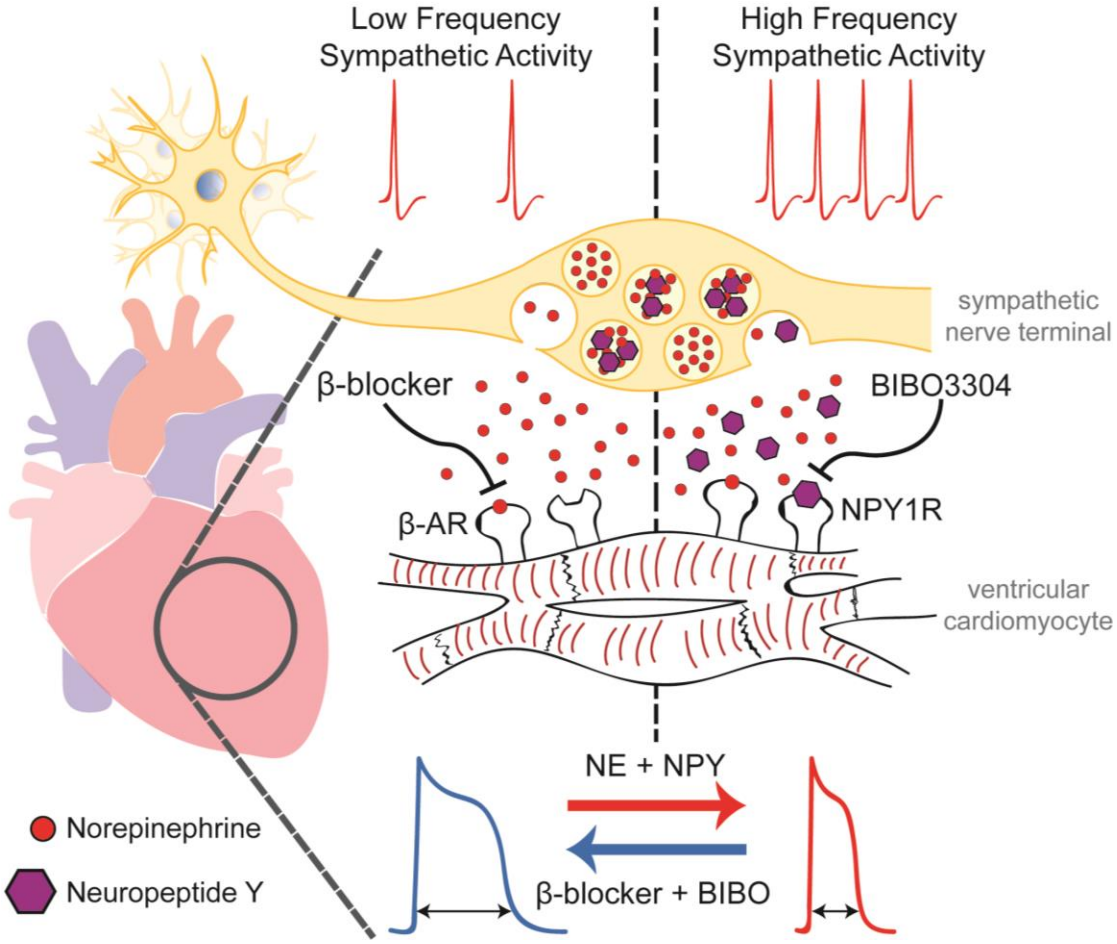

INTRODUCTION

The sympathetic nervous system plays an important role in the occurrence of ventricular tachycardia (VT) and ventricular fibrillation (VF).[1-3] Cardiac sympathetic activation causes triggered activity[4,5] and increases in heterogeneity and dispersion of ventricular repolarization,[6-8] leading to VT, VF, and sudden cardiac death.[9] Beta-blocker therapy, by targeting beta-adrenergic receptors for norepinephrine (NE), remains the cornerstone of sympathetic neuromodulation for treatment of VT and VF.[10] Recently, propranolol has been suggested to be more efficacious for control of recurrent ventricular arrhythmias than metoprolol, especially in the setting of VT/VF (electrical) storm.[11]

However, despite maximally tolerated doses of beta-blocker therapy, patients can continue to experience recurrent VT and VF episodes.[11] It's possible that during states of significantly elevated sympathetic tone, beta-blocker therapy is insufficient to completely suppress the electrophysiological effects of sympathetic activation. This may in part be due to release of sympathetic neuropeptides, such as neuropeptide Y (NPY), which are reported to be released during states of excessive sympathetic activation,[12-14] and as of yet, are not therapeutically targeted. It has been reported that elevated coronary sinus (CS) plasma NPY levels in patients presenting with heart failure portends a poor outcome,[15] and in patients with acute myocardial infarction (MI) is associated with higher ventricular arrhythmia scores [14], greater infarct size, and reduced ejection fraction, despite reperfusion therapy.[16] In a rat Langendorff model, blockade of myocardial NPY Y_1 receptor (NPY1R) by BIBO 3304, increased VF thresholds.[17] These data suggest that NPY has proarrhythmic potential, which could be mediated through its Y_1 receptor on cardiac myocytes.[18] However, direct ventricular electrophysiological effects of NPY *in-vivo* remain to be evaluated.

The purpose of this study was to evaluate the effects of sympathetic activation via bilateral stellate ganglia stimulation (BSS) at different frequencies on cardiac electrophysiological indices, hemodynamic parameters, and NE and NPY levels, in a porcine model *in-vivo*. In addition, we

hypothesized that high doses of propranolol, at several times clinically indicated doses, may not be sufficient to completely block the effects of sympathoexcitation. Finally, we assessed whether any remaining electrophysiological effects may be driven from the release of cardiac NPY and attenuated by infusion of the Y_1 receptor blocker, BIBO 3304.

RESULTS

In order to study the effects of sympathetic stimulation on hemodynamic and electrophysiological parameters and neurotransmitter/neuropeptide profiles with and without propranolol and the Y_1 inhibitor BIBO 3304, 3 protocols involving different groups of animals (protocols 1–3) were used (Figure 1A).

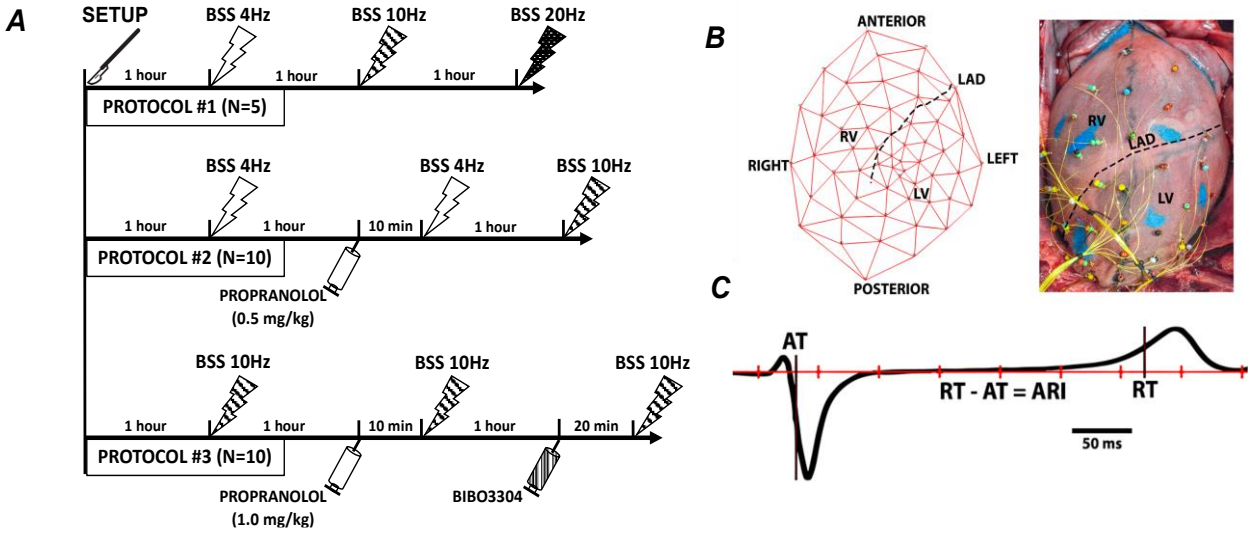

Figure 5-1. ***Study design and methods.*** (**A**) Timeline of protocols used to evaluate effects of BSS under different pharmacological conditions. (**B**) Schematic of the 56-electrode sock used to acquire local electrograms from ventricular epicardium. Electrograms are mapped onto a 2-dimensional plane to assess regional differences. (**C**) ARI, a surrogate for action potential duration, is measured as the time from the most negative d*V*/d*t* of the activation wave-front to the most positive d*V*/d*t* of the repolarization wave-front.

Effects of frequency of sympathetic stimulation on hemodynamic parameters, neurotransmitter/neuropeptide profiles, and electrophysiological parameters

In protocol 1, the effects of frequency on hemodynamic and electrical parameters as well as NE and NPY release profiles were tested at 3 different frequencies (4, 10, and 20 Hz) but at

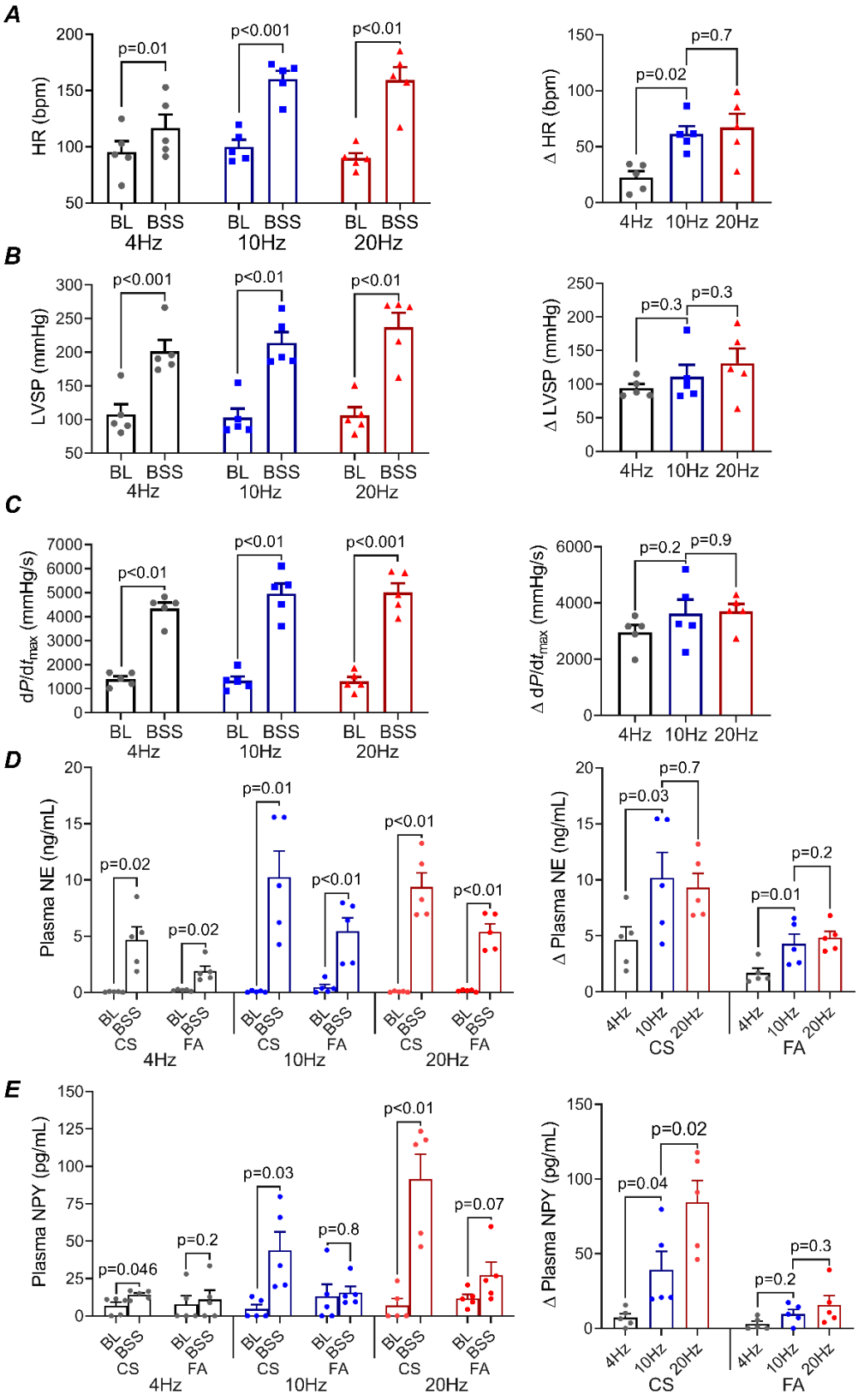

Figure 5-2. ***Effects of different frequencies of BSS on cardiac hemodynamic parameters, NE, and NPY.***

All frequencies of stimulation significantly increased (**A**) HR**,** (**B**) LVSP, (**C**) and d*P*/dt_{max}. HR, unlike LVSP or

dP/dt_{max}, increased significantly more at 10 Hz than 4 Hz. There were no significant differences in hemodynamic parameters between 10 Hz and 20 Hz. (**D**) Plasma NE in the CS with all frequencies of stimulation, but release was significantly greater in the CS than femoral artery (FA). Release of NE was greater at the higher frequencies. There was no difference in the changes in CS NE levels between 10 Hz and 20 Hz of stimulation. (**E**) CS NPY levels at 10 Hz BSS were greater than 4 Hz, with further increases observed at 20 Hz. BL = baseline, n = 5 animals for all comparisons, baseline vs. stimulation comparisons were performed using the two-sided paired Student's t-test and comparisons of changes between different frequencies were performed using one-way ANOVA with post hoc analysis. $P \leq 0.05$ was considered statistically significant.

the same fixed current (defined as 1.2 times the threshold current that led to a 10% increase in heart rate or systolic blood pressure at 4 Hz) in-vivo in 5 Yorkshire pigs to determine NE and NPY release profiles in this species. All tested frequencies of stimulation significantly increased heart rate (HR), left ventricular systolic pressure (LVSP), and dP/dt_{max} from baseline ($P < 0.05$) (Figure 2A-C). BSS at 10 Hz increased HR more than 4 Hz (61.5 ± 7.0 bpm vs. 22.7 ± 5.5 bpm; $P = 0.02$). Further increases in HR at 20 Hz vs. 10 Hz were not observed. There were no significant differences between frequencies of stimulations on increases in LVSP or dP/dt_{max}.

The effects of frequency of BSS on electrical, hemodynamic, and plasma NE and NPY levels are shown in Figure 2, D and E. All frequencies of stimulation increased coronary sinus (CS) NE levels by 100- to 150-fold. BSS at 10 Hz and 20 Hz led to significantly greater release of CS NE compared to 4 Hz. There were no statistically significant differences in NE release profiles at 10 Hz vs. 20 Hz.

BSS at 4 Hz caused a significant, but modest change in CS NPY levels (from 6.7 ± 2.6 pg/mL to 14.1 ± 1.3 pg/mL; $P = 0.046$) but not FA NPY levels (Figure 2E). However, BSS at 10 Hz evoked a 5-fold greater release of CS NPY than 4 Hz (39.3 ± 12.2 pg/mL with 10 Hz vs. 7.2 ± 2.7 pg/mL with 4 Hz; $P = 0.04$). BSS at 20 Hz further increased CS NPY levels compared to 10 Hz (from 7.0 ± 4.7 pg/mL to 91.4 ± 16.7 pg/mL; $P < 0.01$). CS and FA release profiles for NE and NPY are shown in Tables 1 and 2, respectively.

Ventricular activation-recovery intervals, corrected for heart rate, (ARIc), shortened during BSS compared to baseline with all frequencies of stimulation (Figure 3). Stimulation at 4 Hz

Table 5-1. ***Plasma NE concentrations in the coronary sinus and femoral artery at baseline and during bilateral stellate ganglia stimulations for protocols 1 to 3.***

			BL (ng/ml)	BSS (ng/ml)	Δ (ng/ml)
Protocol #1 (n=5)	4 Hz BSS	CS	0.04 ± 0.0	**4.7 ± 1.2***	4.6 ± 1.2
		FA	0.2 ± 0.03	**1.9 ± 0.5***	1.7 ± 0.4
	10 Hz BSS	CS	0.07 ± 0.04	**10.2 ± 2.3***	10.2 ± 2.3
		FA	0.4 ± 0.3	**4.7 ± 1.1****	4.3 ± 0.9
	20 Hz BSS	CS	0.06 ± 0.03	**9.4 ± 1.3****	9.3 ± 1.3
		FA	0.2 ± 0.04	**5.0± 0.6****	4.8 ± 0.6
Protocol #2 (n=10)	4 Hz BSS + 0.5 mg/kg Propranolol	CS	0.2 ± 0.06	**2.2 ± 0.7***	2.1 ± 0.7
		FA	1.4 ± 0.5	**8.9 ± 2.3****	7.5 ± 2.0
	10 Hz BSS + 0.5 mg/kg Propranolol	CS	0.2 ± 0.06	**2.70± 0.4*****	2.5 ± 0.4
		FA	2.4 ± 0.6	**18.7± 4.4****	16.2 ± 4.2
Protocol #3 (n=10)	10 Hz BSS	CS	0.1 ± 0.04	**9.1 ± 1.6*****	9.0 ± 1.6
		FA	0.07 ± 0.03	**4.3 ± 1.5***	4.2 ± 1.5
	10 Hz BSS + 1.0 mg/kg Propranolol	CS	0.1 ± 0.04	**1.14 ± 0.38***	1.0 ± 0.4
		FA	0.1 ± 0.05	**0.8 ± 0.2****	0.7± 0.2
	10 Hz BSS + 1.0 mg/kg Propranolol + BIBO 3304	CS	0.3 ± 0.08	1.50± 0.6	1.2 ± 0.6
		FA	0.2 ± 0.05	**0.83± 0.2*****	0.7 ± 0.1

CS = coronary sinus, FA = femoral artery, BL = baseline, BSS = bilateral stellate ganglia stimulation. *$P \leq 0.05$, **$P < 0.01$, ***$P < 0.001$ vs. baseline.

shortened global ARIc by 75 ± 17 ms (from 397 ± 8 ms to 322 ± 17 ms; $P = 0.01$), whereas BSS at 10 Hz induced further shortening (139 ± 8 ms; from 392 ± 9 ms to 253 ± 10 ms; $P < 0.001$). BSS at 20 Hz also caused a 166 ± 8 ms shortening in global ventricular ARIc (from 415 ± 6 ms to 249 ± 10 ms; $P < 0.001$) but this was not significantly different than changes observed at 10 Hz. No significant regional differences in ARIs at different frequencies of stimulation were noted, Supplemental Figure 1.

Effects of sympathetic stimulation after 0.5 mg/kg propranolol

Given the lack of electrophysiological and ARI differences between 10 Hz and 20 Hz of stimulation frequency, the effects of propranolol 0.5 mg/kg were evaluated during BSS at 4 Hz

Table 5-2. ***Plasma NPY concentrations in the coronary sinus and femoral artery at baseline and during bilateral stellate ganglia stimulations.***

			BL (ng/ml)	BSS (ng/ml)	Δ (ng/ml)
Protocol #1 (n=5)	4 Hz BSS	CS	6.7 ± 2.6	**14.1 ± 1.3***	7.2 ± 2.7
		FA	8.0 ± 5.5	11.0 ± 6.2	3.1 ± 1.8
	10 Hz BSS	CS	4.6 ± 2.9	**43.9 ± 12.3***	39.3 ± 12.2
		FA	12.9 ± 8.2	15.6 ± 4.2	9.6 ± 3.0
	20 Hz BSS	CS	7.0 ± 4.7	**91.4 ± 16.7****	84.5 ± 14.5
		FA	11.7 ± 2.7	27.4 ± 8.5	15.7 ± 6.3
Protocol #2 (n=10)	4 Hz BSS + 0.5 mg/kg Propranolol	CS	9.0 ± 2.3	**11.9 ± 2.0****	2.3 ± 0.7
		FA	8.0 ± 1.8	9.6 ± 1.9	1.9 ± 0.9
	10 Hz BSS + 0.5 mg/kg Propranolol	CS	7.3 ± 1.9	**17.1 ± 3.6****	9.9 ± 2.6
		FA	7.9 ± 2.2	11.25 ± 2.41	3.9 ± 1.5
Protocol #3 (n=10)	10 Hz BSS	CS	7.0 ± 1.7	**16.4 ± 2.1****	9.5 ± 2.4
		FA	12.6 ± 4.2	14.5 ± 2.9	6.3 ± 2.1
	10 Hz BSS + 1.0 mg/kg Propranolol	CS	9.6 ± 1.9	**14.9 ± 1.9****	5.3 ± 1.3
		FA	17.1 ± 6.1	15.9 ± 4.9	2.5 ± 1.2
	10 Hz BSS + 1.0 mg/kg Propranolol + BIBO 3304	CS	9.3 ± 1.5	**16.3 ± 1.5*****	7.0 ± 1.3
		FA	16.1 ± 6.0	17.8 ± 4.4	4.4 ± 1.3

CS = coronary sinus, FA = femoral artery, BL = baseline, BSS = bilateral stellate ganglia stimulation. *$P \leq 0.05$, **$P < 0.01$, ***$P < 0.001$ vs. baseline.

and 10 Hz (n = 10) (Figure 1). Despite propranolol at this high dose, BSS at 4 Hz and 10 Hz significantly increased HR, LVSP, and dP/dt_{max} (Supplemental Figure 2) with greater increases in LVSP and dP/dt_{max} at 10 Hz than 4 Hz.

BSS at 4 Hz and 10 Hz shortened global ventricular ARIc compared to baseline, despite beta-blocker therapy. However, BSS at 10 Hz caused greater global ARIc effects than at 4 Hz (a decrease of 29 ± 4 ms at 10 Hz vs. 9 ± 3 ms at 4 Hz; $P < 0.001$) after propranolol treatment, despite similar levels of NE in the CS, further suggesting a potential role for other co-transmitters in mediating these effects. Raw (uncorrected) ARI values for BSS at 4 Hz and 10 Hz are reported in Supplemental Figure 3.

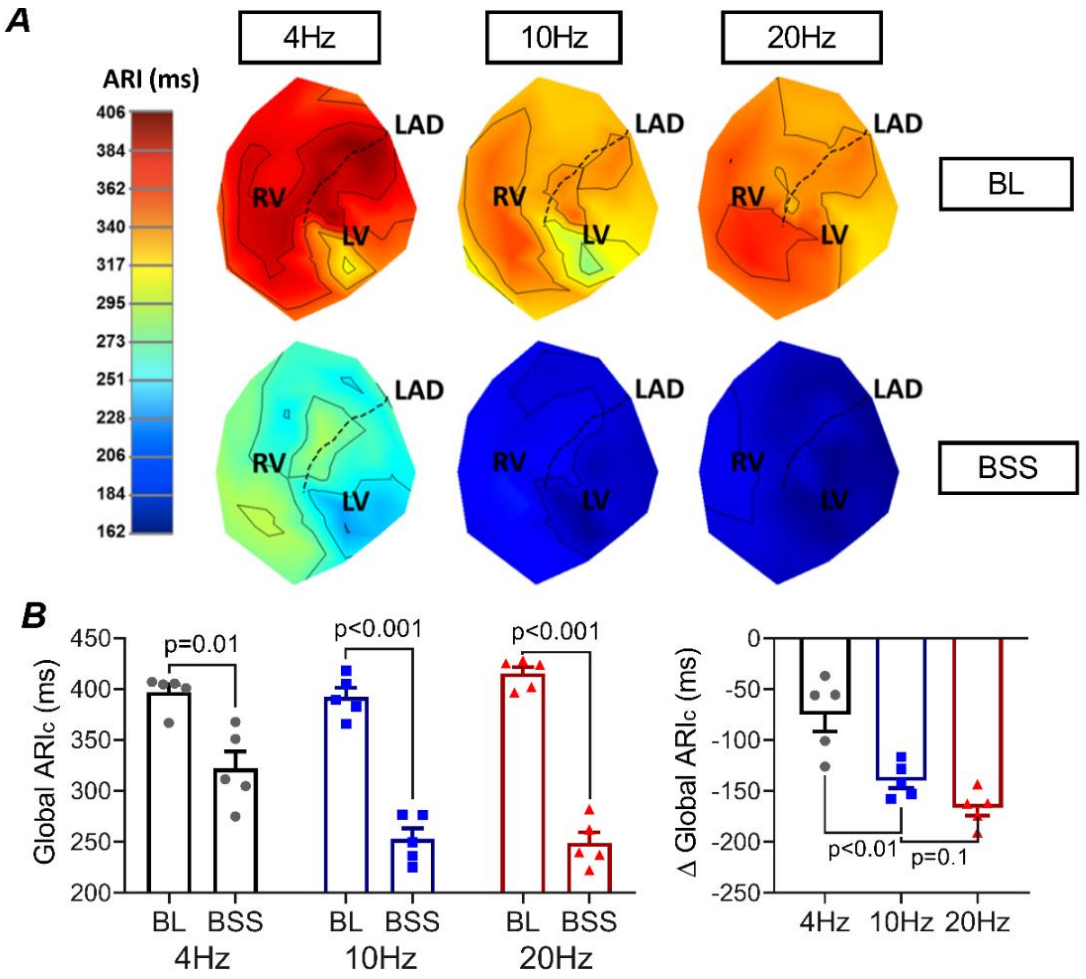

Figure 5-3. ***Effects of frequency of stimulation on ventricular electrophysiology.*** (**A**) Representative polar maps depicting the effects of BSS at 4, 10, and 20 Hz on ventricular ARIs. (**B**) All stimulation frequencies caused significant shortening of corrected ARIs. BSS at 10 Hz and 20 Hz shortened global ventricular ARIs more than 4 Hz, even after correcting for heart rate. There was no difference in ARIc shortening between BSS at 10 Hz vs. 20 Hz. BL = baseline, ARIc = corrected ARI for heart rate, △ = change from BL. *n* = 10 animals for all comparisons, baseline vs. stimulation comparisons were performed using the two-sided paired Student's *t*-test and comparisons of changes between different frequencies were performed using one-way ANOVA with post hoc analysis. $P \leq 0.05$ was considered significant.

Effects of sympathetic stimulation after 1.0 mg/kg of propranolol

Given the results of the above experiments which demonstrated significant residual electrophysiological effects at 0.5 mg/kg of propranolol and significant release of NPY at 10 Hz, in protocol 3 we used stimulations at 10 Hz were used to evaluate effects of BSS after 1.0 mg/kg propranolol (to assure even greater blockade of beta-adrenergic receptors) (Figure 1).

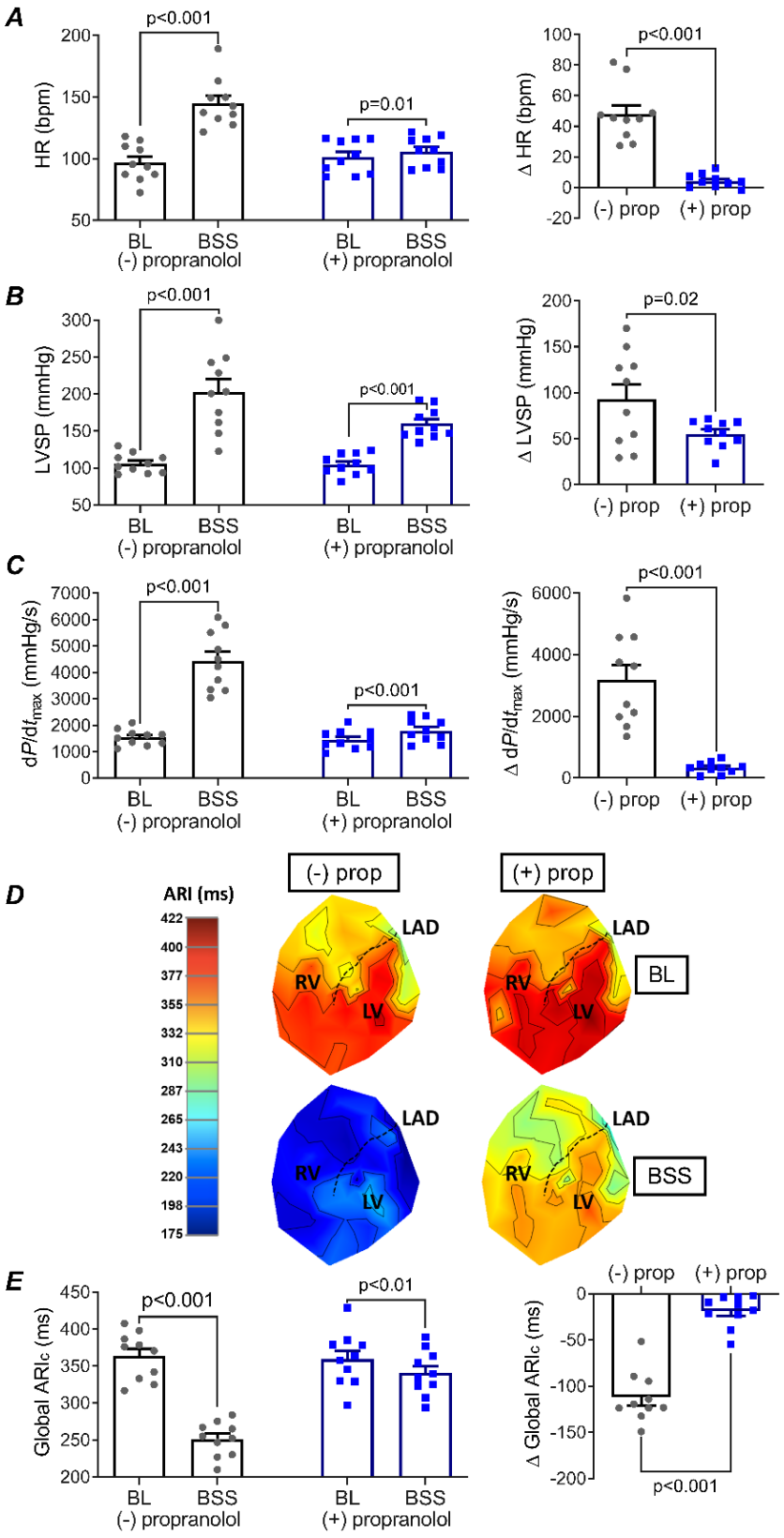

Figure 5-4. ***Effects of 1.0 mg/kg propranolol on BSS induced changes in hemodynamic and electrophysiological parameters.*** Although effects of BSS, especially HR, were mitigated by 1.0 mg/kg

of propranolol, 10 Hz BSS continued to have significant increase (**A**) HR, (**B**) LVSP, and (**C**) dP/dt_{max}. (**D**) Representative polar maps comparing raw ventricular ARIs with and without propranolol. (**E**) Although 1.0 mg/kg propranolol did mitigate BSS-induced changes in global ARIs, it did not completely block the effects of BSS. BL = baseline, ARIc = corrected ARI for heart rate, △ = change from BL. (-) prop = untreated animals, (+) prop = 1.0 mg/kg propranolol. n = 10 animals for all comparisons, analyses were performed using the two-sided paired Student's t-test. $P \leq 0.05$ was considered significant.

Propranolol (1.0 mg/kg) significantly mitigated BSS-induced CS NE release profiles (from 9.0 ± 1.6 ng/mL to 1.0 ± 0.4 ng/mL), while there was only a modest reduction in BSS-induced release of CS NPY (Tables 1 and 2).

Although the effects of BSS on hemodynamic parameters and ventricular ARIs were significantly reduced after infusion of 1.0 mg/kg propranolol, BSS still increased HR, LVSP, and dP/dt_{max} ($P < 0.001$ for all parameters, Figure 4, A-C). Furthermore, after treatment with 1.0 mg/kg propranolol, BSS continued to significantly shorten global ventricular ARIc by 19 ± 5 ms (from 359 ± 12 ms to 341 ± 10 ms; $P < 0.01$; Figure 4, D and E). Raw (uncorrected) ARI values are reported in Supplemental Figure 3.

Expression of NPY1R on the ventricular myocardium

The presence of NPY1R protein in the ventricular myocardium was confirmed by Western blotting (Figure 5B; see complete unedited gel in the supplemental material). A major immunoreactive band was detected at approximately 51 kDa in the apex, mid and base of the left ventricle (n = 3). The higher molecular weight may represent an intermediate N- or O-glycosylated form with bands up to 55 kDa reported in human tissue.[19]

The localization of NPY1R was further validated by immunohistochemistry, Figure 5. High expression of NPY1R was noted in the vascular smooth muscle of cardiac blood vessels with adjacent NPY-immunoreactive nerve fibers. While highly expressing NPY, cardiac ganglia expressed only low levels of NPY1R. Adjacent myocardium showed moderate expression of NPY1R with NPY-immunoreactive nerve fibers running between myocytes. Neither NPY nor NPY1R immunoreactive puncta were observed in negative controls of any area.

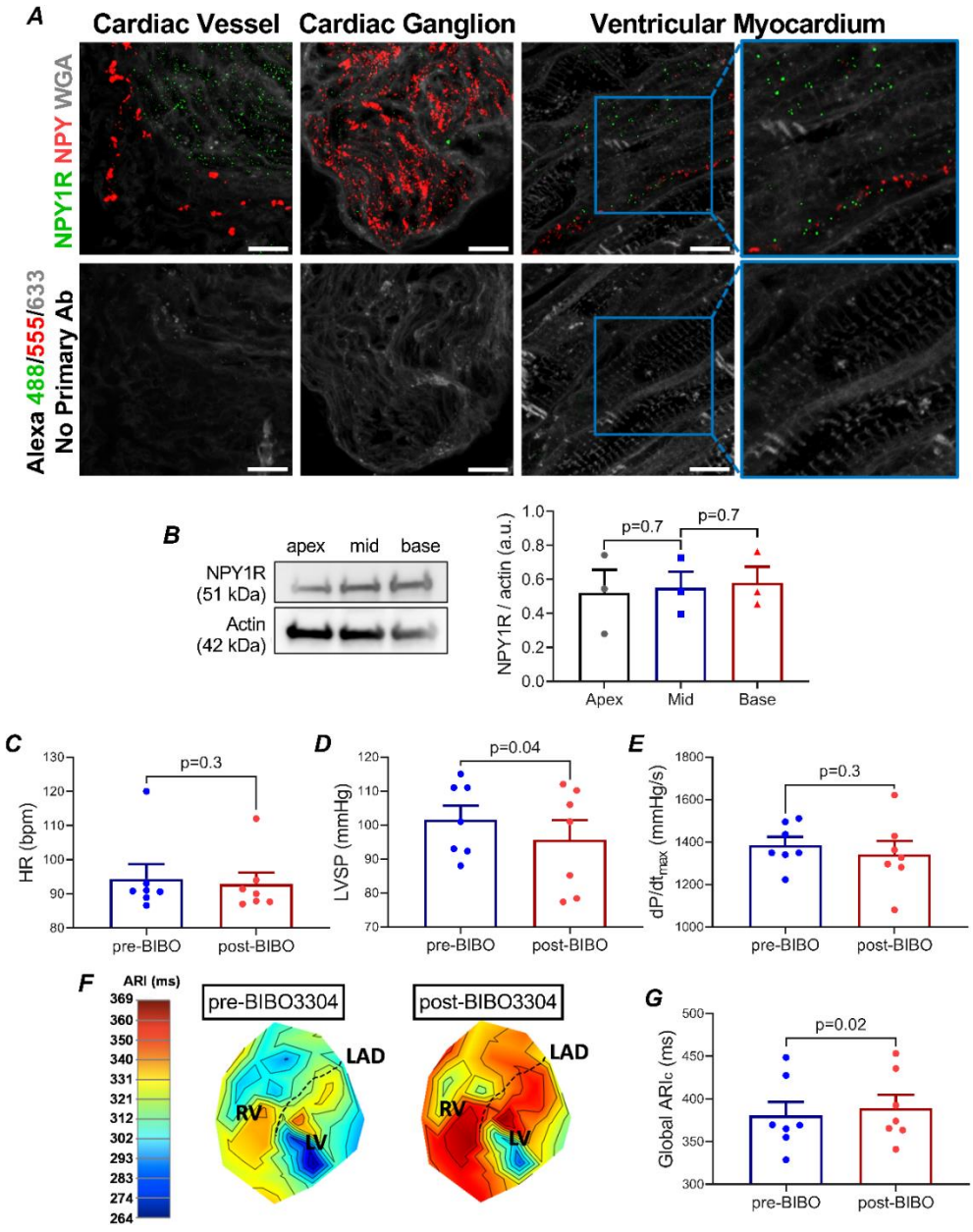

Figure 5-5. ***Expression of NPY1R in the porcine ventricular myocardium and the effects of infusion of BIBO3304 on hemodynamic parameters and ARIs.*** (**A**) NPY1R expression was confirmed in the porcine heart. High expression of NPY-Y1R (green) is evident in the vascular smooth muscle with moderate expression in intracardiac ganglia and the myocardium. NPY-immunoreactive nerve fibers (red) directly appose the NPY-1R immunoreactive vessels and myocardium. (**B**) Presence of NPY-1R is confirmed by western blot analysis of ventricular whole cell lysate and shows no regional differences in expression. BIBO 3304 had no significant effect on resting (**C**) HR or (**D**) d*P*/dt_{max} while a modest reduction in (**E**) LVSP (101.6 ± 4.1 mmHg to 94.7 ± 5.7 mmHg) was observed (**F**) Representative polar maps comparing the effects of BIBO 3304 on raw ARIs. (**G**) Global corrected ventricular ARIs significantly prolonged following the

administration of BIBO 3304. Scale bars are 10 μm. BL = baseline, ARIc = corrected ARI for heart rate. *n* = 7 animals for all comparisons. Comparisons were performed using the two-sided paired Student's *t*-test, pre-BIBO 3304 refers to data just prior to infusion of BIBO3304 but after infusion of propranolol 1.0 mg/kg for protocol #3, while post-BIBO 3304 represents data after 20 mins of BIBO 3304 infusion.

Effects of adjuvant NPY1R antagonism on BSS-induced hemodynamic and electrophysiological changes

To assess the role of NPY via Y_1 receptors in mediating the observed residual effects of sympathoexcitation in the setting of high-dose propranolol, BIBO 3304, a selective NPY1R antagonist, was administered in the same animals that received 1.0 mg/kg propranolol.

Infusion of BIBO 3304 after propranolol had no significant additional effect on HR or dP/dt_{max} (Figure 5, C and E). However, it caused a modest reduction in LVSP (P = 0.04) and, importantly, prolonged global ventricular ARIc (from 381 ± 16 ms to 389 ± 15 ms; P = 0.02; Figure 5, F and G).

Following adjuvant therapy with BIBO 3304, BSS at 10 Hz continued to increase LVSP (from 98.1 ± 4.7 mmHg to 147.0 ± 10.9 mmHg; P < 0.001) and dP/dt_{max} (from 1234.6 ± 84.4 mmHg/s to 1780.1 ± 124.1 mmHg/s; P < 0.001) (Figure 6, B and C). Unlike with intravenous propranolol at 1.0 mg/kg, there was no longer a significant HR effect with BSS after treatment with BIBO 3304 and propranolol (103.7 ± 4.9 bpm to 104.7 ± 5.5 bpm; P = 0.6; Figure 6A). Thus, BSS-induced increases in HR in the setting of propranolol alone were inhibited after administration of BIBO 3304 (4.4 ± 1.4 bpm vs. 1.0 ± 1.9 bpm, respectively; P = 0.02). There was no significant difference in BSS-induced increases in LVSP, however, between propranolol alone and propranolol with BIBO 3304, suggesting that BSS continues to have significant effects on systolic blood pressure. Of note, inotropy, as measured by dP/dtmax, improved after BIBO 3304 infusion during BSS (an increase of 333.6 ± 59.8 mmHg/s before vs. 545.5 ± 78.3 mmHg/s after BIBO 3304 with BSS; P = 0.047; Figure 6C).

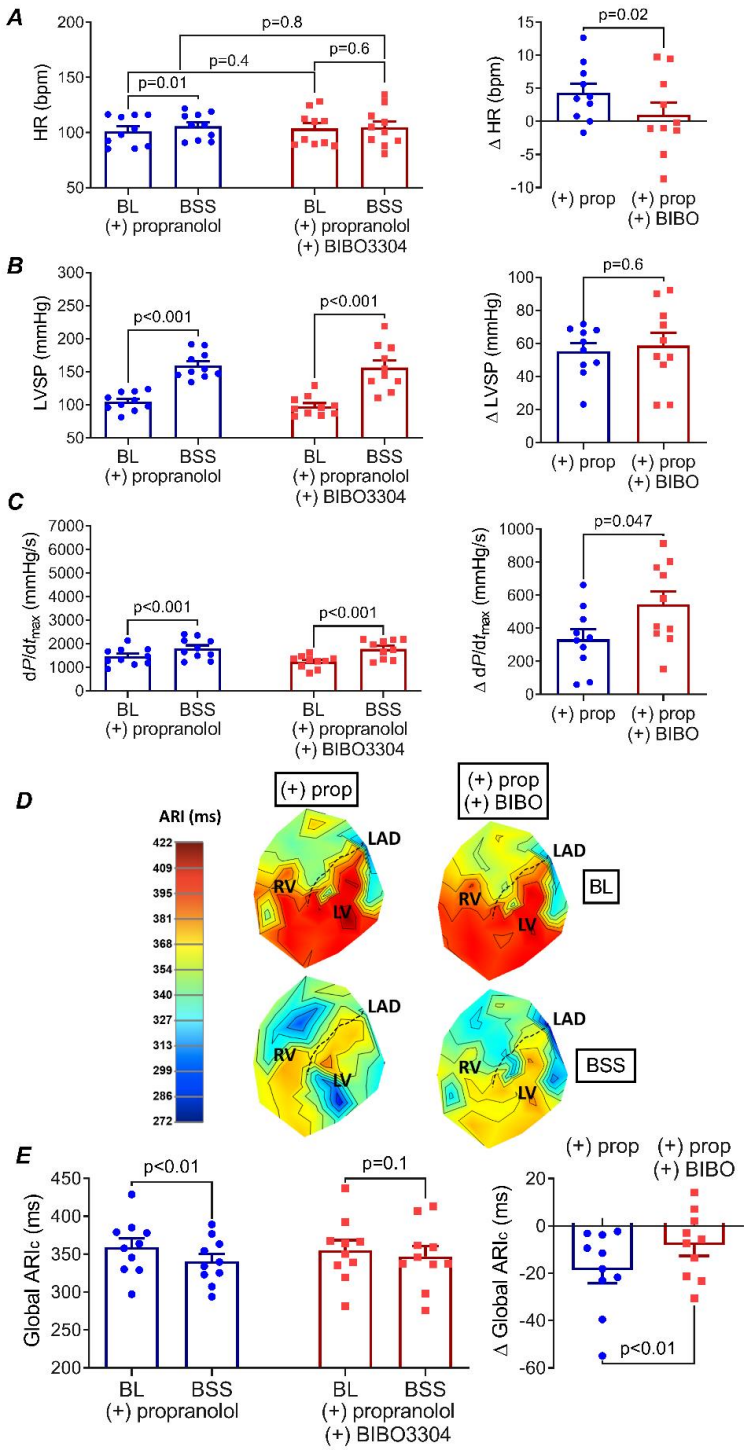

Figure 5-6. ***Effects of BSS on hemodynamic and electrophysiological parameters after 1.0 mg/kg propranolol i.v. and BIBO 3304 as compared to propranolol alone.*** BIBO 3304 completely blocked effects of BSS on (**A**) HR, while residual effects on (**B**) LVSP, and (**C**) d*P*/dt_{max} continued to be observed. BIBO 3304 augmented the changes in d*P*/dt_{max}. (**D**) Representative polar maps comparing effects of BSS on raw ventricular ARIs in the setting of high-dose propranolol, with and without BIBO 3304. (**E**) Global corrected ventricular ARIs significantly shortened despite administration of high-dose propranolol, but not after

administration of BIBO 3304. Additional treatment with BIBO 3304 significantly reduced BBS-induced shortening of ARIc. BL = baseline, ARIc = corrected ARI for heart rate, △ = change from BL. (+) prop = 1.0 mg/kg propranolol, (-) BIBO = NPY1R blockade, (+) BIBO = 0.2 mg/kg + 0.4 mg/kg/hr BIBO 3304. *n* = 10 animals for all comparisons, analyses were performed using the two-sided paired Student's *t*-test. $P \leq 0.05$ was considered significant.

Despite high-dose propranolol, BSS significantly decreased global ventricular ARIc (from 359 ± 12 ms to 341 ± 10 ms; $P < 0.01$; Figure 6, D and E). After additional administration of BIBO 3304, however, effects of BSS on ventricular ARIc were reduced (from 355 ± 13 ms to 347 ± 14 ms; $P = 0.1$). A mean difference in ARIc shortening of approximately 11 ms was observed after combined propranolol and BIBO 3304 compared with propranolol alone (19 ± 5 ms with propranolol alone to 8 ± 4 ms with propranolol + BIBO 3304; $P < 0.01$).

DISCUSSION

Major findings

In the present study we tested the hypothesis that elevated sympathetic tone circumvents the effects of high dose propranolol and that its electrophysiological effects may, in part, be mediated via NPY. Using a porcine model, we first confirmed the frequency-dependent release of NPY *in-vivo* in this species. We initially tested propranolol at 0.5 mg/kg i.v. to assess whether this dose would block electrophysiological effects of sympathoexcitation, as it represents 5 times the maximal clinically recommended doses for ventricular arrhythmias.[10] Surprisingly, while 0.5 mg/kg propranolol reduced effects of BSS, significant effects on ARIs (APD) persisted, especially at 10 Hz of stimulation, suggesting that high doses of propranolol are insufficient to block effects of sympathoexcitation and providing insight as to why patients may suffer from recurrent arrhythmias despite high doses of beta blocker therapy. Subsequently, in order to further isolate effects of NPY vs. NE, 1.0 mg/kg propranolol was used to evaluate electrophysiological effects of NPY. Detailed *in-vivo* evaluation showed shortening of ventricular ARIs despite high dose beta blocker therapy, effects which were mitigated by Y_1 receptor blockade. Our findings are in line

with previous *ex-vivo* data in rats and studies suggesting elevated arrhythmic risk in myocardial infarction patients with higher NPY levels.[14]

Other key findings of this study include:

1. While cardiac NE release is significant at 4 Hz, this release profile plateaus at 10 Hz *in-vivo*. Only modest amounts of NPY are released at 4 Hz of stimulation, with pronounced releases of NPY at 10 Hz and 20 Hz of BSS.
2. Beta-blocker therapy decreases release of NE but does not affect NPY release.
3. Although Y_1 receptor blockade caused a modest decrease in systolic blood pressure, suggesting afterload reduction, it did not affect dP/dt_{max} at baseline or during sympathetic activation, suggesting lack of deleterious inotropic effects.
4. Y_1 receptor blockade demonstrated a significant, and clinically meaningful reduction in ventricular ARIs, similar in magnitude to other neuromodulatory therapies, such as cardiac sympathetic denervation (CSD),[20] that are known to be anti-arrhythmic. However, it did not inhibit BSS induced increase in LVSP.

Beta-blocker therapy and ventricular arrhythmias

Beta-blocker therapy is the standard of care for patients that present with life-threatening VT. Recently, propranolol was shown to have better outcomes in treatment of patients presenting with VT storm than metoprolol. Despite treatment with beta-blocker medications, however, many patients experience recurrent VT and VF.[11,21,22] In this study, 0.5 mg/kg of intravenous propranolol, which is 5 to 10 times ACLS recommended doses for treatment of VT,[10] did not completely inhibit the effects of sympathoexcitation. Our data provide insight as to why beta-blocker therapy may be insufficient to prevent electrophysiological effects of sympathoexcitation. As a neuromodulatory therapy, CSD has shown benefit in treatment of refractory VT in patients already treated with beta blocker therapy and in reducing VT inducibility in infarcted porcine hearts.[20,23] It's also possible that one of the mechanisms behind the beneficial effects of CSD is a reduction in NPY. CSD, by reducing

afferent neurotransmission, can decrease efferent sympathetic outflow. In addition, by disrupting efferent sympathetic fibers, CSD can reduce both NE as well as NPY levels.

Beta-blocker therapy can also act by pre-synaptic mechanisms to reduce NE release from sympathetic nerve terminals,[24] as also observed in this study. We did not, however, observe a substantial reduction in NPY release after propranolol infusion. NE is stored in two different type of vesicles, small clear vesicles that primarily carry catecholamines and large dense vesicles that also carry NPY.[25-27] It's possible that beta-blockers have differential pre-synaptic effects on the release of these vesicles. Unlike beta-blocker therapy, which reduces the release of NE, it appears that Y_1 receptor-antagonism lacks presynaptic effects and does not affect the release of NPY, as shown in Table 2.

NPY, cardiovascular disease, and ventricular arrhythmias

NPY levels are increased in the setting of heart failure.[28-30] Patients with MI who have higher CS NPY levels are at a greater risk of ventricular dysfunction, even despite reperfusion therapy,[31] and those with higher plasma NPY were recently shown to have increased incidence of VT.[14] Of note, in a rat Langendorff model, NPY significantly increased incidence of ischemia-driven ventricular arrhythmias.[14] However, evaluation of *in-vivo* effects of NPY on ventricular APDs, especially in large animal models is lacking. This is largely due to the overwhelming effect of NPY in causing vasoconstriction when given intravenously, which has prevented a detailed assessment of its electrophysiological effects. In this study, blockade of NPY1R with BIBO 3304 further mitigated ventricular effects of sympathetic nerve stimulation on ARIs, a surrogate of APDs. Our study showed that on average, BIBO 3304 can mitigate ARI shortening by approximately 10 ms, even after correcting for HR, beyond beta-blocker therapy. Although this is a modest reduction, previous studies of neuromodulation, such as CSD and vagal nerve stimulation, have shown that even 5-10 ms increases in ventricular ARIs or refractoriness are sufficient to significantly reduce VT/VF inducibility.[20,32,33] Along this line, recently published data have shown that in an innervated rat Langendorff model, BIBO 3304 is able to increase VF threshold during sympathetic stimulation

above and beyond beta-blocker therapy with metoprolol, suggesting that Y_1 receptor blockade is anti-arrhythmic *ex-vivo.*[17] Also, recent human data suggests that patients with ST elevation myocardial infarction who have higher NPY levels also have higher incidences of ventricular arrhythmias, suggesting that NPY may be pro-arrhythmic in humans.[17]

The effects of NPY on ventricular myocyte APD have been explored in cell culture using patch-clamping techniques. NPY has been shown to reduce action potential duration in ventricular myocytes of guinea pigs.[34] In addition, optical imaging of ex-vivo rat hearts has shown that NPY significantly increases the calcium transient amplitude, accompanied by a significant shortening of the calcium transient duration.[17] It has also been suggested that NPYY1R activation enhances myocyte calcium release due to NE, acting in a synergistic fashion.[35] While this mechanism can partly explain NPY-mediated APD shortening, the residual effects of BIBO 3304 beyond high dose propranolol may also suggest that the NPY1R has an independent mechanism for shortening APD in cardiomyocytes. We also noted a mitigation of effects of BIBO 3304 on HR, despite similar increases in LVSP, similar NE and NPY release profiles, and greater increases in inotropy with BSS. These data are in line with a previous study suggesting that NPY can cause NPY1R-mediated stress evoked tachycardia.[36] The observed similar or greater effects on other hemodynamic parameters in this study suggest that repeat stimulation "fatigue," which may occur with multiple stimulations of stellate ganglia if a sufficient waiting period between stimulations is not allowed, was not a factor in our studies (with a minimum of a 60 min waiting period between stimulations).

NPY is a potent vasoconstrictor,[37] but its effects on inotropy are unclear. A study in isolated rat cardiomyocytes suggested NPY1R-agonism may improve inotropy,[38] while an *in-vivo* study suggested that NPY inhibits inotropic effects of sympathetic stimulation.[39] It's also possible that by causing significant coronary vasoconstriction,[16] NPY can interfere with myocardial metabolism and, thereby, cardiac function. Interestingly, NPY1R blockade with BIBO 3304 did not reduce dP/dt_{max} and augmented the inotropic effects of BSS. Taken together these data suggest that adjuvant myocardial blockade of NPY1R may be hemodynamically well-tolerated. Despite

combination of BIBO 3304 and propranolol, a modest residual effect on ARIs still remained during BSS. This may be due to other sympathetic co-transmitters, such as galanin,[13] whose levels are also elevated with cardiovascular disease,[15] but whose electrophysiological effects remain unclear.

Of note, we tested effects of BIBO 3304 at 10 Hz stimulation, given that we did not see electrophysiological differences between 10 Hz and 20 Hz. It's important to note that the levels of NPY observed in the CS of pigs in this study at 10 Hz (43.9 ± 12.3 pg/mL) were comparable to those observed in the CS of patients with acute MI (29.3 pg/mL with a range of 23.6 to 51.4 pg/mL), who had poorer outcomes at 6 months, as compared to patients who had lower levels of NPY.[16]

Clinical implications

Recurrent ventricular arrhythmias occur in patients with cardiomyopathy, despite therapy with beta blocker medications, anti-arrhythmic drugs, and catheter ablation, posing a significant therapeutic challenge.[21,22] Cardiac sympathetic activation is known to both trigger and maintain ventricular arrhythmias.[1,9] This study demonstrates that high dose beta-blocker therapy, at an order of magnitude higher than clinically recommended doses, still cannot overcome the electrophysiological effects of sympathoexcitation in normal porcine hearts, and that NPY has independent ventricular electrophysiological effects that are mediated through the Y_1 receptor. No adverse effects on inotropy were observed with Y_1 receptor blockade. As treatment of ventricular arrhythmias primarily relies on beta-blocker therapy to reduce effects of sympathetic activation, our results in-vivo in a large animal model provide some insight as to why patients may continue to experience recurrent arrhythmias despite this therapy. Studies in diseased hearts, however, are needed to further confirm our findings and evaluate the effects of Y_1 receptor blockade on ventricular arrhythmia inducibility.

Limitations

This study evaluated effects of BSS and Y_1 receptor blockade acutely; chronic effects of BIBO 3304 remain to be investigated. General anesthesia with isoflurane is known to blunt autonomic responses. To limit this effect, once surgical procedures had been completed,

anesthesia was switched to α-chloralose. In this study atropine was administered to prevent reflex bradycardia in response to rises in blood pressures that can occur as result of BSS. This may have led to an underestimation of effects of NPY acting via other receptors, such as Y_2 receptors, which are known to decrease release of acetylcholine from parasympathetic fibers.[13,40] It's possible that a portion of the changes in ARIs during BSS were driven by heart rate. We did not correct for heart rate changes with pacing due to known effects of cardiac pacing on further exacerbating sympathoexcitation, cardiac NE levels, and cardiac autonomic neural activity.[41,42] I Instead, we corrected ARIs at different heart rates using Friedrichs formula for QT as no formula exists for ARI correction and QT formula is without limitation. Of note, ventricular ARIs prolonged with BIBO 3304 infusion, even after correcting for HR, and results of BSS on ARI pre- and post-BIBO 3304 were noted to be at the same heart rate. Finally, ventricular stimulation was not performed in these animals. Ventricular stimulation rarely causes VT in normal pig hearts (< 10%), and very aggressive programmed stimulation can produce non-specific VF. Therefore, to observe the effects of BIBO 3304 on VT inducibility above and beyond beta-blocker therapy, very large numbers of animals would be required to obtain sufficient power to see an effect. Studies on the effects of BIBO 3304 in the setting of chronic myocardial infarction, where VT is more readily induced, could be used to evaluate effects of BIBO 3304 on the incidence of ventricular arrhythmias.

CONCLUSIONS

This study demonstrates that high doses of beta-blockers cannot completely prevent the electrophysiological effects of sympathetic activation. *In-vivo* NPY can act directly on the ventricles and modulate cardiac APDs via a Y_1 receptor-mediated mechanism. Cardiac contractility was preserved with NPY1R antagonism. Adjuvant NPYY1R blockade may present a promising therapeutic target in patients with refractory ventricular tachyarrhythmias.

METHODS

Ethical approval

Yorkshire pigs (*Sus scrofa*; 3.6 ± 0.1 months old; *N* = 25) were used in the study. Pigs were housed for a minimum of a week to allow for acclimatization at the UCLA animal housing facility and subjected to a standard 12-h light-dark cycle. Care of the animals conformed to the National Institutes of Health Guide for the Care and Use of Laboratory Animals. The study protocol was approved by the University of California, Los Angeles, Institutional Animal Care and Use Committee.

Experimental protocol

Three groups of animals were used for the following studies (Figure 1):

Group 1 (49.1 ± 1.0 kg; *n* = 5) These animals underwent sequential bilateral stellate ganglia stimulations (BSS) to evaluate the effect of a range of stimulation frequencies on hemodynamic, electrophysiological, and neurotransmitter/neuropeptide profiles in the porcine model, given lack of previous data in this species. Stimulations were performed at 4 Hz, 10 Hz, and 20 Hz, with a 60 min wait period in between stimulations.

Group 2 (52.2 ± 3.5 kg; *n* = 10) These animals underwent BSS at 4 Hz and 10 Hz (given results of group 1) with and without 0.5 mg/kg of propranolol i.v. and a minimum of a 60 min wait period between stimulations.

Group 3 (44.8 ± 1.4 kg; *n* = 10) These animals underwent BSS at 10 Hz and repeat 10 Hz stimulations with propranolol 1.0 mg/kg i.v. and a combination of propranolol 1.0 mg/kg i.v. and BIBO 3304 infusion. A minimum of 60 mins was allowed in between stimulations.

Experimental preparation

All animals were sedated with tiletamine-zolazepam (4−8 mg/kg, i.m.) and intubated. General anesthesia was maintained with isoflurane (1−2%) and analgesia managed by intermittent boluses of fentanyl (total 20 mcg/kg, i.v.) during surgical preparation. Following the completion of surgical procedures, anesthesia was maintained by α-chloralose (50 mg/kg initial bolus, subsequently 20–30 mg/kg/hr continuous infusion, i.v.). Hourly arterial blood gases were monitored, and appropriate ventilator adjustments were made to maintain pH at 7.35–7.45. Rectal temperature was assessed and adjusted to maintain body temperature at 35−38 °C. Bilateral femoral veins and

arteries were accessed and used for continuous saline and drug infusion and blood sampling, respectively. Right external jugular vein was used for insertion of a catheter into the coronary sinus for blood sampling. Left carotid artery was used for catheter insertion into the left ventricle (LV) for the assessment of left ventricular pressures and blood pressure measurements, respectively. Twelve-lead surface ECG were obtained via a Prucka Cardiolab System and precordial leads were placed on the dorsal aspect of the animal given sternotomy. Animals underwent median sternotomy to expose the heart as well as bilateral stellate ganglia. Animals were euthanized by induction of ventricular fibrillation under deep anesthesia. General anesthesia was maintained with isoflurane during surgical preparation and transitioned to α-chloralose following completion of surgical procedures.

Stellate ganglia stimulation

After median sternotomy, the right and left stellate ganglia were carefully isolated behind the parietal pleura and bipolar platinum needle electrodes were placed in the ganglia for BSS as previously described.[8,20] The electrodes were connected to a stimulator (Grass Stimulator Model S88) and PSIU6 stimulation isolation units (Grass Technologies, Warwick, RI) for stimulation. The stimulation current that led to a 10% increase in HR and/or LVSP was determined unilaterally at 4 Hz, 4 ms pulse width (square wave) for each animal and defined as the threshold current. BSS was then performed at 2 times threshold according to one of three experimental protocols (Figure 1A). A minimum of 60 min was allowed for electrophysiological and hemodynamic parameters and neurotransmitter/peptide profiles to return to baseline in between stimulations.

Drug infusions

To evaluate whether beta-blocker therapy could prevent BSS-induced changes in hemodynamic and electrophysiological parameters, effects of two high doses of i.v. propranolol were evaluated: 0.5 mg/kg (average dose of 26.1 ± 1.7 mg per animal; n = 10) and 1.0 mg/kg (average dose of 44.8 ± 1.4 mg per animal; n = 10). Both doses of propranolol were given as a bolus infusion over a 5 to 10 min period. Both of these doses are more than five and ten-fold above

American College of Cardiology/American Heart Associated guideline recommend doses of 1 to 3 mg (0.01 mg/kg to 0.04 mg/kg) i.v. and up to 5 mg (0.07 mg/kg) i.v. for treatment of ventricular arrhythmias in 70 kg adult patients,[10] respectively. Repeat BSS was performed 10 mins after infusion of propranolol, to allow for stabilization of hemodynamic parameters. Propranolol 1.0 mg/kg was evaluated in a different set of animals after data from animals that received 0.5 mg/kg of propranolol showed significant residual sympathetic effects during BSS. Atropine sulfate 0.04 mg/kg was used to prevent reflex bradycardia during BSS induced rises in blood pressure. The NPY Y_1 receptor antagonist, BIBO 3304 (Tocris, Minneapolis, MN) was dissolved in DMSO and diluted in saline to a final concentration of 660 mM (0.5 mg/mL) BIBO 3304 in 0.5% DMSO/saline. BIBO 3304 was administered at a dosage of 0.2 mg/kg followed by a 0.4 mg/kg/hr infusion (average dose 9.0 ± 0.3 mg bolus followed by 17.9 ± 0.6 mg/hr infusion of BIBO 3304; n = 10) for 20 min before BSS and for the duration of the stimulation. BIBO 3304 was administered to the same animals that had received 1.0 mg/kg propranolol (Figure 1). All drugs were administered intravenously.

Hemodynamic assessment

A 5-Fr Millar pressure-conductance pressure catheter was placed in the left ventricle (LV) for continuous measurements of LVP throughout the experiment. Raw signals were digitized and recorded by CED Power1401 and subsequently analyzed using Spike2.

Cardiac electrophysiological recordings and analysis

A 56-electrode sock was placed over the ventricles to continuously record unipolar epicardial electrograms connected to a Prucka CardioLab System (Prucka CardioLab System) and band pass filtered at 0.05-500 Hz. Global ARIs, a surrogate of action potential duration, was analyzed from these 56 unipolar electrograms using a customized software, iScaldyn (University of Utah, Salt Lake City, UT) as previously described.[43,44] Activation time (AT) was measured as the interval from onset to minimal dV/dt of the depolarization wave-front and repolarization time (RT) from onset to maximal dV/dt of the repolarization wave-front, respectively. The difference between RT and AT was calculated as ARI, which has been shown to reflect the local APD at the electrode

site (ARI = RT-AT).[44,45] Polar maps and regional analyses reflect raw ARIs. Global ARIs were adjusted for the differences in heart rate using the Fridericia formula, to correct for the effect of heart rate on action potential duration, and corrected ARIs are reported in all figures.[46,47] Unadjusted ARIs were used for regional analysis, as changes in various regions were compared at the same heart rate, as shown in Supplemental Figure 1.

Measurement of sympathetic neurotransmitter/neuropeptide concentrations

CS and FA blood were collected at baseline and during BSS to measure plasma NE and NPY concentrations. Blood was collected into K_2 EDTA blood collection tubes (BD Vacutainer, Franklin Lakes, NJ) followed by immediate centrifugation at 1,500 rcf for 15 min. The plasma was separated, snap frozen in liquid nitrogen, and stored at -80 °C until assay. NE and NPY were measured by ELISA (BA E-6200, sensitivity 0.093 ng/mL, Rocky Mountain Diagnostics, Colorado Springs, CO; EZHNPY-25K, sensitivity 2.0 pg/mL, EMD Millipore, Burlington, MA, respectively) according to manufacturer's instructions.

Evaluation of NPY Y_1 receptor expression

Left ventricular tissue was collected after euthanasia from naïve normal animals (n = 3) and snap-frozen in liquid nitrogen for Western blot or immersion fixed in 4% paraformaldehyde for 24 hours for immunohistochemistry. These animals did not undergo any type of sympathetic stimulation.

Snap frozen tissues were Dounce homogenized and lysed in 8M SDS-urea and total protein concentrations were quantified by bicinchoninic acid assay. 20 µg of protein were loaded per lane on 4-20% polyacrylamide gels (BioRad; 4561093) and proteins were transferred by Trans-Blot Turbo (BioRad; 1704150) onto 0.2 µm PVDF membranes. Membranes were blocked with 5% milk in tris buffered-saline with 0.2% tween, incubated overnight with rabbit anti-NPY1R (1:1000; Abcam; ab91262) or rabbit anti-actin (1:2500; Sigma; A2066) followed by peroxidase anti-rabbit IgG (Jackson Immunoresearch; 711-035-152) for 1 hr at room temperature. Proteins were detected by chemiluminescence with Clarity Western ECL Substrate (BioRad; 1706061) and imaged on

ChemiDoc MP (BioRad; 17001402). Densitometry was performed using ImageJ (NIH) to compare regional expression of NPY1R.

Fixed tissue was embedded in paraffin, sectioned (5 μm), and rehydrated in two xylene washes followed by here ethanol washes and water. Epitopes were unmasked by heat-induced epitope retrieval in EDTA buffer pH 8.0 (Abcam; ab64216) at 90 °C. Slides were then blocked for 1 hr in 3% BSA-TBS-0.2% Triton X-100 with 5% donkey serum and incubated overnight at 4 °C with rabbit anti-NPY1R (1:200; Alomone Labs; ANR-021) and mouse anti-NPY (1:500; Abcam; ab112473) followed by 2 hr incubation at room temperature with Alexa Fluor 488 donkey anti-rabbit IgG and Alexa Fluor 555 donkey anti-mouse IgG (1:200; Invitrogen). Slides were then incubated with wheat germ agglutinin conjugated to Alexa Fluor 633 (Thermo Fisher; W21404) for 30 mins at room temperature and mounted with Antifade Mounting Medium with DAPI (Vector Laboratories; H-1200). Negative controls were performed on serial sections processed in tandem by omission of primary antibody. Slides were imaged on a Zeiss LSM 880 with Airyscan at ×630 magnification and processed with Zen 2 (Zeiss).

Statistical analysis

Data are reported as mean ± SEM. Global ventricular ARIs were calculated as the mean ARI across all 56 electrodes and corrected for heart rate using the Fridericia formula. After confirmation of normality, paired Student's *t*-test was used to compare parameters between baseline and BSS during each condition and responses to BSS between different conditions within each animal. Comparisons of changes in parameters between different frequencies (Protocol #1) were performed using a one-way repeated measures ANOVA with the false discovery rate corrected for by the Benjamini-Hochberg procedure. A P value ≤ 0.05 was considered statistically significant. All statistical analyses were performed with GraphPad Prism software (GraphPad Prism, v8).

FUNDING SUPPORT AND AUTHOR DISCLOSURES

This study was funded by NIHDP2HL132356 and SPARC OT2OD023848 to MV.

REFERENCES

1 Vaseghi, M. & Shivkumar, K. The role of the autonomic nervous system in sudden cardiac death. Prog Cardiovasc Dis 50, 404-419, doi:10.1016/j.pcad.2008.01.003 (2008).

2 Zipes, D. P. & Inoue, H. in Neurocardiology (eds Kulbertus H.E. & G. Frank) 787-796 (Futura Publisher, 1988).

3 Herring, N., Kalla, M. & Paterson, D. J. The autonomic nervous system and cardiac arrhythmias: current concepts and emerging therapies. Nat Rev Cardiol 16, 707-726, doi:10.1038/s41569-019-0221-2 (2019).

4 Ben-David, J. & Zipes, D. P. Differential response to right and left ansae subclaviae stimulation of early afterdepolarizations and ventricular tachycardia induced by cesium in dogs. Circulation 78, 1241-1250 (1988).

5 Priori, S. G., Mantica, M. & Schwartz, P. J. Delayed afterdepolarizations elicited in vivo by left stellate ganglion stimulation. Circulation 78, 178-185 (1988).

6 Opthof, T. et al. Dispersion of refractoriness in normal and ischaemic canine ventricle: effects of sympathetic stimulation. Cardiovasc Res 27, 1954-1960 (1993).

7 Opthof, T. et al. Dispersion of refractoriness in canine ventricular myocardium. Effects of sympathetic stimulation. Circ Res 68, 1204-1215 (1991).

8 Yagishita, D. et al. Sympathetic nerve stimulation, not circulating norepinephrine, modulates T-peak to T-end interval by increasing global dispersion of repolarization. Circulation. Arrhythmia and electrophysiology 8, 174-185, doi:10.1161/CIRCEP.114.002195 (2015).

9 Shivkumar, K. et al. Clinical neurocardiology defining the value of neuroscience-based cardiovascular therapeutics. J Physiol 594, 3911-3954, doi:10.1113/JP271870 (2016).

10 Al-Khatib, S. M. et al. 2017 AHA/ACC/HRS Guideline for Management of Patients With Ventricular Arrhythmias and the Prevention of Sudden Cardiac Death: Executive Summary: A Report of the American College of Cardiology/American Heart Association Task Force on

Clinical Practice Guidelines and the Heart Rhythm Society. J Am Coll Cardiol 72, 1677-1749, doi:10.1016/j.jacc.2017.10.053 (2018).

11 Chatzidou, S. et al. Propranolol Versus Metoprolol for Treatment of Electrical Storm in Patients With Implantable Cardioverter-Defibrillator. J Am Coll Cardiol 71, 1897-1906, doi:10.1016/j.jacc.2018.02.056 (2018).

12 Burnstock, G. Autonomic neurotransmission: 60 years since sir Henry Dale. Annu Rev Pharmacol Toxicol 49, 1-30, doi:10.1146/annurev.pharmtox.052808.102215 (2009).

13 Herring, N. et al. The cardiac sympathetic co-transmitter galanin reduces acetylcholine release and vagal bradycardia: implications for neural control of cardiac excitability. Journal of molecular and cellular cardiology 52, 667-676, doi:10.1016/j.yjmcc.2011.11.016 (2012).

14 Herring, N. et al. Pro-arrhythmic effects of the cardiac sympathetic co-transmitter, neuropeptide-Y, during ischemia-reperfusion and ST elevation myocardial infarction. Faseb J 30 (2016).

15 Ajijola, O. A. et al. Coronary Sinus Neuropeptide Y Levels and Adverse Outcomes in Patients With Stable Chronic Heart Failure. JAMA Cardiol, doi:10.1001/jamacardio.2019.4717 (2019).

16 Herring, N. et al. Neuropeptide-Y causes coronary microvascular constriction and is associated with reduced ejection fraction following ST-elevation myocardial infarction. Eur Heart J 40, 1920-1929, doi:10.1093/eurheartj/ehz115 (2019).

17 Kalla, M. et al. The cardiac sympathetic co-transmitter neuropeptide Y is pro-arrhythmic following ST-elevation myocardial infarction despite beta-blockade. Eur Heart J, doi:10.1093/eurheartj/ehz852 (2019).

18 Herring, N. Autonomic control of the heart: going beyond the classical neurotransmitters. Exp Physiol 100, 354-358, doi:10.1113/expphysiol.2014.080184 (2015).

19 El Karim, I. A., Lamey, P. J., Linden, G. J. & Lundy, F. T. Neuropeptide Y Y1 receptor in human dental pulp cells of noncarious and carious teeth. Int Endod J 41, 850-855, doi:10.1111/j.1365-2591.2008.01436.x (2008).

20 Irie, T. et al. Cardiac sympathetic innervation via middle cervical and stellate ganglia and antiarrhythmic mechanism of bilateral stellectomy. Am J Physiol Heart Circ Physiol 312, H392-H405, doi:10.1152/ajpheart.00644.2016 (2017).

21 Tung, R. et al. Freedom from recurrent ventricular tachycardia after catheter ablation is associated with improved survival in patients with structural heart disease: An International VT Ablation Center Collaborative Group study. Heart Rhythm 12, 1997-2007, doi:10.1016/j.hrthm.2015.05.036 (2015).

22 Sapp, J. L. et al. Ventricular Tachycardia Ablation versus Escalation of Antiarrhythmic Drugs. New Engl J Med 375, 111-121, doi:10.1056/NEJMoa1513614 (2016).

23 Vaseghi, M. et al. Cardiac Sympathetic Denervation for Refractory Ventricular Arrhythmias. J Am Coll Cardiol 69, 3070-3080, doi:10.1016/j.jacc.2017.04.035 (2017).

24 Berg, T. beta1-Blockers Lower Norepinephrine Release by Inhibiting Presynaptic, Facilitating beta1-Adrenoceptors in Normotensive and Hypertensive Rats. Front Neurol 5, 51, doi:10.3389/fneur.2014.00051 (2014).

25 Lundberg, J. M. & Hokfelt, T. Multiple co-existence of peptides and classical transmitters in peripheral autonomic and sensory neurons--functional and pharmacological implications. Prog Brain Res 68, 241-262 (1986).

26 Lundberg, J. M., Franco-Cereceda, A., Lacroix, J. S. & Pernow, J. Neuropeptide Y and sympathetic neurotransmission. Ann N Y Acad Sci 611, 166-174, doi:10.1111/j.1749-6632.1990.tb48930.x (1990).

27 Lundberg, J. M., Rudehill, A., Sollevi, A., Fried, G. & Wallin, G. Co-release of neuropeptide Y and noradrenaline from pig spleen in vivo: importance of subcellular storage, nerve impulse frequency and pattern, feedback regulation and resupply by axonal transport. Neuroscience 28, 475-486, doi:10.1016/0306-4522(89)90193-0 (1989).

28 Ullman, B., Hulting, J. & Lundberg, J. M. Prognostic value of plasma neuropeptide-Y in coronary care unit patients with and without acute myocardial infarction. Eur Heart J 15, 454-461, doi:10.1093/oxfordjournals.eurheartj.a060526 (1994).

29 Hulting, J., Sollevi, A., Ullman, B., Franco-Cereceda, A. & Lundberg, J. M. Plasma neuropeptide Y on admission to a coronary care unit: raised levels in patients with left heart failure. Cardiovasc Res 24, 102-108, doi:10.1093/cvr/24.2.102 (1990).

30 Maisel, A. S. et al. Elevation of plasma neuropeptide Y levels in congestive heart failure. Am J Med 86, 43-48, doi:10.1016/0002-9343(89)90228-3 (1989).

31 Cuculi, F. et al. Relationship of plasma neuropeptide Y with angiographic, electrocardiographic and coronary physiology indices of reperfusion during ST elevation myocardial infarction. Heart 99, 1198-1203, doi:10.1136/heartjnl-2012-303443 (2013).

32 Waxman, M. B. & Wald, R. W. Termination of Ventricular Tachycardia by an Increase in Cardiac Vagal Drive. Circulation 56, 385-391, doi:Doi 10.1161/01.Cir.56.3.385 (1977).

33 Ellenbogen, K. A., Smith, M. L. & Eckberg, D. L. Increased Vagal Cardiac Nerve Traffic Prolongs Ventricular Refractoriness in Patients Undergoing Electrophysiology Testing. Am J Cardiol 65, 1345-1350, doi:Doi 10.1016/0002-9149(90)91325-Z (1990).

34 Bryant, S. M., Ryder, K. O. & Hart, G. Effects of neuropeptide Y on cell length and membrane currents in isolated guinea pig ventricular myocytes. Circ Res 69, 1106-1113, doi:10.1161/01.res.69.4.1106 (1991).

35 Wier, W. G., Zang, W. J., Lamont, C. & Raina, H. Sympathetic neurogenic Ca2+ signalling in rat arteries: ATP, noradrenaline and neuropeptide Y. Exp Physiol 94, 31-37, doi:10.1113/expphysiol.2008.043638 (2009).

36 Zhang, W. G., Lundberg, J. M. & Thoren, P. Neuropeptide Y Y1 receptor antagonist (BIBP 3226) attenuates stress evoked tachycardia in conscious spontaneously hypertensive rats. Cardiovasc Drug Ther 11, 801-806, doi:Doi 10.1023/A:1007726626924 (1997).

37 Franco-Cereceda, A., Lundberg, J. M. & Dahlof, C. Neuropeptide Y and sympathetic control of heart contractility and coronary vascular tone. Acta Physiol Scand 124, 361-369, doi:10.1111/j.1748-1716.1985.tb07671.x (1985).

38 Heredia Mdel, P. et al. Neuropeptide Y rapidly enhances [Ca2+]i transients and Ca2+ sparks in adult rat ventricular myocytes through Y1 receptor and PLC activation. Journal of molecular and cellular cardiology 38, 205-212, doi:10.1016/j.yjmcc.2004.11.001 (2005).

39 Awad, S. J., Einstein, R., Potter, E. K. & Richardson, D. P. The effects of neuropeptide Y on myocardial contractility and coronary blood flow. Br J Pharmacol 104, 195-201, doi:10.1111/j.1476-5381.1991.tb12407.x (1991).

40 Smith-White, M. A., Iismaa, T. P. & Potter, E. K. Galanin and neuropeptide Y reduce cholinergic transmission in the heart of the anaesthetised mouse. Br J Pharmacol 140, 170-178, doi:10.1038/sj.bjp.0705404 (2003).

41 Taylor, J. A., Morillo, C. A., Eckberg, D. L. & Ellenbogen, K. A. Higher sympathetic nerve activity during ventricular (VVI) than during dual-chamber (DDD) pacing. Journal of the American College of Cardiology 28, 1753-1758, doi:Doi 10.1016/S0735-1097(96)00389-0 (1996).

42 Rajendran, P. S. et al. Myocardial infarction induces structural and functional remodelling of the intrinsic cardiac nervous system. J Physiol-London 594, 321-341, doi:10.1113/Jp271165 (2016).

43 Coronel, R. et al. Monophasic action potentials and activation recovery intervals as measures of ventricular action potential duration: experimental evidence to resolve some controversies. Heart Rhythm 3, 1043-1050, doi:10.1016/j.hrthm.2006.05.027 (2006).

44 Millar, C. K., Kralios, F. A. & Lux, R. L. Correlation between refractory periods and activation-recovery intervals from electrograms: effects of rate and adrenergic interventions. Circulation 72, 1372-1379 (1985).

45 Haws, C. W. & Lux, R. L. Correlation between in vivo transmembrane action potential durations and activation-recovery intervals from electrograms. Effects of interventions that alter repolarization time. Circulation 81, 281-288 (1990).

46 Vandenberk, B. et al. Which QT Correction Formulae to Use for QT Monitoring? J Am Heart Assoc 5, doi:10.1161/JAHA.116.003264 (2016).

47 FRIDERICIA, L. S. Die Systolendauer im Elektrokardiogramm bei normalen Menschen und bei Herzkranken. Acta Medica Scandinavica 53, 469-486, doi:10.1111/j.0954-6820.1920.tb18266.x (1920).

SUPPLEMENTAL TABLES AND FIGURES

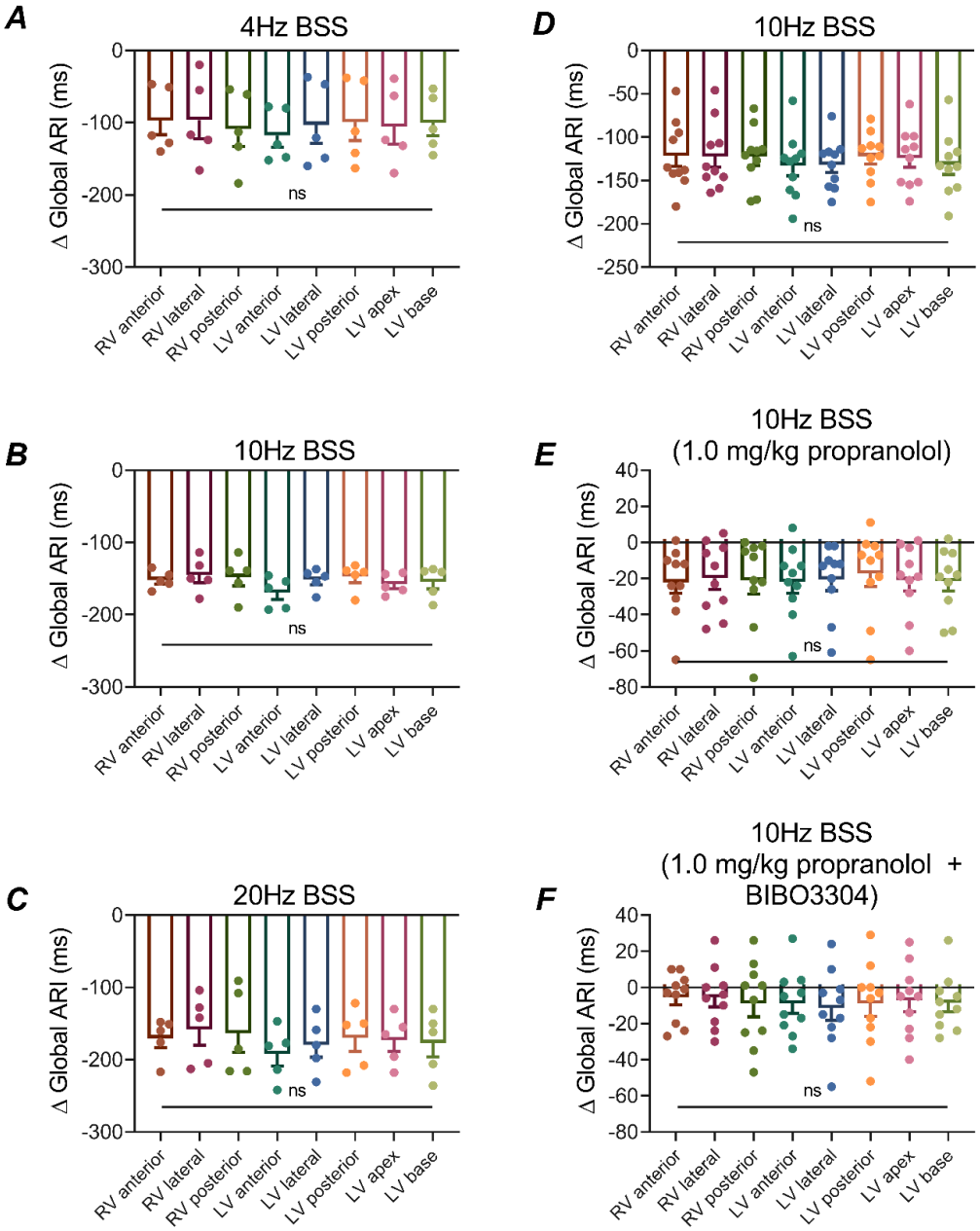

Supplemental Figure 5-1. ***Regional raw ARIs during BSS.*** There were no significant regional differences in the change in ARI between RV anterior, lateral, posterior and LV anterior, lateral, posterior, apex and base with **(A)** 4 Hz, **(B)** 10 Hz, or **(C)** 20 Hz of stimulation or with 10 Hz stimulation **(D)** without drug, **(E)** with 1.0 mg/kg propranolol, or with **(F)** 1.0 mg/kg propranolol + BIBO3304. BL = baseline, BSS = bilateral stellate ganglia stimulation; RV = right ventricle, LV = left ventricle. **(A-C)** *n* = 5 animals for all comparisons, **(D-F)** *n* = 10 animals for all comparisons; comparisons of changes between different regions were performed using one-way ANOVA.

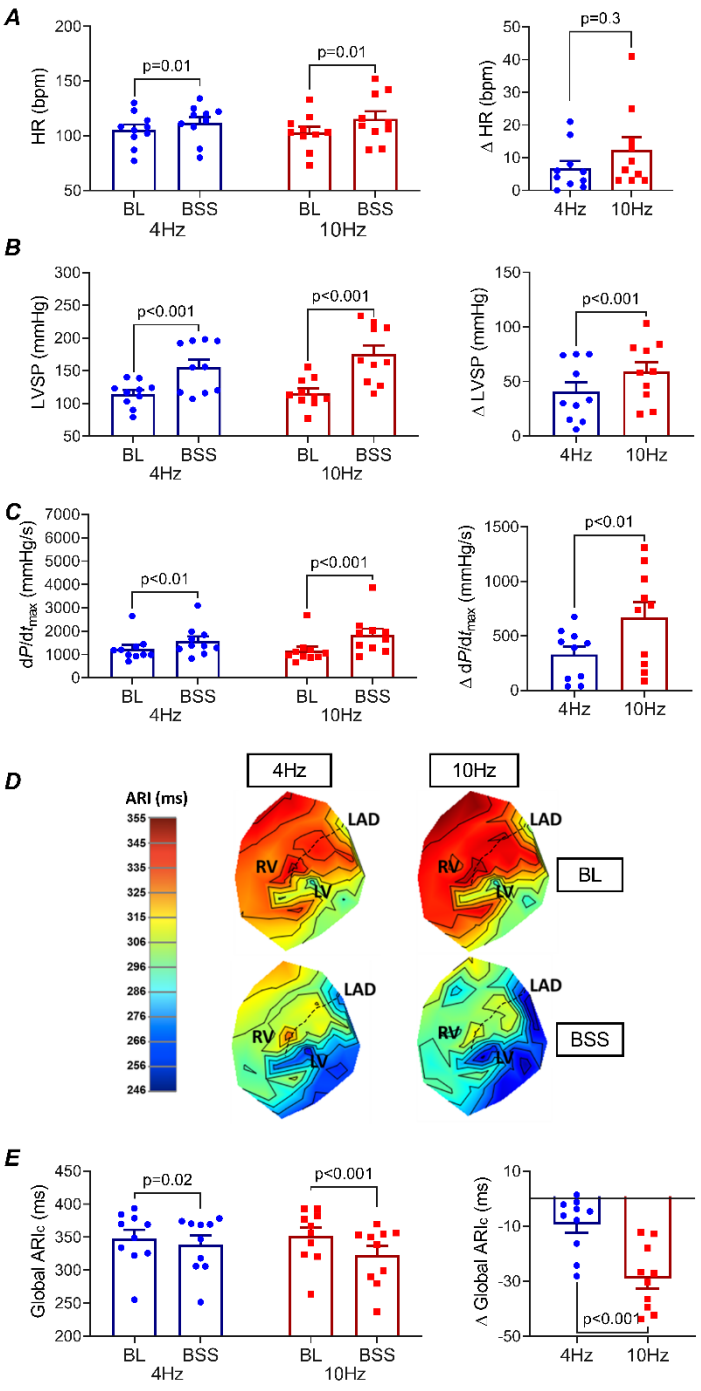

Supplemental Figure 5-2. ***Effects of BSS after 0.5 mg/kg propranolol.*** Both BSS at 4 Hz and 10 Hz significantly increased **(A)** HR, **(B)** LVSP, and **(C)** d*P*/dt_{max} despite administration of 0.5 mg/kg propranolol. BSS at 10 Hz caused significantly greater increases in LVSP and d*P*/dt_{max} vs. 4 Hz. BL = baseline. **(D)** Representative polar maps depicting the effects of BSS at 4 Hz and 10 Hz on raw ARIs after 0.5 mg/kg propranolol. **(E)** Both frequencies caused significant shortening in raw and corrected ARIs despite propranolol with greater effects at 10 Hz vs. 4 Hz. BL = baseline, △ = change from BL. *n* = 10 animals for all comparisons, comparisons were performed using the two-sided paired Student's *t*-test. $P \leq 0.05$ was considered significant.

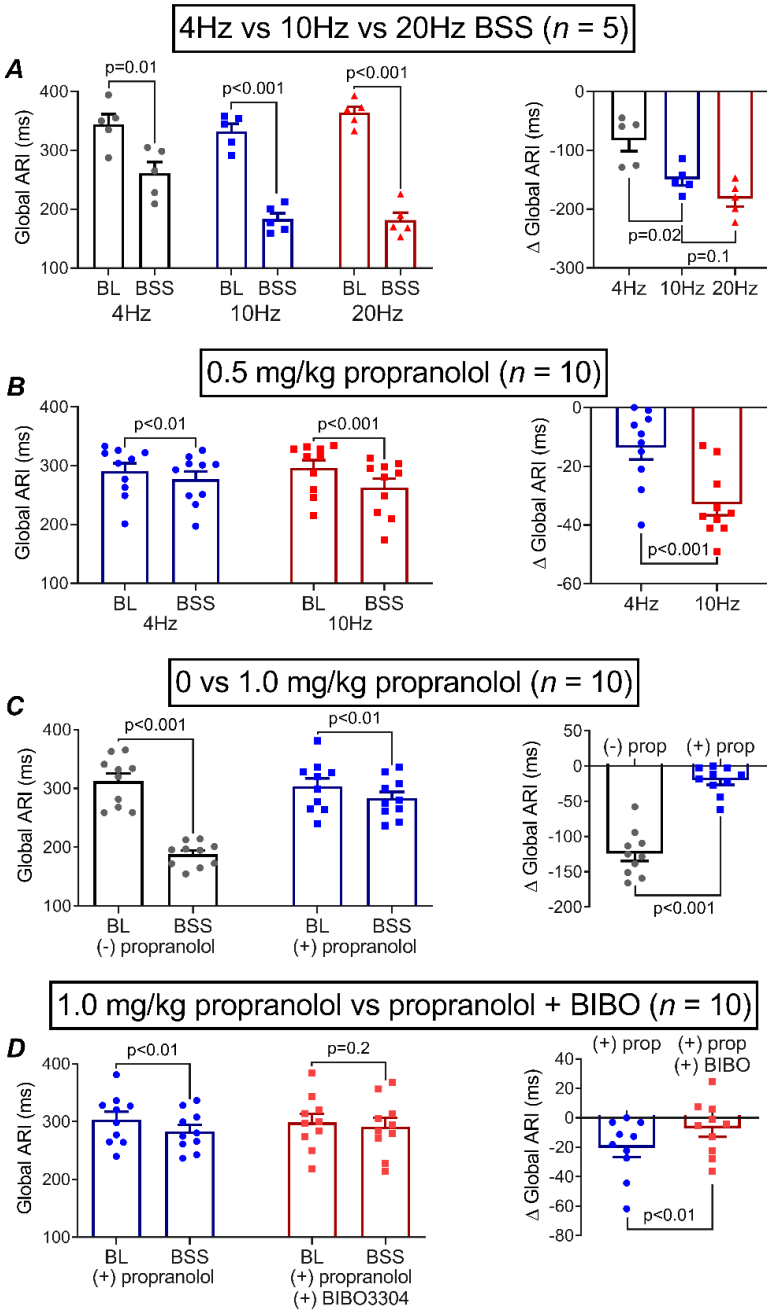

Supplemental Figure 5-3. ***Uncorrected/raw global ventricular ARIs.*** **(A)** Global ARI significantly shortened at all frequencies of stimulation with significantly more shortening at 10 and 20 Hz than 4 Hz BSS. **(B)** ARI shortening persisted at 4 and 10 Hz BSS despite treatment with 0.5 mg/kg propranolol with **(C)** residual electrophysiological effects in the setting of 1.0 mg/kg propranolol with 10 Hz BSS. **(D)** However, further administration of BIBO 3304 abrogated the electrophysiological effects of 10 Hz BSS. Comparisons were performed using the two-sided paired Student's *t*-test. $P \leq 0.05$ was considered significant.